HUNGARIAN UNIVERSITY OF AGRICULTURE AND LIFE SCIENCES

Performance evaluation of solar chimney applied for drying processes

DOI: 10.54598/003170

PhD Dissertation

by

Gebremicheal Gedion Habtay

Gödöllő
2022

Doctoral school

Denomination: Doctoral School of Mechanical Engineering

Science: Mechanical Engineering

Leader: Prof. Dr. Gábor Kalácska, DSc
Institute of Technology
Hungarian University of Agriculture and Life Science, Gödöllő, Hungary

Supervisor: Prof. Dr. István Farkas, DSc
Institute of Technology
Hungarian University of Agriculture and Life Science, Gödöllő, Hungary

Co-Supervisor: Dr. János Buzás, PhD
Institute of Technology
Hungarian University of Agriculture and Life Science, Gödöllő, Hungary

…… ……

Affirmation of supervisor Affirmation of head of school

CONTENTS

NOMENCLATURE AND ABBREVIATION

A	Area (m^2)
C_p	Specific heat of air (J kg^{-1} °C^{-1})
d.b.	Dry basis
D_{eff}	Moisture diffusivity (m s^{-1})
Ex	Exergy (W)
F_R	Heat removal factor
g	Acceleration due to gravity (m s^{-2})
H	Height (m)
h_e	Effective heat transfer coefficient between the absorber and moving air ($Wm^{-2}K^{-1}$)
h_{fg}	Latent heat of vaporization (J kg^{-1})
h_{fp}	Heat transfer coefficient between air and absorber plate ($Wm^{-2}K^{-1}$)
h_r	Radiative heat transfer coefficient ($Wm^{-2}K^{-1}$)
I_b	Hourly beam radiation (W m^{-2})
I_d	Hourly diffuse radiation (W m^{-2})
I_g	Hourly global radiation (W m^{-2})
I_0	Extra-terrestrial radiation (W m^{-2})
I_T	Instantaneous global solar irradiance (W m^{-2})
m	Mass (kg)
$\dot{m}$	Mass flow rate (kg s^{-1})
MC	Moisture content (%)
Nu	Nusselt number
P	Pressure (Pa)
Pr	Prandtl number
Ra	Rayleigh number
Q	Heat gain (W)
r_b	Tilt factor for beam radiation
r_d	Tilt factor for diffuse radiation
r_r	Tilt factor for reflected radiation
S	Flux absorbed in the absorber plate (W m^{-2})
SEC	Specific energy consumption (kWh kg^{-1})
S_{cs}	Solar constant (W m^{-2})
t	Time (s), air gap thickness (mm)
T	Temperature (°C)
U_0	Overall heat loss coefficient ($Wm^{-2}K^{-1}$)
V_w	Wind velocity (m s^{-1})
w.b.	Wet basis

Greek symbols

α	Absorptance of the collector absorber plate
$\acute{\alpha}$	Thermal diffusivity (m^2 s^{-1})
β	Collector tilt angle (°)
β'	Thermal expansion coefficient (K^{-1})
δ	Declination angle (°)
Δ	Change

ε	Emissivity
η	Efficiency
θ_z	Zenith angle (°)
λ	Thermal conductivity (W $m^{-1}K^{-1}$)
μ	Dynamic viscosity (kg $m^{-1}s^{-1}$)
ν	Kinematic viscosity (m^2 s^{-1})
ρ	Density (kg m^{-3})
σ	Stefan-Boltzmann constant (W $m^{-2}K^{-4}$)
τ	Transmissivity of the glass cover
$(\overline{\tau\alpha})$	Effective transmissivity–absorptivity product
Φ	Latitude (°)
ψ	Azimuth angle (°)
ω	Hour angle (°)

Subscripts

a	Ambient, air
c	Collector
ch	Solar chimney
cha	Drying chamber
d	Drying
f	Fluid, final
g	Glass
h	Horizontal surface
i	Inlet/initial
o	Outlet, overall
p	Absorber plate, apple
s	Sky
u	Useful
w	Water
I	Relates to 1st law of thermodynamics
II	Relates to 2nd law of thermodynamics

Abbreviations

DSD	Direct type solar dryer
ISD	Indirect type solar dryer
MSD	Mixed type solar dryer
OSD	Open sun dryer
SAC	Solar air collector
SC	Solar chimney

1. INTRODUCTION, OBJECTIVES

The research work's background and significance, as well as the main research goals, are discussed in this chapter.

1.1. Introduction

The demand for energy has increased due to fast world population growth and economic development. The majority of energy is produced from non-renewable sources, such as fossil fuels like coal, oil, and gas, which supply about 80% of the world's energy and will run out completely within a century or so (Bentley, 2002). Besides, using fossil fuels to generate heat and electricity poses several risks to human health and ecosystems. As reported by Soeder (2021), fossil fuels and industry accounted for 89% of global CO_2 emissions. In addition, there is a serious energy crisis that is currently affecting the global economy. The crisis has brought attention to the necessity of energy resiliency and a push toward renewable energy source. Solar energy is a limitless resource with the potential to meet a significant portion of the world's future energy demands. It is one of the most promising sources of energy alternative, particularly for low-temperature applications like solar dryers. Solar dryers are one of the most cost-effective ways to guarantee food security and are suited for farmers in both developing and developed countries (Zarezade and Mostafaeipour, 2016). According to Prakash et al. (2016) report, the use of solar drying technique cut conventional energy consumption by up to 27–80% and reduces the CO_2 emissions.

Agricultural product drying is important for preserving and extending the shelf-life of the product after harvesting by reducing the moisture content to an acceptable level, which is usually between 10–20% (Eltawil et al., 2018). According to Chakraverty report in 2003, 20% of the world's perishable agricultural products are dried to increase their shelf-life and promote food security. As a result, with advancements in drying operation conditions and product quality, drying research remains a vital topic. Moreover, harnessing solar energy is a viable strategy in order to meet the technical, economic and environmental demands posed by the drying process (Farkas, 2011).

Numerous designs of solar dryers have been described in the literature, and they are categorized based on the airflow mechanism and heat transfer mode as forced or natural convection dryers (Singh and Kumar, 2012; Matavel et al., 2021). Natural type solar dryers are cheaper than forced type dryers due to the absence of external driving mechanisms such as fans and blowers. However, it has been reported that their ineffective performance is caused by a low air flow rate (Ekechukwu and Norton, 1997). Their drying effectiveness typically ranges from 20 to 40% (Udomkun et al., 2020). Single pass solar air collectors (SAC) are best suited for natural type solar dryers (Bassey, 1986) which have the lowest efficiency compared to other types of solar air collector due to their poor heat transfer coefficient. Numerous studies have been conducted to enhance the heat transfer rate of the SAC of indirect solar dryers including adding fins, baffles, wire mesh etc... to the absorber plate to create artificial roughness. However, the cost of fabrication is higher. Utilizing a solar chimney, which increases the system's air flow rate, is another method of enhancing the effectiveness of these dryers (Forson et al., 2007;

Afriyie et al. 2009). Solar chimney is one of the buoyancy-based technologies that heats air by using the greenhouse effect generated by solar radiation.

1.2. Objectives

According to a survey of the available literature, a minimal experimental work has addressed the effect of the solar chimney particularly on the performance of natural convection indirect type solar dryers (ISD). To the best of our knowledge, there has no experimental work on ISD that use solar chimney with different chimney gaps and chimney heights to improve the air flow rate, which enhances the performance of the ISD. The lack of reliable experimental investigations for both theoretical and modeling studies is a major issue. In this work, seven detachable solar chimneys were introduced with cardboard absorber plate and an aluminum fin. Therefore, the present work is focused on improving the ISD performance through experimentation. The detailed research objectives are as follows:

- To study the effect of solar radiation and ambient temperature on the performance of ISD.
- To examine the effect of the type of solar chimney (SC) height and air gap thickness on temperature rise and air flow rate of the dryer under both no-load and load conditions.
- To change the SC's stack height and air gap thickness, then evaluate how these changes affect the dryer unit's energy efficiency (energy and exergy analysis).
- To estimate moisture loss of dried product (apple slices) using proposed SC designs and compare them with the conventional dryer and open sun drying (OSD).
- To investigate and compare the effect of types of SC on energy consumption and drying efficiency.
- To perform experiments in order to compare the collected data and recommend the optimum arrangement for achieving the highest level of performance.

The following is a breakdown of the thesis's structure. The motivations for using solar dryers are discussed in chapter 1 as well as the study's main objectives. The literature review in chapter 2 presents research papers that are relevant to the thesis topic and finds out the research gaps. The experimental setup of the ISD with solar chimney integrated on it, the equipment used to collect data, and the theoretical model of the proposed solar chimney design are all detailed in Chapter 3. The experimental results from various chimney layouts are presented in Chapter 4. The data acquired on several days of the trials is displayed in figures and thoroughly explained. The thesis statements, as well as new scientific findings, are also presented here. Chapter 5 presents the main conclusions and recommendations, as well as future work.

2. LITERATURE REVIEW

This chapter provides a full overview of various types of solar dryers used in food applications, including fundamental drying concepts, solar drying system classification, and highlighting their performance in terms of drying kinetics, energy, exergy, and end-product quality. Recent advancements in this field have been thoroughly investigated, and a research gap has been identified.

2.1. Concepts of drying and theory

The fundamentals of drying, such as drying mechanisms, drying rates, drying kinetics, and dryer performance indicators, are covered in this section.

2.1.1. Fundamental concepts of drying

Drying is a food preservation technique that involves removing water from food to avoid bacterial growth, which accounts for more than a quarter of the energy needed in the food industry (Mohana et al., 2020). Therefore, the fundamental principle of a solar dryer is to lower product moisture content to a level that prevents spoilage while also reducing product weight for easier storage and transportation (Jangam, 2011; Belessiotis and Delyannis, 2011; Sangamithra et al., 2014). The agricultural product's moisture content is expressed on either a wet or dry basis, and the percentage of moisture content varies by product (Stiling et al., 2012; Kumar et al., 2014; Kumar et al., 2016). The basic knowledge that governs the drying process will enable a better understanding of any solar dryer (Ekechukwu, 1999; Morgan et al., 2006). Fig. 2.1 shows a schematic that describes the general principle of a solar dryer.

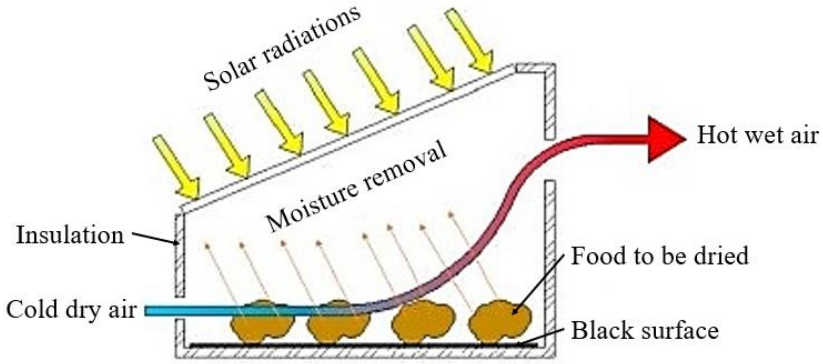

Fig. 2.1. Principle of the solar dryer (El Hage et al., 2018)

In most cases, drying is accomplished by the vaporization of water that is contained in the food. There are two important processes which are encountered in the unit of operation of drying (Shringi et al., 2014; Chauhan et al., 2015):

1) The heat transfer that is required to provide the latent heat of vaporization.
2) The water vapor passes through the food product and then away from it, affecting water separation from the product.

The conversion of liquid water into vapor consumes most of the energy utilized for drying. Heat is transmitted to the food item during the drying process by conduction, convection, or radiation to evaporate the moisture present on the surface of the food Fig. 2.2. Internal moisture

migration to the drying surface, on the other hand, occurs simultaneously. Evaporation process is accelerated by the heat given by the drying air. Diffusion, which is considered the principal mechanism in drying, also occurs when water molecules move from higher to lower concentrations (Kumar and Sharma, 2022). Depending on the food product, the safe moisture content value varies. Table 2.1 shows the level of permissible moisture content for various items along with their maximum allowable temperature during the drying process (Sharma et al., 2009).

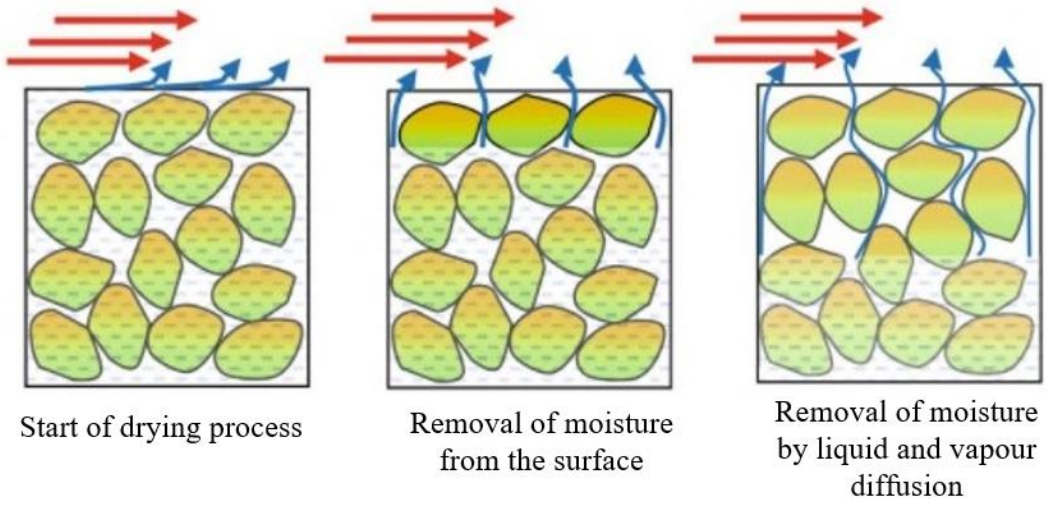

Fig. 2.2. Moisture distribution during food drying

Table 2.1. Initial and final *MC* and maximum allowable temperature for drying some crops

Crop	**Initial MC (% w.b.)**	**Final MC (% w.b.)**	**Maximum temperature (°C)**
Potato	75-83	13	75
Apple	80	24	70
Banana	80	15	70
Tomato	96	10	60
Carrot	70	5	75
Apricot	85	18	65

Psychrometry (Appendix A3) is significant in the study of drying phenomena because it refers to the properties of the air-vapor mixture that govern the drying rate. Psychrometric charts are made in orthogonal coordinates, with temperature as the abscissa and humidity as the ordinate and are most typically used to determine air humidity based on wet and dry bulb temperatures (Kumar and Sharma, 2022). The temperature and rate at which liquid vaporizes depends on the vapor concentration in the surrounding atmosphere when appropriate heat is provided for drying operations. Although direct computer calculations have replaced psychrometric charts in big convectional drying systems, their use in small and medium drying systems remains a rapid and reliable estimation and check.

2.1.2. Drying theory

The rate of drying is critical in terms of both engineering and economics, as it defines the dryer's production capacity. Due to the hygroscopic nature of agricultural products, controlling the drying rate is crucial. Drying is a process in which heat and mass are transferred simultaneously within the product as well as between the material's surface and the surrounding medium. Heat is necessary to evaporate the moisture that is removed from the drying product surface by the external drying medium, usually air. Several biological, products, when drying as single particles under constant external conditions, exhibit a constant rate of moisture loss during the initial drying period, followed by a falling rate drying period.

The drying period, which is governed by the temperature and moisture content of the product, as well as the relative humidity and velocity of the drying air, is the most significant metric to consider when evaluating a dryer. Agricultural products are dried in two distinct stages after a warm-up preheating time: constant-rate evaporation period followed by a falling-rate drying period, both of which have an impact on the overall drying process (Özbek and Dadali, 2007; Babu et al., 2018).

The rate of drying during a constant rate drying period is determined by external variables such as temperature, humidity, and airflow. The rate of drying during the falling-rate drying stage, on the other hand, is controlled by the internal flow of liquid. The rate of fall is mostly determined by the type of product, and it entails moisture transfer from within the product to the surface via liquid diffusion, as well as moisture removal from the surface (Hussain et al., 2021). Drying of most high moisture items, such as fruits and vegetables, the falling rate further divided into two stages: first falling rate, and second falling rate. Fig. 2.3 depicts a possible depiction of the various stages of drying.

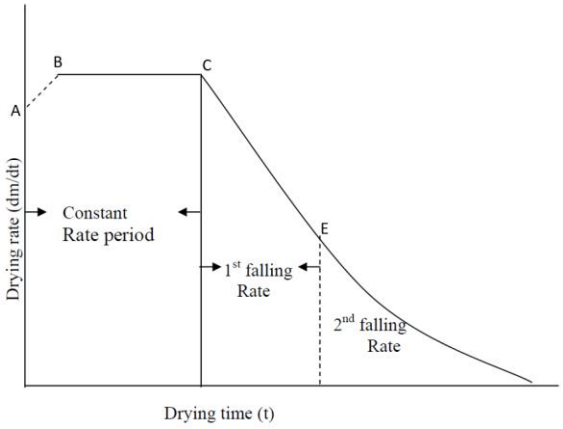

Fig. 2.3. Drying rate curve (Belessiotis and Delyannis, 2011)

The rate of moisture migration from the inside of the product to the surface is sufficiently high in the early stages of drying to keep the surface totally wetted. The rate of drying is controlled at this stage by the rate of evaporation from the surface, which is controlled by the condition of air adjacent to the surface. This results in a constant rate drying period as portion *BC* of the curve shown in the Fig. 2.3. The critical moisture content is the point at which the drying rate begins to drop (point C), and it is a function of the type of product and product thickness (Yaciuk, 1982). The rate of drying reduces below the critical moisture content, eventually

reaching zero at the equilibrium moisture content. When the critical moisture content is reached, the constant rate period ends, and the falling rate period *CE* begins.

In general, agricultural products are placed in drying chambers in two ways namely: thin layer and deep bed drying. In thin layer drying, the product depth is limited to 200 mm where the rate of drying is proportional to the difference between the vapor pressure of moisture in the dried product and vapor pressure of moisture in the drying air. In deep layer drying however, the depth of grain is more than 200 mm, and the rate of moisture removal is maximum for the bottom layer and decreases exponentially for subsequent layer (Sekyere et al., 2016). Fruit, vegetables, and sliced fruits should be dried in thin layers, whereas grains should be dried in a deep bed layer.

2.1.2.1. Thin layer drying

The behavior of the product while drying is completely dependent on drying process. Airflow rate, air temperature, initial moisture content of product, and product thickness are a factor that can affect the drying behavior of the product. Cutting the apple into a thin layer had the greatest impact on drying rate followed by drying air temperature, initial moisture content, and relative humidity, with air velocity having the least impact (Doymaz, 2009). Thin layer drying modeling has been used to forecast the drying performance of a variety of agriculture products based on the assumption that drying rate is only determined by the product size, airflow rate, drying air and product initial moisture content (Da Silva et al., 2014; Odewole and Falua, 2021).

The drying process for various agricultural goods has been described using a variety of models: theoretical, semi-theoretical, and empirical equations. Ertekin and Firat (2017) conducted a detailed evaluation of over 100 semi-theoretical and empirical thin layer drying models utilized in agricultural products, evaluating the statistical criteria for selecting the appropriate model. They are generally based on the premise that the air to crop volume ratio is extremely large. When this assumption is taken into account, the drying rate is solely determined by the qualities of the material to be dried, its size, the drying air temperature, and the moisture content.

In the literature, the thin layer drying of an agricultural product is often described by two basic types of models: empirical models and diffusion models. Empirical models are useful not just for describing thin layer water removal, but also for describing heat penetration when hot air is used. Empirical models have been tested on a variety of vegetables and fruits by several researchers, such as pumpkins, green peppers, green beans, and onions (Yaldýz and Ertekýn, 2001), apples, figs, seedless grapes, green peas, tomatoes and onions (El-Sebaii et al., 2002), grapes (Belessiotis and Delyannis, 2011), fenugreek leaves (Sunil et al., 2014), fresh pineapple (Bena and Fuller, 2002), sliced bitter gourd (Vijayan et al., 2016), banana (Lingayat et al., 2017), cashew (Dhanushkodi et al., 2017).

Surface diffusion on the pore surfaces and liquid diffusion due to capillary action are the two mechanisms for drying agricultural products (Chasiotis et al., 2021). Liquid diffusion, however, is the dominant mechanism due to the mass transfer process, which is driven by the removal of moisture from the product. The moisture contents were expressed on dry basis, which makes modeling more convenient. The most widely used theoretical models to describe

the mass and heat diffusion is derived from Fick's second law of diffusion (Kucuk et al., 2014). The diffusion equation governs heating in this scenario, which includes the drying rate in the energy balance, which can be estimated using an empirical model. A list of some drying kinetics models used for fruits and vegetables are presented in Table 2.2.

Table 2.2. Thin layer models to describe drying kinetics

Model name	Empirical expression	Reference
Lewis	$\mathrm{MR} = \exp(-\mathrm{kt})$	(Lewis, 1921)
Modified Page	$\mathrm{MR} = \exp(-\mathrm{kt})^{\mathrm{n}}$	(Page, 1949)
Logarithmic	$\mathrm{MR} = \mathrm{a}\exp(-\mathrm{kt}) + \mathrm{c}$	(Ali et., 2016)
Wang and Singh	$\mathrm{MR} = 1 + \mathrm{at} + \mathrm{b}t^2$	(Wang and Singh, 1978)
Midilli Kucuk	$\mathrm{MR} = \mathrm{a}\exp(-\mathrm{kt}^{\mathrm{n}}) + \mathrm{bt}$	(Midilli et al., 2002)
Weibull	$\mathrm{MR} = \exp\left(-\left(t/a\right)^{b}\right)$	(Corzo et al., 2008)
Verma et al	$\mathrm{MR} = \mathrm{a}\exp(-\mathrm{kt}) + (1-\mathrm{a})\exp(-\mathrm{gt})$	(Demir et al., 2007)

Several kinetics drying models were employed in many literatures for modeling fruit drying. However, those listed in Table 2.2 are the most frequently used to describe drying of different agricultural products. Various authors have studied the modeling of the product drying process, e.g., drying of bitter gourd (Vijayan et al., 2016), tomato slices (Samimi et al., 2016), apricot (Zhang et al., 2016). Noori et al. (2021) performed a thin layer modelling on apple slices and found that out of 11 thin layer models the Page, approximation diffusion, Verma et al and Midilli and Kacuk models were the best fitting that describe apple slices.

2.1.2.2. Deep bed drying

In deep-bed drying, all the grains in the dryer are not fully exposed to the same condition of drying air, which at any point in the product mass changes with time and with the depth of the product bed. Fig. 2.4 presents a schematic illustration of deep bed drying, where drying takes place in zones (Belessiotis and Delyannis, 2011). Mostly, drying is performed in a "drying zone" which moves through the grain in the direction of air movement. Evaporation cools the air as it moves up to the upper zones, increasing moisture content. As a result, between the lower and upper zones, a temperature and relative humidity gradient is generated, which is a measure of the drying rate. The air flow rate, drying air temperature, and the depth of the bed are all important drying parameters. The recommended thickness of each layer is only 0.45 m or less if the heated air at temperatures ~45 °C is employed. The free flow of air through the drying bed is caused by a pressure drop across it, resulting from the difference between the densities of relatively cool ambient air and the warm air inside the dryer (Sekyere et al., 2016).

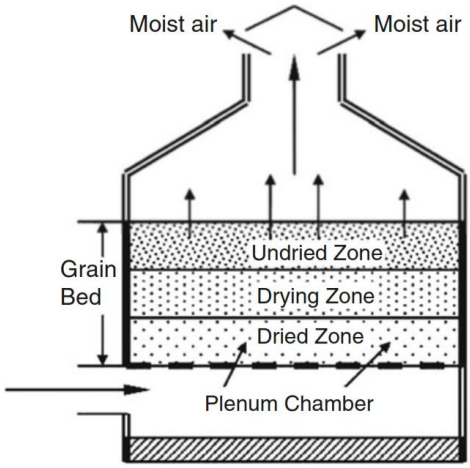

Fig. 2.4. Schematic illustration of deep bed drying zones

2.2. Classification of the solar drying system

The first idea of the solar dryer was developed to avoid open sun drying problems by Everitt (1980) which was a box-shaped housing unit having a transparent sunlight cover to overcome the deficiencies of open sun drying (OSD). Many solar dryers have been developed over the last two decades for drying various products efficiently by utilizing the solar energy, and their selection should take into account the available insolation rate in the target region, the type of product to be dried, and operational and investment costs. Several researchers presented an overview of various designs, construction, and operational principles of a wide variety of solar-assisted solar dryer systems (Chaudhari and Salve, 2014; Chauhan et al., 2015; Vijayavenkataraman et al., 2012). According to Mujumdar and Law (2010), out of 500 different types of dryers, about 100 are commercially used whereas (Fudholi et al., 2010), highlighted several solar driers and their potential costs for local production.

A thorough examination of the design, development, and performance assessment of various types of solar dryers has been presented by Kumar et al. (2016), whereas Chauhan and Rathod (2020) were also defined briefly in terms of their technological, economic, and physical features. A review of solar drying was presented by El-Hage et al, (2018). The authors investigated the latest trend on solar dryer development, classifications, parameters that affects the performance of solar drying, and limitations of such technology. Besides, economic, and environmental studies were conducted for the Lebanese case to determine the payback period and CO_2 reduction. Method of airflow and the utilization of solar energy is used to classify solar drying systems. The dryers are classified as active type and passive type solar dryers based on the airflow method as shown in Fig. 2.5.

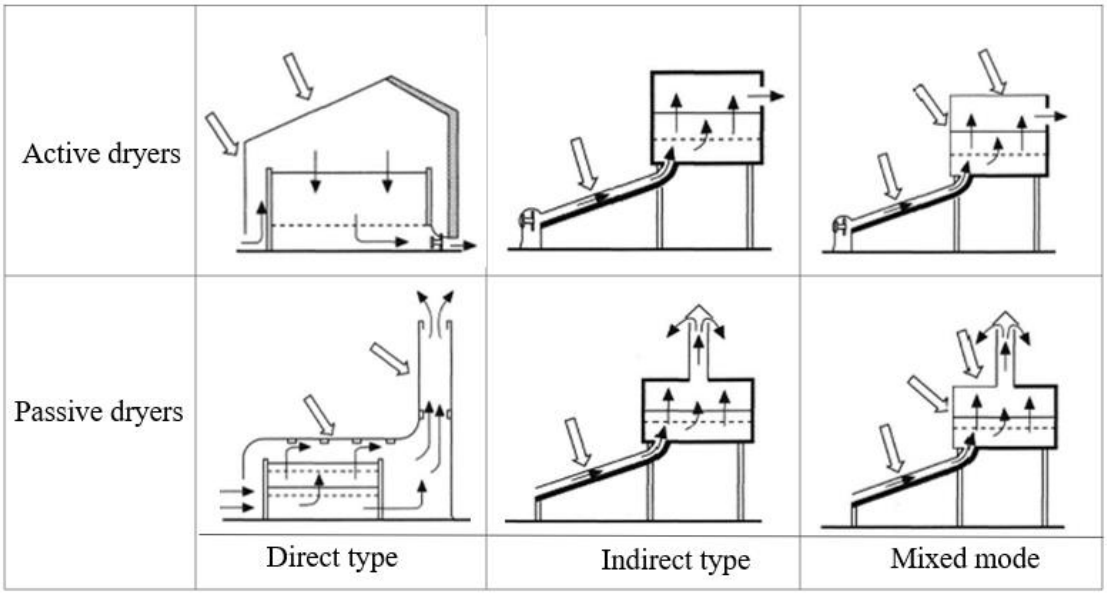

Fig. 2.5. Typical solar dryer designs (Ekechukwu and Norton, 1999)

Active solar dryers required fans to duct air through the dryer components which can be mounted either at the inlet or at the exit of the solar collector, but it is operated either by an electricity/ photovoltaic (PV) module. In terms of efficiency, active solar dryers are higher efficient than passive ones. This is because of the airflow rate in the active mode dryer. On the other hand, the collector outlet temperature is higher for passive mode than active mode (Khama et al., 2016). A controlled blower, forced convention, should provide a required amount of airflow through the dryer system (Gulcimen et al., 2016). The primary goal of a blower is to keep the proper airflow rate in the drying system, resulting in homogeneous moisture evaporation from the product (Ghatrehsamani and Zomorodian, 2012). The first step in the design of a blower system is the calculation of the quantity of the air to be handled and the amount of heat, which must be imparted to it (Saxena et al., 2015). Some designs have tended to locate the fan between the air heater and the drying chamber. This keeps the collector under negative pressure, ensuring that all air leakages and the additional heat generated by the fan are in the system.

Passive solar dryers (natural convection) depend on the natural movement of air due to buoyancy force, wind pressure difference, or combination of them and need minimum expenditure for controlling the drying temperature. However, its drying rate is limited. The presence of a chimney has in the passive convective solar dryer can improve the airflow rate of the dryer. Mathematical and experimental methodologies were employed in several studies to increase airflow by introducing varied sizes and shapes of chimneys (Chung et al., 2015; Ekechukwu and Norton, 1998; Ferreira et al., 2008; Sudprasert et al., 2016; Tan and Wong, 2013).

According to the utilization of solar energy, the drying system is also divided into two categories: uncontrolled (OSD) and controlled solar drying as illustrated in Fig. 2.6. The controlled sun drying systems further divided into: direct type (DSD), indirect type (ISD), and mixed-mode type solar dryers (MSD).

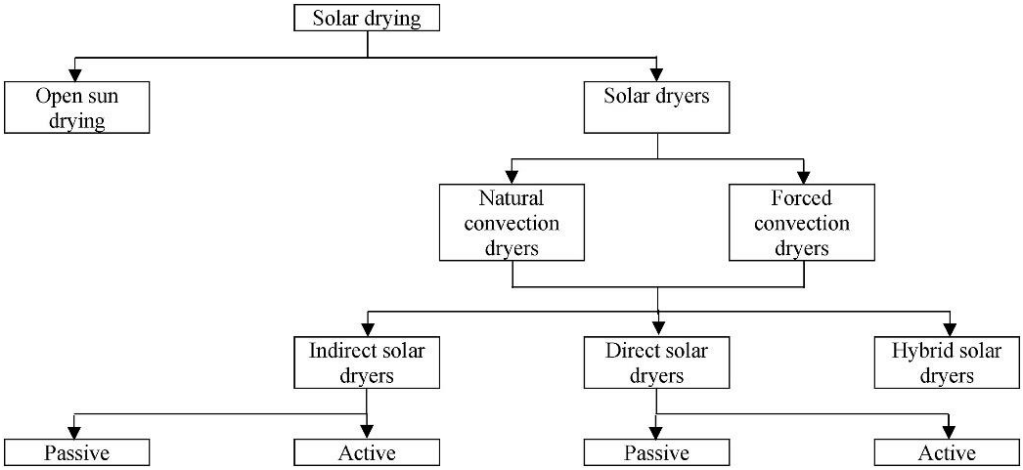

Fig. 2.6. Broad classification of solar dryers (Udomkun et al., 2020)

Mustayen et al. (2014) investigated the drying potential of direct, indirect, mixed-mode, passive convection, and active convection solar dryers in drying agricultural products in tropical and subtropical countries. they concluded that the passive convection dryers are more advantageous and practical than other types. The thermal performance of direct, indirect, and mixed mode passive solar dryers was evaluated experimentally under no load conditions (Mahapatra and Tripathy, 2019). For comparison purposes, the efficiency and convective heat transfer coefficient between the absorber and moving air were determined. Their research revealed that the efficiency of direct, indirect, and mixed mode dryers was determined to be 31.40, 27.55, and 41.43%, respectively, while the corresponding average convective heat transfer coefficients were 16.31, 14.92, and 23.81 $Wm^{-2}°C^{-1}$.

2.2.1. Open sun drying

Open sun drying (OSD) has been the technique of choice for food preservation. During the time of drying process, it does not require any additional energy sources, Furthermore, the use of skilled labor is not required. This type of dryer has the least expensive and most appropriate drying method for rural areas (Vengsungnle et al., 2020). However, it has some restrictions and drawbacks, such as the possibility of dust and insect contamination of the product. The amount of solar energy absorbed at the product surface raises the product temperature, resulting in the emission of long wavelength radiation and convective heat loss when drying in the open sun. The mass transfer of moisture from the surface of the product to the ambient air during drying dependent on the rate at which moisture diffuses to the surface, which varies depending on the product type (Tomar et al., 2017).

2.2.2. Direct type solar dryers

In direct-type solar dryers (DSD), the product to be dried is directly exposed to solar radiation with or without natural air circulation (Ekechukwu and Norton, 1999). The basic design of a direct mode dryer is an enclosure with a transparent glass cover (Sharma et al., 2009). When compared to other types of dryers, this kind of dryer does not require an air preheater and is easy to construct, economical, and low maintenance. Drying small amounts of crops, fruits, and vegetables is more efficient using DSD. Fig. 2.7 shows a schematic representation of a

DSD. The moisture in the product is eliminated due to the heat generated by solar radiation absorption within the items and on the enclosure's surface. However, as compared to other types of dryers, DSD has low efficiency due to the lack of an air preheater and uncontrolled heat inside the chamber.

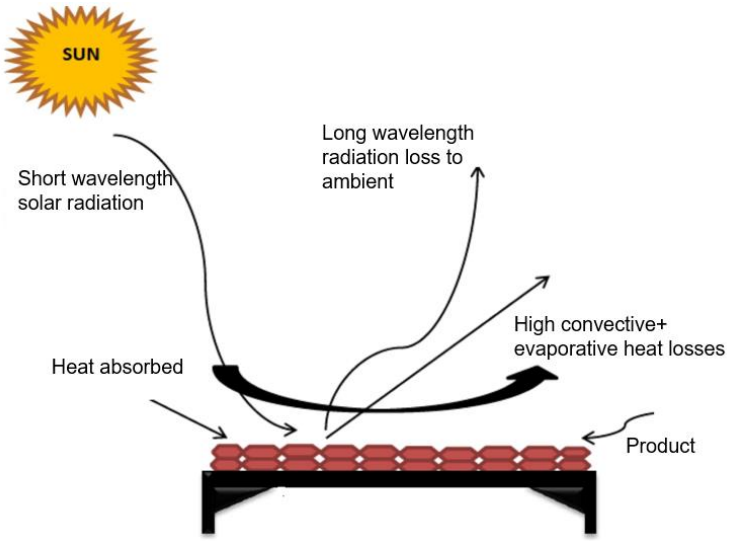

Fig. 2.7. Schematic diagram of direct solar drying (Bhardwaj et al., 2021)

Several studies have been conducted on the improvement of such type dryers. Bena and Fuller (2002), combined a direct convection solar dryer with biomass burner to dry fruit and vegetables. They reported that the overall efficiency of the unit was 9% with a capacity of 20-24 kg fresh pineapple arranged in a single layer of 0.01 m thick slices.

The dryer's airflow rate can be improved by adding a chimney to the top of the drying cabinet. Afriyie et al. (2009) conducted three trials on a direct passive solar crop dryer, one with a standard chimney, one with a solar chimney, and one with the roof of the drying chamber tilted to form a tent dryer. The temperatures at similar heights in the solar chimney were much higher than in the normal chimney. The roof that is more inclined toward the vertical plane leads to an increased airflow under no-load trials Fig. 2.8. This explains that tent dryers perform better than cabinet dryers of the same loading capacity under similar environmental conditions. In their conclusion, such dryer performed very well in an atmosphere of low humidity and thus it is location specific.

Afriyie and Bart-Plange (2012) performed experimental investigation on chimney-dependent direct solar crop dryer for different inlet areas with a fixed outlet area. In their experimental setup, three-chamber roof angles of 81°, 64°, and 51° to vertical plane were constructed. In addition, three different inlet designs with inlet gaps of 70, 50, and 300 mm were built. The chimney had a rectangular cross-section with a width of 440 mm, a uniform gap of 80 mm, and a height of 625 mm. Three sides of the solar chimney walls were glazed, and the fourth wall was made of a wooden board, with an inner surface painted black as shown in Fig. 2.8. The result showed that a high inlet gap for a given exit gap can result in a high mass flow rate. This can also be used in conjunction with a solar chimney and a proper drying chamber roof angle.

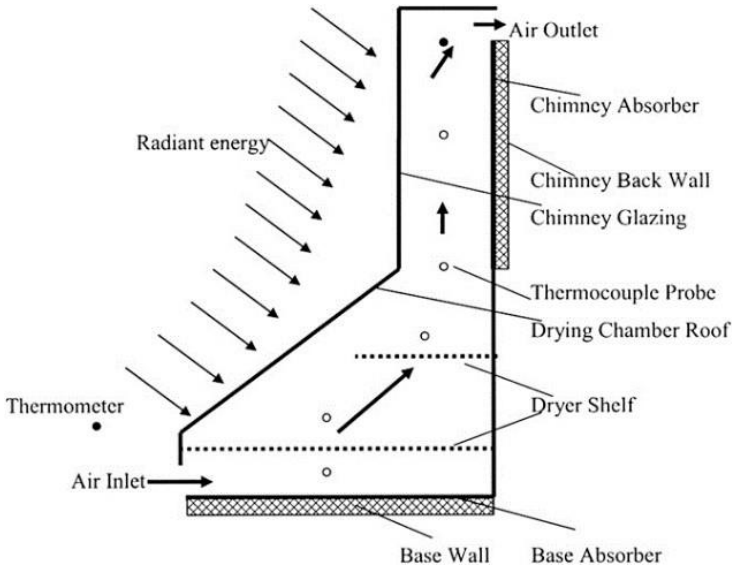

Fig. 2.8. Chimney dependent direct mode solar crop dryer (Afriyie et., 2009)

2.2.3. Indirect type solar dryers

Indirect (distributed type) solar drying (ISD) is the latest technique of drying. This type of dryer is useful for drying fruits and vegetables in rural areas. The ISD is made up of a solar collector, drying chamber a fan (active type) or a chimney (passive type). It has an advantage over DSD in terms of managing drying temperature, air velocity, and product loading. Furthermore, it protects product quality by avoiding direct sunlight exposure. This is due to the air being heated separately in a device known as a solar air collector. The ambient air is heated using a solar air collector. The warm air is then ducted to the drying chamber, where it transfers heat and evaporates moisture from the material.

The indirect type of solar dryers was reviewed and compared to other types of dryers, as well as open sun drying and numerous design modifications were performed (Phadke et al., 2015). The authors discussed the comparison of various technologies of indirect solar dryers to direct solar dryers and to one another. New ways for increasing the efficiency of solar dryers have also been implemented. Different designs, construction details, and performance evaluation of the ISD were also reported by Lingayat et al. (2020b).

Farkas (2008) developed an indirect type forced convection solar drying. A PV panel with a maximum power: 2 x 20 W was installed in the front side of the dryer with a changeable elevation angle that suitable for different sunshine angle throughout the year as shown in Fig. 2.9. Several types of fruits were tested using this dryer. The influence of various drying parameters on solar air collectors, particularly air flow rate, was investigated, as well as the calculation efficiency. An indirect type of solar dryer was developed to evaluate dryer performance under both natural and forced convection for drying tomatoes (Gupta et al., 2012). The dryer consists of a flat plate solar collector and drying chamber with three trays. The average drying temperature reached 45 °C in natural and 40 °C in forced convection and the mass flow rates of 0.00653 and 0.014 kg/s were found for natural and forced convection respectively. The overall efficiency of the drying chamber was 17% and the efficiency of the collector was found to be 30%.

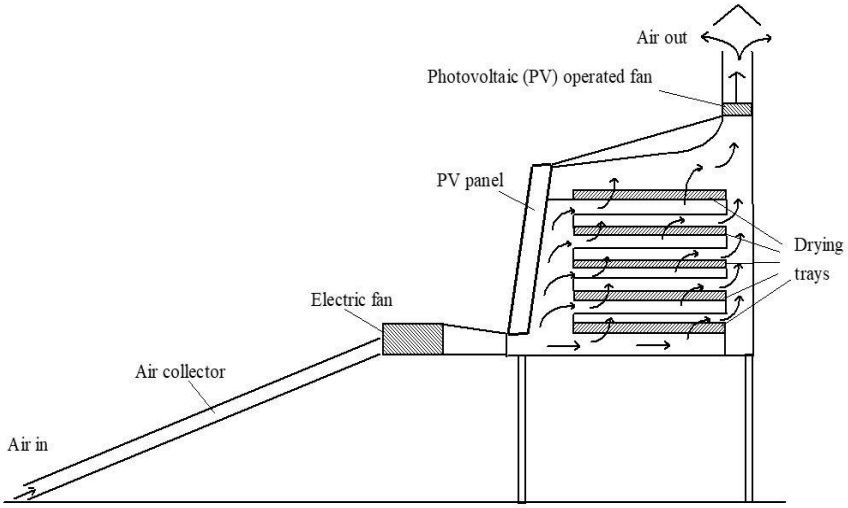

Fig. 2.9. Schematic diagram of the indirect solar dryer (Fakas, 2008)

Sreekumar et al. (2008) have constructed and tested an efficient and cost-effective solar dryer for drying vegetables (bitter gourd). The product was loaded beneath the absorber plate, which prevented the problem of discoloration due to direct exposure to solar radiation Fig. 2.10. The solar dryer was put through three different tests: no-load with the axial fans turned off, no-load with the axial fans turned on, and axial fans turned on with the load. The dryer absorber plate attained a temperature of 97.2 °C and the maximum air temperature was 78.1 °C under no-load conditions. The payback period was calculated as 3.26 years.

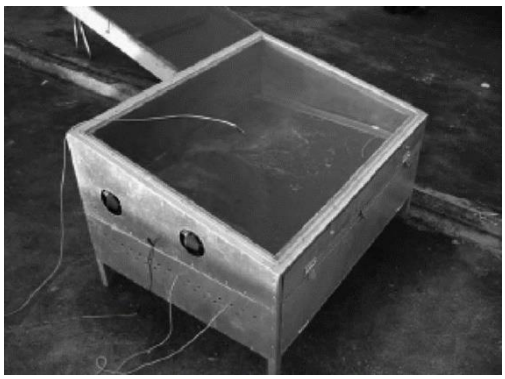

Fig. 2.10. An illustration of the photograph of the solar dryer (Sreekumar et al., 2008)

Dissa et al. (2009) performed a simulation on a thin layer indirect solar drying system and validated it experimentally. The system has a solar collector, drying unit, chimney (PVC material) with 0.25 m long and 0.12 m diameter and is used to dry mango slices as provided in Fig. 2.11. The products were placed on four rectangular trays with 81 mm by 44 mm dimensions. Each tray was constructed of a wooden frame and separated 20 mm from each other. The experiments have been done during the harvesting time of mangoes. It was observed that drying rates were reached a maximum value of 0.18 g kg^{-1} s^{-1} on the first day, 0.13 g kg^{-1} s^{-1}, and 0.04 g kg^{-1} s^{-1} on the second and third day respectively.

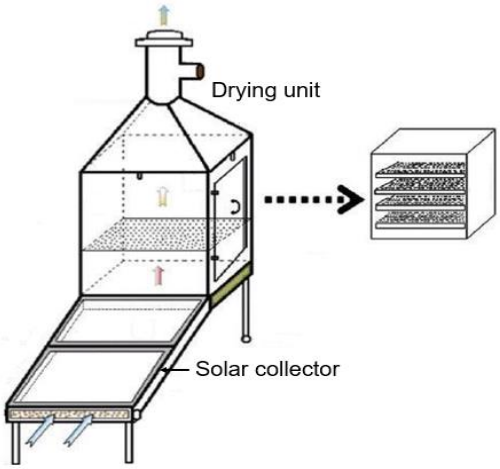

Fig. 2.11. Prototype of the indirect solar dryer (Dissa et al., 2009)

Bolaji (2005) developed and evaluated the performance of an indirect solar dryer using a box-type absorber collector for crop drying. A solar air heater, an opaque crop bin, and a chimney make up the dryer as shown in Fig. 2.12. The heated air rises in the unit because the box-type absorber collector, which is formed of a glass transparent cover and a black absorber plate, is inclined at an angle of roughly 20° to the horizontal. The temperature inside the dryer was 15.3 °C higher than the ambient temperature throughout the day, according to the author, and the system's maximum efficiency was 60.5%, while flat plate absorber and fin-type absorber efficiency was 21 and 36%, respectively. He calculated that the maximum average temperature inside the collector and drying was 64 °C and 57 °C, respectively, whereas the maximum ambient temperature was 33.5 °C.

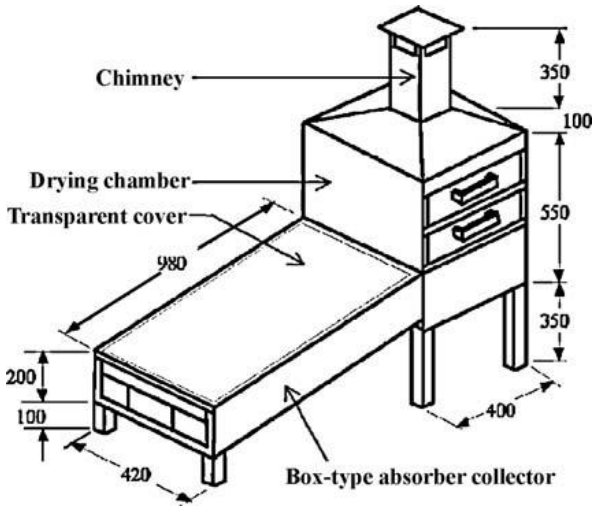

Fig. 2.12. Indirect natural convection solar dryer (Bolaji, 2005)

El-Sebaii et al. (2002) constructed and tested an indirect type of natural convection solar dryer under Tanta climate conditions as illustrated in Fig. 2.13. The system consists of a solar collector, drying chamber, storage material (the sand was used), and chimney. They experimented with drying various fruits with and without storage materials. They found that the maximum temperature is reaching about 60 °C in the drying chamber and that the storage material cut the drying time by 12 hrs.

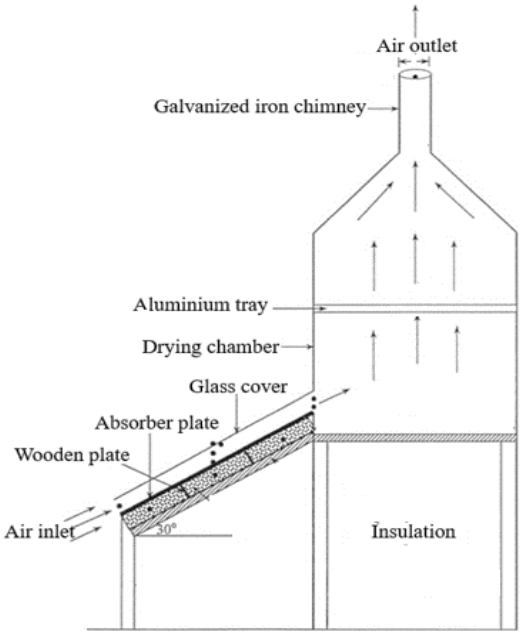

Fig. 2.13. Indirect type natural convection solar dryer (El-Sebaii et al., 2002)

Aissa et al. (2014) used an indirect solar dryer forced convection to dry sponge-cotton for five days in the ranges of 35 to 49 °C ambient air temperature, 35.2 to 69.8 °C drying air temperature, 30 to 1258 $W.m^{-2}$ solar radiation, and 0.016 to 0.08 kg/s air flow rate. The mass flow rate of air remained constant throughout each trial. A painted black cylindrical chimney, made from galvanized iron connected to the top of the drying chamber to increase the movement of airflow. The result showed the overall efficiency recorded between 1.85% and 18.6%. In addition, empirical correlations of temperature lapse and moisture ratio in the drying chamber are found to describe the drying curves of the sponge-cotton.

Mathematical modeling of indirect natural convection solar dryer was designed by Tashtosh et al. (2014) for drying dairy products in Jordan called Jameed. The dryer comprises a solar collector with proportions of 0.1 m in height, 0.8 m in width, and 1.2 m in length. The drying chamber consists of four trays separated equally from each other at a distance of 0.2 m and used to dry 4 kg of jameed, each tray holds 1 kg. The author also studied the effect of outlet air temperature and mass flow rate by varying the width or length of the solar collector. The result showed that the average collector efficiency was 37% and the maximum outlet temperature was recorded at 41 °C at 1 pm.

Experimental tests under natural convection were carried out by Hajar et al. (2017) to evaluate the thermal performance of the indirect solar dryer for drying pear. A solar air collector, a drying chamber, and a chimney makes up the solar dryer. The absorber plate was made of two corrugated aluminum sheets painted in matt blank paint. These corrugated plates were fixed to form parallel cylinders allowing air to circulate along with the collector. The drying chamber was fabricated from a wooden sheet and well insulated from all sides with glass wool of 5 mm thick to keep the drying chamber temperature always above the ambient temperature. The vertical chimney is made of aluminum of 700 mm in height. The experiment was carried out in April 2016. The result showed that a maximum outlet temperature of 57 °C under natural

convection can be reached. The average energy efficiency of the drying chamber was 11.11% and the drying took 24 hours to reduce the mass of the sample from 997.3 g to 135.13 g.

Khaldi et al. (2017) presented a mathematical model of an indirect solar dryer for improving airflow distribution and achieving a homogeneous temperature by adding a second air inlet to the drying chamber Fig. 2.14. Figs were chosen as drying fruit and placed in the two trays in the dryer chamber. The model was carried out for a typical day of August under the climatic conditions of Tlemcen (Algeria). The air heated by the absorber-1 flows towards the packed bed to warm up the gravel and then to dry the figs. The inclined chimney (35°) is placed on top of the cabinet composed of the glass cover, absorber-2 (aluminum), and heat storage material (granite).

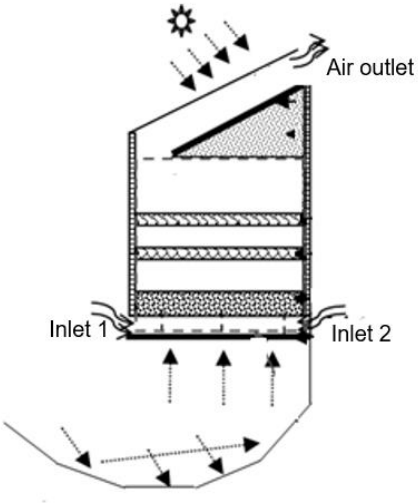

Fig. 2.14. Schematic view of the indirect solar dryer with two absorbers and a reflector (Khaldi et al., 2017)

When compared to a single inlet dryer, the results showed that employing two opposed inlets improves the drying process by lowering temperature fluctuation by about 67% and enhancing mass flow rate by about 18%.

Tedesco et al. (2019) designed and built an indirect passive solar dryer with chimney for apple drying. During the two days drying experiments, 2456 g of fresh apples were dehydrated, and 271 g of dehydrated apples remained after removing 89% of their moisture, requiring 32.78 MJ of sunlight energy. They also discovered that this type of solar dryer may function normally even under high relative humidity.

Lingayat et al. (2017) designed and developed an indirect solar dryer for drying banana slices. The dryer consists of a solar air heater, insulated drying chamber with four trays provided with chimney for exhaust air Fig. 2.15. The solar air heater consists of a V-shape corrugated (42 in number) absorber of 2 m^2 area was made from 0.4 mm thick copper sheet and painted black color. The result showed that the temperature of the air is the most important factor followed by the humidity of air and air velocity for improving the drying rate.

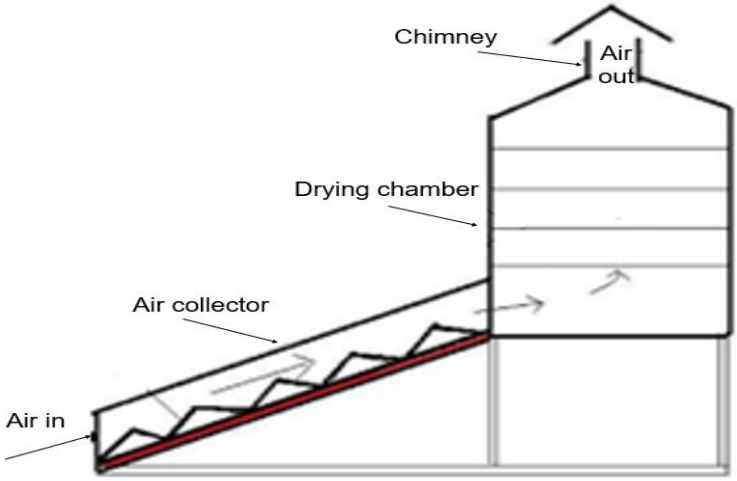

Fig. 2.15. Schematic view of the experimental setup

Vijayan et al. (2016) designed and investigated an indirect forced solar drying technique for bitter gourd using a sensible heat storage medium (Fig. 2.16). The effect of porous thermal storage and air mass flow rate was investigated using various drying models. The moisture content of the product from this method decreased from 92% to 9% in 7 hours, whereas open sun drying took 10 hours to achieve the same level. The average solar collector and drying efficiencies were both 22% and 19%, respectively. They suggested that drying in heat-sensitive storage was more uniform and resulted in a higher-quality output.

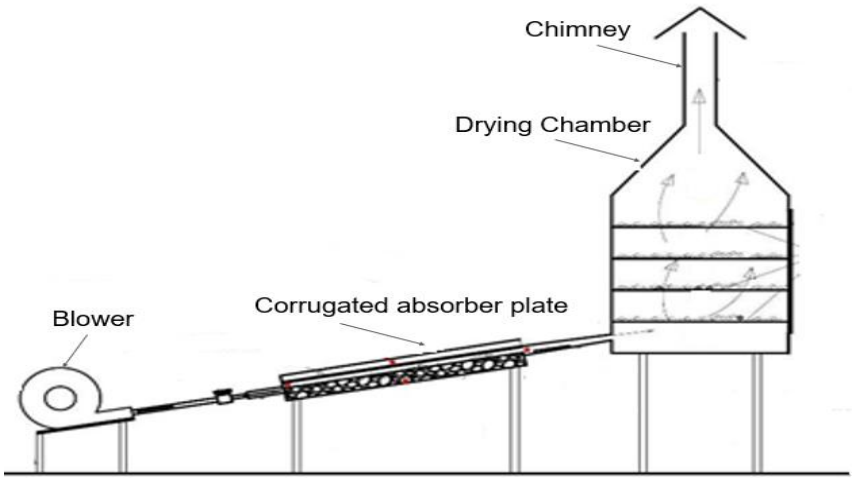

Fig. 2.16. Schematic view of the experimental setup (Vijayan et al., 2016)

2.2.4. Mixed-type solar dryers

Mixed type solar dryers (MSD) combine the basic characteristics of direct and indirect type solar dryers. The product to be dried is heated in two ways, through the direct absorption of solar radiation and the pre-heater air coming from the solar collector (El-Sebaii and Shalaby, 2012). Ayensu and Asiedu-Bondzie (1986) designed a mixed-mode passive solar dryer consisting of a solar air collector with heat storage, a drying chamber with three trays, and a

cylindrical chimney. The chimney of 300 mm diameter and 1.9 m height were made from matt black painted galvanized iron sheets fitted with a metal cap.

Simate (2003) developed and compared mixed-mode with indirect-mode natural convection solar dryers for drying maize. To optimize the dryers and compare their performance, the models were tested under varying solar conditions. The findings indicated that for the same grain capacity, the mixed-mode optimization yielded a shorter collector length than that of the indirect mode.

The Mixed mode convection solar crop dryer was designed and evaluated experimentally by Forson et al. (2007) in Kumasi, Ghana. This dryer consists of a primary collector (solar air collector) of collector area 42.4 m^2, a drying chamber, and a chimney. Sidewalls and top cover of the drying chamber were made transparent so that serve as a secondary collector. The dryer was used to dry a batch of cassava that weighed 160 kg by mass and had an initial moisture content of 67% (w.b.), which was reduced to 17% (w.b.) by removing 100 kg water. The drying efficiency was evaluated as 12.3% under load conditions with a drying time of 35.5 h.

Kumar et al. (2013) designed and constructed a low-cost mixed-type solar cabinet dryer. The dryer unit is intended for drying low moisture content food products such as pepper, turmeric, and cauliflower. The temperature inside the drying chamber was 77 °C during midday and an average of 64 °C to 66 °C on a full sunny day in the month of March-August. An experimental mixed-mode natural convection solar crop dryer with a backup heater was designed, constructed, and evaluated by Sekyere et al. (2016) to dry freshly pineapples under four distinct Scenarios for four typical seasons in Ghana (Fig. 2.17).

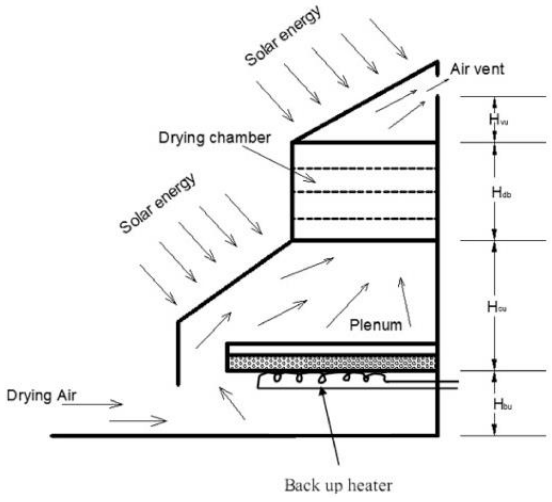

Fig. 2.17. Schematic illustration of mixed-type passive solar dryer

The dryer is designed to operate with solar radiation as the main source and a backup heater at night for continuous drying. The dryer reduces the moisture content of pineapple slices from about: 1) 1049% to 144% (d.b.) in 23 h; 2) 924% to 106% in solar drying with back up heater in 19 h; 3) 1049% to 184% only with backup heater in 10 h; 4) 912% to 155% in hybrid mode in 7 h for drying in scenarios. The average moisture pickup efficiency values obtained were 27%, 24%, 11% and 32% for scenarios 1, 2, 3, and 4, respectively.

Baniasadi et al. (2017) evaluated the performance of a mixed-mode solar drier with phase change material at the bottom of the drying chamber. They concluded that because of the improved performance of the solar collector, a continuous constant drying rate was obtained, and the solar dryer's energy efficiency was 11%.

2.3. Solar radiation intensity in Hungary

If one is considering installing a solar energy system (PV module or solar air collector), it is necessary to understand the fundamental features of solar radiation. Without this, it is impossible to determine what thermal opportunities solar radiation provides, as well as when and to what degree conventional energy sources can be replaced by solar collectors. For a given location, the cloud cover, the frequency of clear sky days, and the solar radiation that can be measured on the earth's surface are all determined by meteorological data gathered over many years. Hungary is between 45.8° and 48.6° north latitude in the northern temperate zone. According to data, annual average sunshine hours range between 1,900 and 2,200 hours, and the yearly amount of heat reaching the horizontal surface is 1,280 kWh/m^2/year (3.38 kWh/m^2/day) (Kafui et al., 2019), which is about 0.44 kWh/m^2/day less than the average world amount reported (3.82 kWh/m^2/day), making solar energy a cost-effective option for drying (Qasaimeh, 2012). The annual maximum amount of heat reaching the south-facing surface at 45° in Hungary is 1370 kWh/m^2 (Naplopo, 2014). For optimal annual energy production, the solar collectors have to be tilted to face south with a tilt angle equal to the geographical latitude (El-Sebaii et al., 2010; Zang et al., 2016). Rusirawan (2012) compared annual energy output to different surface orientations (collector tilt and azimuth angles). According to the author's findings, the maximum yearly power output can be achieved when the collector tilted angle is between 30-34° and the azimuth angle is 0° (true facing south). In terms of solar radiation, there are no notable differences between locations of Hungary. The sunniest part of the country is in the center and southern parts, while the north and west have the least amount of sunshine. The highest disparity between regions of the country is roughly 8% (Naplopo, 2014). Figs 2.18 and 2.19 show the intensity of Hungary's global horizontal solar irradiation (GHI) and direct normal solar irradiation (DNI).

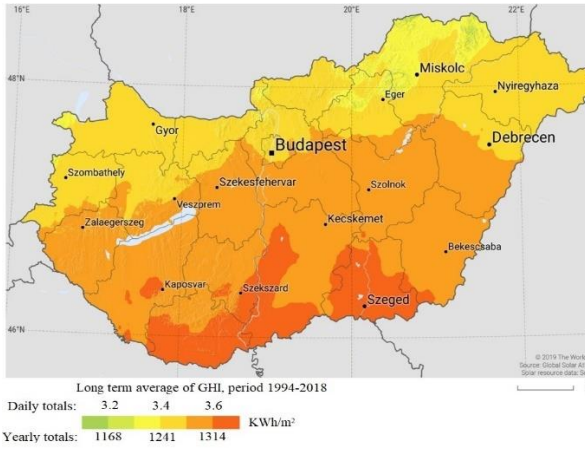

Fig. 2.18. GHI intensity of Hungary (Solargis, 2020)

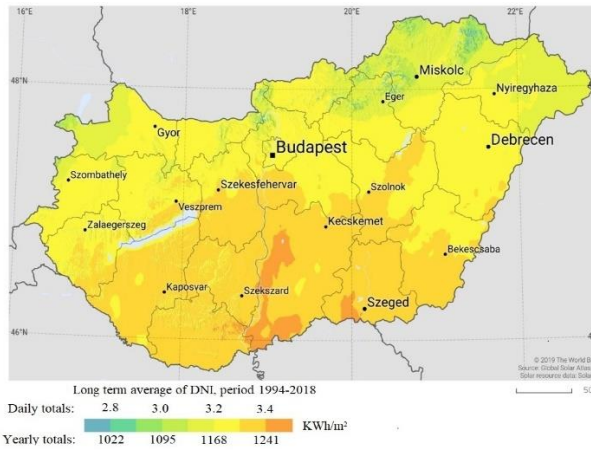

Fig. 2.19. DNI intensity of Hungary (Solargis, 2020)

2.4. Factors affecting drying processes

According to the literature, several factors influence the drying rate of solar dryers. The variety of biological product, pretreatment, drying air temperature, drying air flow rate, and local climate, amount of material to be dried are the most vital factors that influence solar dryer performance (Farkas, 2008; Arunsandeep et al., 2018; Pagukuman and Ibrahim, 2021). The impact of various characteristics on the solar dryer's performance was discussed by Kapadiya and Desai (2014). Leon et al. (2002) presented a comprehensive study of the characteristics used to evaluate solar dryers. In addition to other variables, they highlighted the impact of air temperature, relative humidity, and airflow rate in addition to other parameters. Kucuk et al. (2014) examined the drying behavior of 67 thin-layer drying curves models by taking into account numerous affecting parameters such as product type, temperature, air velocity, and pretreatment. Correia et al. (2015) investigated the impacts of drying air temperature, drying time, and tomato fruit thickness during the drying process. The best drying conditions were found to be at 60 °C, with the lowest thickness layer (15 mm) and the shortest drying time. The effects of drying air temperature and sliced apple thickness were also studied by Meisami-Asl et al. (2010).

The quantity of dried products is an important factor that influences the performance of solar dryers. A higher load of products requires a greater amount of drying air. Due to the failure to achieve the necessary moisture level inside the materials, the danger of receiving poor quality dried products increases. A small amount of dried product, on the other hand, increases the solar dryer's drying rate, although this can lead to energy waste in some situations.

Pretreatment of samples before to drying is critical since it increases the drying rate and decreases the drying time. Hence, less energy consumption and high quality of product will be achieved (Hedayatizadeh and Chaji, 2016). Sharma et al. (1992) investigated and tested a variety of fruits with and without chemical pretreatment under various drying circumstances using an indirect type of multi-shelf fruit and vegetable dryer. They observed that chemical pretreatment increases not just the drying rate but also the dryer efficiency, resulting in a higher quality dried product. Rayaguru and Routray (2012) discussed the effect of pretreatments used before apple drying on product quality and drying kinetics. Pretreatment may also include slicing the fruits. In many drying processes the product being dried is cut into a thin layer to reduce the amount of energy required to dry the product and the drying time. Vijayan et al. (2016) study a bitter gourd was cut into 5-7 mm thick slices.

The type of product to be dried has an impact on the drying rate, as some materials are heat sensitive. Fudholi et al. (2010) examined a variety of solar dryer designs for drying several agricultural and marine products.

Temperature is another parameter which can influence the drying rate and the final properties of a sample (Lingayat et al., 2017). According to Farkas (2013) suggested that appropriate temperature range and the amount of energy needed to remove moisture the most crucial factors in designing a safe and cost-effective drying system. The amount of moisture removed is determined by the temperature of the dried air, with warm air catching moisture more readily than cold air. A higher temperature is required when the initial moisture content is high to shorten the drying duration. At low moisture content, however, the temperature has little

influence since just a small amount of heat is necessary to evaporate the moisture. Bennamoun and Belhamri (2003) stated that drying is essentially affected by the air temperature. For 60 °C, the time required to achieve the desired moisture was 500 min and it took 900 min for temperature equal to 40 °C. The optimal temperature range for desiccating various agriculture-based products inside the drying chamber was found to be 45 to 60 °C. The most serious concerns in this field, on the other hand, are the irregular nature and improbability of solar radiation (Agrawal and Sarviya, 2016).

Airflow rate is another key factor that influences drying time and energy efficiency. Condorí et al. (2017); Fudholi and Sopian (2019) created and tested three parallel-pass solar collectors with double, single, and no baffles using numerical and experimental approaches. According to the data, the parallel-pass solar collector double baffles with the highest mass flow rate had the best efficiency. Because of the small rise in temperature, an increase in air flow rate reduces conduction losses. At a high flow rate, however, air may not have enough contact time with the substance to remove moisture. Insufficient flow rate increases the dryer temperature, which leads to the burning of the product. According to Karim and Hawlader (2006a), most agricultural products should be dried at a rate of 0.035 kg/m^{2}s. Ekka et al. (2020) used two successive air mass flow rates to expedite the drying of black ginger in a forced convection mixed mode horizontal solar dryer. When this dryer was operated with varied air mass flow rate during initial and falling period rather than constant flow rate, there was a considerable improvement in thermal performance and moisture diffusivity.

Relative humidity of air is also a significant parameter on the performance of the solar dryer. Air with low relative humidity can capture more moisture from the dried product and drying duration become shorter. However, air with high relative humidity cannot capture moisture from the dried product due to saturation. It can be shown also that increase in relative humidity with increased surface temperature can enhance the convection heat transfer coefficient (Zhang et al., 2007).

2.5. Single-pass solar air collectors performance evaluation

A solar air heater (SAC) is a simple device that uses the sun's energy to heat air. It has a wide range of uses, including drying agricultural products–fruits and vegetables. It consists of an absorber surface (typically a dark, thermally conducting surface), a glass that transmits short-wavelength solar radiation while blocking the longer-wavelength radiation from the absorber; a heat-transfer medium i.e., air, a panel made of wood or other materials, and some thermal insulation behind the absorber surface as shown in Fig. 2.20. Meteorological parameters (solar radiation, humidity, and wind speed), absorber area and material, orientation, collector type (single or double pass), inlet temperature, and volume flow rate all influence the thermal performance of a SAC. Due to the air having a low heat capacity and the low convective heat transfer coefficient between the absorber and the air, a larger heat-transfer surface area and higher flow rates are required. Solar air collectors that are energy-efficient should absorb the incident solar radiation, convert it to thermal energy, and deliver it to the air stream with minimum losses.

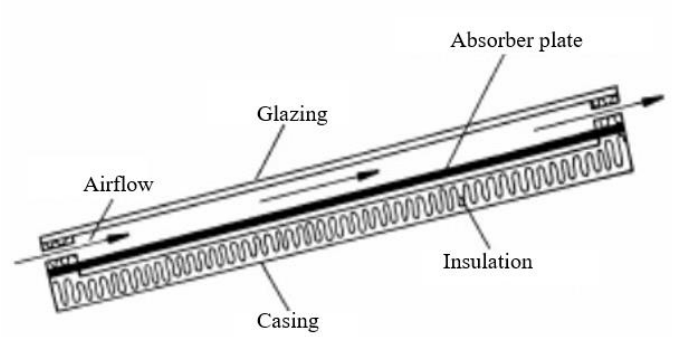

Fig. 2.20. Conventional single-pass solar collector (Ekenchukwu and Norton, 1999)

Various types of SACs can be utilized in the drying process due to their low cost and simple form. SACs can be employed in a range of drying applications with various types of dryers. Numerous studies investigating various SACs have been published in the literature. The majority of studies have focused on how absorber design characteristics affect collector efficiency. Artificial roughness, such as fins, baffles, and a wire mesh layer, is one of the most extensively utilized solutions for enhancing collector efficiency (Karim and Hawlader, 2004; Pramanik et al., 2017; Al-Neama and Farkas, 2019; Kumar et al., 2019; Khanlari et al., 2020). The absorber plate with V-shaped baffles was used by Karim and Hawlader. (2006a) and Lingayat et al. (2017). Another way to improve SAC performance is to use a double-pass solar air collector (DPSAC). Omojaro and Aldabbagh. (2010) studied the thermal performance of single and double-pass solar air collectors using wire mesh as a packed bed, finding that the air mass flow rate increased from 0.012 kg/s to 0.038 kg/s, the efficiency increased significantly, but the temperature difference between the outlet flow and the ambient air decreased. For the same air mass flow rate, the DPSAC was 7 to 19.4% more efficient than the SPSAC, according to their findings. Krishnananth and Murugavel. (2013) used thermal energy storage (paraffin wax) on DPSAC and found that the collector efficiency increased not only during daytime but also during evening hours.

The concept of thermodynamics laws is used for study of energy and exergy analysis in solar air collectors (SAC's). Energy analysis is essential for determining how successful a process is, and exergetic analysis is a vital concept for examining how process operated in actual behavior under various energy losses and internal irreversibility (Ghritlahre and Sahu, 2020). According to Ajam et al. (2005), the concept of exergetic is a superior method for developing and optimizing SAC's.

The energy efficiency of a finned SPSAC was constructed and tested by Ibrahim et al. (2013). The experimental setup is composed of two modules: a collector module and an air handling model. As shown in Fig. 2.21, the collection module has glazing and a black-painted aluminum absorber with fins, while the air handling module includes a fan and duct. The findings revealed that collector efficiency improved as solar radiation intensity and mass flow rate rose. Experimental studies on the effectiveness of SAC were conducted by Ozturk and Demirel (2004). The dimension of the designed SAC is 1.9 m by 0.9 m and absorber plate made of aluminium. According to their research, the average energy and exergy efficiency are 17.51 and 0.91%, respectively and both efficiencies rise as collector outlet temperature rises. Gupta and Kaushik (2008) presented that when the inlet air temperature is low, the flat-plate SAC's

maximum exergy output obtained with the lowest flow rate. Another study found that the solar radiation intensity and geometry of absorber plate effects the efficiency of SAC's (Akpinar and Kocyigit,2010).

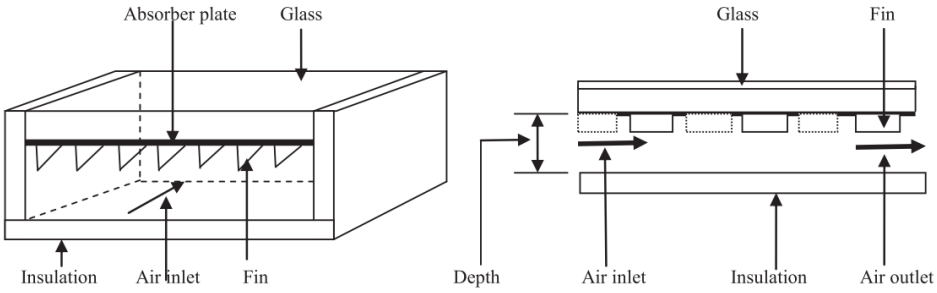

Fig. 2.21. The schematic of a SPSAC with a finned absorber: a) front view and b) cross-sectional view.

Pramanik et al. (2017) designed and investigated a double-pass wire-packed SAC both analytically and experimentally as illustrated in Fig. 2.22. Fins made of 0.3 mm thick Aluminum material are extended downward from the absorber plate up to 0.50 mm. The airflow rate was increased by using a DC suction fan at the outlet, which sucks the air to flow over extended surfaces. Instantaneous efficiency and air outlet temperature both increased up to 69% and 94 °C, respectively.

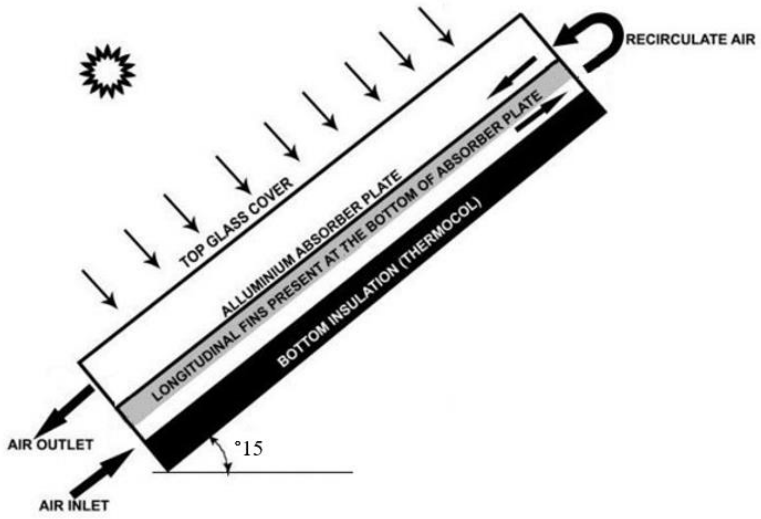

Fig. 2.22. Schematic diagram of a double pass solar air heater (Pramanik et al., 2017)

Singh (2017) carried out simulation work on an arched plate with an equilateral triangle turbulator and a dimply turbulator on the inner side of the absorber plate wall. Results showed that an arched-shaped absorber plate can significantly improve the overall performance of the solar air heater system using various turbulators and he provided a new direction of the work trend in this area.

Using newly constructed SAC, Gulcimen et al. (2016) evaluated drying parameters experimentally and theoretically. To enhance the collector's efficiency, three different mass flow rates (0.012 kg/s, 0.026 kg/s, 0.033 kg/s) with fins with angles of 30°, 45°, and 60° were

mounted inside the airflow. The maximum collector efficiency was 47% for the mass flow rate of 0.033 kg/s and fin angle of 60°, according to their results.

Al-Neama (2018) designed and investigated experimentally the performance of the solar air collector by introducing four absorber plate designs: horizontal fin, inclined 45° fin, vertical fin, and helical fins. The result showed that the direction and shape of fins are played a significant factor to improve the thermal performance of SACs. The horizontal direction of rectangular fins attachment is the most efficient direction to get the maximum percentage of useful heat gained as compared with vertical and 45° inclined fins. The helical finned absorber plate gave a significant thermal improvement of solar air collectors by about 18% of daily energy efficiency and useful heat gain.

2.6. Effect of air gap thickness on solar air collector performance

There are many methods to minimize the convective heat losses from the SAC such as fluid properties, geometry, angle of inclination of the SAC, air gap thickness confined between the absorber and the glass cover etc. however, air gap thickness plays a great effect to reduce the heat losses while improving the convective heat transfer from the absorber to the fluid. Utilizing of experimental approaches is necessary for controlling this complex heat transfer.

Dheyab et al. (2019) created four solar air collectors, each with a different air gap thickness of 30, 50, 70, and 90 mm. The maximum air temperature difference was observed for an air gap thickness of 30 mm, whereas the highest mass flow rate was recorded for an air gap thickness of 90 mm, according to their findings. They also discovered that as the air gap thickness increased beyond 50 mm, the mass flowrate and collector efficiency increased insignificantly. The optimal air gap of a solar air collector has been studied in several studies. Nahar and Gupta (1989) used three air gaps of 25, 50, and 150 mm, with the 50 mm gap outperforming better in overall collector efficiency. According to Macedo and Altemani (1978), the energy efficiency of the solar collector was improved when using an air gap thickness of 9–11 mm. Ferahta et al. (2012) performed numerical study on the effect of air gap thickness on heat transfer between the absorber plate and the glass cover of a SAC. According to their findings, conduction is shown to be dominant for small air gaps whereas convection is found to be dominant for large thicknesses.

2.7. Effect of solar chimney on dryer performance

In recent years, there has been a lot of interest in developing solar chimney (SC) technology for various applications due to the rising use of solar energy. Researchers are increasingly interested in SCs as a viable technique for enhancing natural ventilation because of its long-term energy saving (Shi et al., 2016). SCs employ solar energy to raise the temperature and induce a density drop in the air, with the buoyancy force causing the air stream to travel inside the system. The greenhouse effect warms the air passing through a transparent collector. Although many theoretical and experimental studies have been conducted in this area, there hasn't been much attention paid to chimney modeling for indirect passive solar dryers. Kasaeian et al (2017) reported around 20% out of 200 studies on solar chimneys have been done experimentally. Lacking reliable experimental validation stands as a major hurdle for both theoretical and modeling studies. In addition, based on application types, 36 applied papers

were investigated. The result showed that the contribution to drying application was only 6%. There is a paucity of chimney optimization in the domain of drying, despite the fact that various ideas have already been documented. Ekechukwu and Norton (1997) represented the method attempt to improve the chimney by testing a solar radiation absorber surface around the chimney in order to keep the heated air inside the chimney above ambient temperature. thus, enhancing the buoyance-induced airflow. The authors came to the conclusion that a well-designed chimney can keep the mean air temperature inside the chimney higher than the temperature of the surrounding temperature.

A chimney operates by increasing the buoyancy force to aid the airflow through a structure. The buoyancy force is determined by the difference between the mean air density inside the chimney and the density of outside air. (Koyuncu, 2006) developed and tested two different types of natural convection greenhouse type dryers with and without chimneys to determine the effect of the chimney on the air flows. The chimney was constructed from a galvanized iron sheet with a rectangular shape. The test was made experimentally with no product load and with product (pepper) load in summer conditions of 2001. He found that chimneys provide better natural circulation of air than dryers without a chimney.

Several researchers have suggested that heated chimneys can improve the ventilation in a room. The use of a heated chimney in passive solar dryers is highly appreciable to enhance the continuous airflow inside the drying cabinet to achieve this density difference. Madhlopa et al. (2002) suggested that increasing the height of an added chimney improved the thermosiphon abilities of a solar dryer. Furthermore, as airflow in a convective air system is directly linked to the change in air density due to temperature, the thermosiphon abilities of the dryer and airflow are proportional.

Yaciuk (1982) stated that solar energy is collected in the air heaters utilizing the greenhouse effect using transparent cover and absorber. Because of the buoyancy effects, the warm air rises through the sloped collector and into the drying chamber where the crops are placed. Many designs are possible depending on the mode of circulating the air. The agent for moving the air in most available designs is mechanical such as the fan (forced indirect dryers). The effect of buoyancy can be enhanced by using a chimney, which creates a draft that can cause an adequate mass flow of air to pass through the collector and then through the crops. There is not a great deal of interest in this method.

Zambrano and Alvarado (1984) designed and tested two chimneys with different shapes but the same chimney height to reduce the excessive solar radiation and/or low internal air velocity (insufficient chimney draft). The authors selected two chimneys one with a cylindrical shape and the other one with a truncated inverted cone and both shapes have the same height of 4.3 m and base diameter of 0.3 m. The experimental result showed that the velocity of air at the basal section of the conical chimney was approximately twice that of a cylindrical shape. In the drying chamber, the temperature recorded was 78 °C for cylindrical shape and 66 °C for the truncated inverted cone respectively. Moreover, the temperature of the product reduced approximately by 10 °C.

Bassey (1986) designed and tested an indirect free convection solar dryer using various parameters (temperatures of drying chambers, airflow, and chimney) under no-load and loaded

conditions using rice in Sierra Leone. One of the dryers had a single-pass air heater whereas the other had a double-pass air heater. Five different chimney configurations were used on the dryers over three years. Based on his result, a chimney with short height (about 50 mm) and painted black covered with transparent material affects the flow of air through the dryer. In addition, a single-pass air heater is considered better as compared with a double-pass air heater due to higher temperatures recorded in the drying chamber. A vertical flat plate collector chimney designed by Das and Kumar (1989) for drying 20 kg of field harvest high-moisture paddy. The dryer unit consists of an inclined collector (20.6°), a batch dryer, and a vertical collector chimney, all joined in series and positioned due south. The absorber and the cover for both the collectors were 2 m by 2 m black-painted corrugated G.I. sheet and 3 mm poly-methyl-methacrylate, respectively. The system could generate an adequate flow of hot air to enhance the drying rate.

Vlachos et al. (2002) designed and tested a new low-cost indirect solar dryer equipped with a solar air collector, a heat storage cabinet, and a solar chimney. The solar chimney has a trapezoid base placed right on top of the drying chamber and the chimney duct that has the shape of a narrow parallelepiped. The external measurement of the duct was 0.73 x 1 x 0.12 m, and its front side is a glass 3 mm thick. Five holes are opened to facilitate the insertion of measuring probes. The dryer is built up in the city of Serres (latitude 41°07', longitude 23°34', altitude 32 m) of Greece. Based on theoretical consideration as well as preliminary tests under operating conditions, they found a model to calculate the volumetric airflow rate inside the chimney which is given as:

$$V_a = 0.113\ \pi\ D_h^2 \left[\frac{D_h g}{\rho_a}(T_{ch} - T_a)\right]^{0.5}, \tag{2.1}$$

where T_{ch} is the average temperature of the chimney, T_a is the ambient temperature, and ρ_a is the air density.

Chen et al. (2003) made experiments to study a full-scale solar chimney as a ventilation device. The results showed that by changing the chimney gap while maintaining all the other conditions, the airflow rate increased with increasing the chimney gap and the airflow rate reached a maximum at a chimney inclination angle of around 45° which is about 45% higher than that for a vertical chimney. The increase in flow rate is due to the relatively even airspeed inside the chimney, which significantly reduces the pressure loss at the chimney inlet and outlet compared to the corresponding vertical chimney.

Senadeera and Kalugalage (2004) presented an experimental performance evaluation of a solar tunnel dryer constructed with two chimneys, GI sheet metal, and a wooden frame covered with polyethylene. The results showed that chimneys with polyethylene gave a higher efficiency than sheet metal chimneys.

Ferreira et al. (2008) studied the technical feasibility of a solar chimney to dry agricultural products. To assess this drying device, a prototype solar chimney was built and the drying tests of food, based on theoretical and experimental studies, assure the technical feasibility of solar chimneys used as solar dryers, in which the air velocity, temperature, and humidity parameters were monitored as a function of the solar incident. The constructed chimney generates a hot

airflow with a temperature rise of 13±1 °C. They concluded that thermal diffuser plastic film is more suitable to be used in the solar chimney's cover because of its low weight and reduced costs (Fig. 2.23). An experimental investigation into the performance of a solar crop dryer with a solar chimney and no air preheating was described by Afriyie et al. (2009). According to the authors, a direct passive solar dryer can be assumed as one large chimney. The experimental tests were performed on the cabinet dryer, using a normal chimney, and repeated with a solar chimney. The trails were carried out with the roof of the drying chamber at different angles. Such types of solar dryers are suitable for low humid air. For high humid air conditions, it is necessary to provide a certain amount of preheating to the air. The result showed that the solar chimney can increase the airflow rate of a direct-mode dryer especially when it is well designed with the appropriate angle of the drying chamber roof.

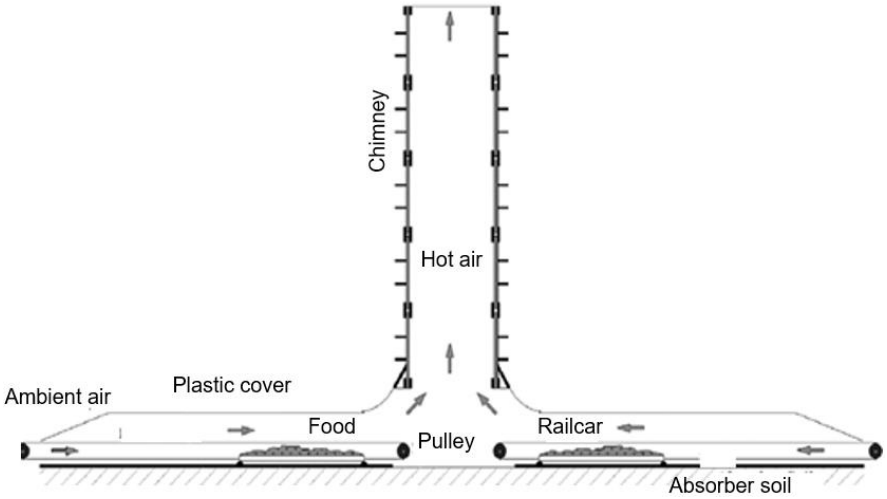

Fig. 2.23. Schematic representation of the solar chimney prototype as a solar dryer

Maia et al. (2009) presented a practical study of the airflow through a solar chimney to dry agricultural products. The prototype was built on the campus of Universidad Federal de Minas Gerais, Brazil. The solar chimney has a dimension of 1 m diameter and 11 m height tower which was supported by six mechanical tubes 1.3 m above the ground. The tower was made of wood and fiberglass. Ambient condition and total water mass removed were evaluated to assess the performance of the solar chimney.

Russon et al. (2009) designed a solar food dryer to optimize the dryer's efficiency. They developed a model which describes the total efficiency as a function of chimney height. In this study, four chimney heights were used 0 mm, 234 mm, 798 mm, 1361 mm, and 1595 mm. These heights were derived using scaling factors of central composite design. Potatoes, thinly sliced to a thickness of 3 mm, were chosen as the test product. They concluded that chimney height had a positive impact on enhancing the dryer's overall efficiency and air mass flow rate. Total efficiency increased by 4% for each additional meter of chimney height. A developed model is found in Eq. 2.2.

$$\eta_{\text{total}} = 0.439 + 4.01 \cdot 10^{-5} \text{chimney height}_{\text{mm}}. \tag{2.2}$$

Afriyie et al. (2011) developed mathematical models to simulate and optimize the ventilation concerning the design of chimneys under no-load conditions. Their investigations revealed that

inlet-exit area ration, drying chamber, roof inclinations and chimney height are the critical parameters to achieve maximum airflow inside the dryer. The same authors (Afriyie et al., 2013) developed a simulation procedure that describes the drying process within a chimney-dependent direct solar crop dryer. Their work on the development of simulation code to help optimize ventilation in such dryers.

Chen and Qu (2014) developed a solar chimney-based indirect-mode solar drying system with the porous absorber and evaluated the heat transfer and flow in the system. With the height of the solar dryer increasing from 1.41 m to 1.81 m, the higher airflow velocity and lower temperature at the chimney outlet can be accomplished. This is due to the inclined angle of the porous absorber, which has a significant impact on the airflow and temperature field in the system.

According to Chung et al. (2015), the efficacy of stack ventilation is significantly influenced by solar chimney width gap and length. In their investigation, the height was fixed, and nine different combinations of width and length were investigated. Their research showed that no reverse flow was noticed up to the solar chimney's 2 m length and 0.6 m cross-sectional gap.

Ghaffari and Mehdipour (2015) presented a new approach for numerically modeling an indirect solar dryer using computational fluid dynamics. In their study, the outlet air temperature of the chimney was calculated using the equation:

$$T_{ch,o} = T_{am} + \left(T_{ch,i} - T_{am}\right)e^{-UPl/\dot{m}C_p}, \tag{2.3}$$

where $T_{ch,i,}$ and $T_{ch,o}$ are the chimney inlet and outlet air temperatures, p is the chimney's base perimeter, $\dot{m}$ is the mass flow rate, l is the height of the chimney and U is the chimney's general heat transfer coefficient.

The effect of moist air on the performance of a vertical solar chimney was explored by Sudprasert et al. (2016). In a solar chimney, a numerical model was created to simulate the heat transfer and fluid flow of dry air and wet air with a relative humidity of 30 - 80%. The overall air temperature was higher for a solar chimney with wet air, according to the results. Furthermore, raising the vapor in the mixture by increasing the relative humidity from 40% to 80% reduced the average velocity and hence buoyant force in the solar chimney.

2.8. Summary of literature review

The literature review indicates that interest in the development of natural air circulation has been sparked by research on the use of solar chimneys due the energy crisis and environmental issues. A solar chimney is used for a variety of applications such as passive cooling and ventilation of buildings, power generations etc. The basic principle of a solar chimney is to create an updraft along a channel using the sun. In natural solar dryers, installation of a solar chimney improves air movement inside the dryer unit. The effective design of solar chimneys, however, has received little consideration.

Due to the lack of a pre-heater in direct type solar dryers, the effect of the solar chimney is more obvious when utilizing these dryers, making the solar chimney one of the key components of the DSD. There hasn't been much investigation into the effect of solar chimney in natural

indirect type solar dryers, though, because of the pre-heater. It has been stated that various solar dryer chimney designs have been reported in the literature such as using opaque metal materials without insulation, chimney with absorber painted black and covered with transparent plastic etc. However, no experimental research on the parametric analysis of a solar chimney has been conducted. When evaluating a chimney, it's necessary to take into account its height and the air gap between the absorber and the glass cover. High air circulation is produced by chimney height, and heat transfer between the heated absorber and adjacent air is facilitated by air gaps. Nevertheless, increasing the height of the chimney does not necessarily result in improving airflow. Furthermore, there isn’t any conclusive evidence in the literature that a high or a small air gap thickness (based on the air gap in solar air collector) improved on heat transfer.

According to the research analysis, it could be concluded that the current study has the intended goals to answers to the knowledge gap. Therefore, the current study has been carried out both experimentally and theoretically focused on parametric evaluation of various solar chimney designs, including solar chimney stack height, chimney air gap and their effects on the functionality of the dryer unit. Energy and exergy analysis and equations of drying will be employed to analyze, compare and select the best solar chimney design that can improve the performance of the dryer unit.

3. MATERIALS AND METHODS

This chapter covers the description of the materials, techniques, and equipment used, as well as the scientific methodologies employed in the experimental measurements to accomplish the research goals, such as how the study was conducted, how data was obtained, and what graphical analyses were performed.

3.1. Study location and orientation

The novel indirect solar dryer (ISD) was designed, constructed, and tested using seven different solar chimney configurations at the forecourt of the laboratory of mechanical engineering of the Hungarian University of Agriculture and Life Sciences (MATE) (former Szent Istvan University), Gödöllő, Hungary, between June–August 2020, 2021, and July 2022. The geographical locations of the setup are 47° 35' 39" N and 19º 21' 59" E as shown in Fig. 3.1.

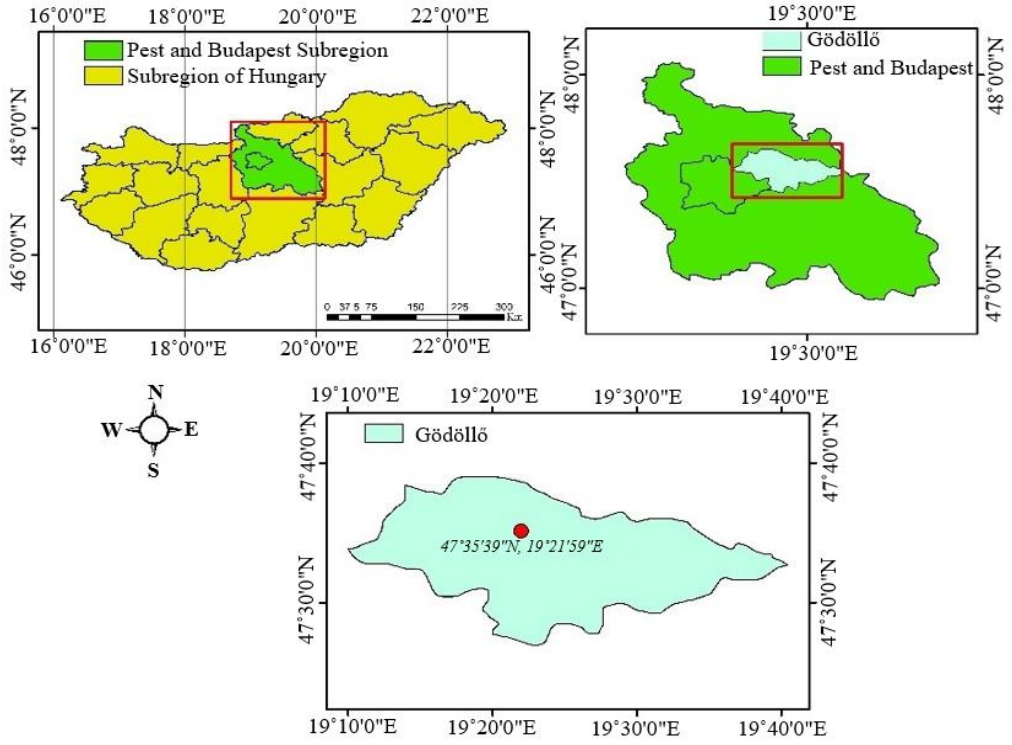

Fig. 3.1. Study area and location of the setup

In order to produce the maximum quantity of hot air, solar collectors must face the sun directly. This requires that the sun must strike the surface of the solar collectors at right angles and not be subjected to any shade. However, during the time of experiment, practically all solar air collectors are fixed and do not track the sun. According to several studies, solar collectors should be tilted up from the horizontal the same number of degrees as the latitude (Zang et al., 2016). The amount of solar radiation that reaches the collector surface varies depending on the tilt angle. The collectors and solar chimneys should be oriented toward the equator, which in Hungary means facing true south (Duffie and Beckman, 2013). In this research location, the collector's best named angle is at a 45° angle to the horizontal (Al-Neama and Farkas, 2019), while maintaining the solar chimney in its vertical orientation due to structural stability.

3.2. Description and experimental set up

A single-pass solar air collector, a drying chamber, and a solar chimney are all part of the solar-based drying system (ISD). A solar air collector is made up of an absorber and a glass cover that is connected to a drying chamber at a particular inclination, which is determined by the location. When solar radiation strikes the glass cover, some of the energy is absorbed by the absorber plate, which subsequently heats the air next to it before flowing into the drying chamber. In the drying chamber, the product that needs to be dried absorbs heat from the solar collector and loses moisture. After absorbing moisture from the products, the air becomes more humid, flows through the solar chimney, where it is heated once more, loses density, and is then forced upward to exit through the top vent into the environment, creating a continuous flow where cold, dense air is drawn in to replace the warm air through the dryer. The complete experimental setup of the novel ISD and its schematic diagram along with the measuring experiment are shown in Fig. 3.2. and 3.3, respectively. The dryer unit is held in place by a metallic framework. The design and setup of the ISD's components are described in detail in following sections.

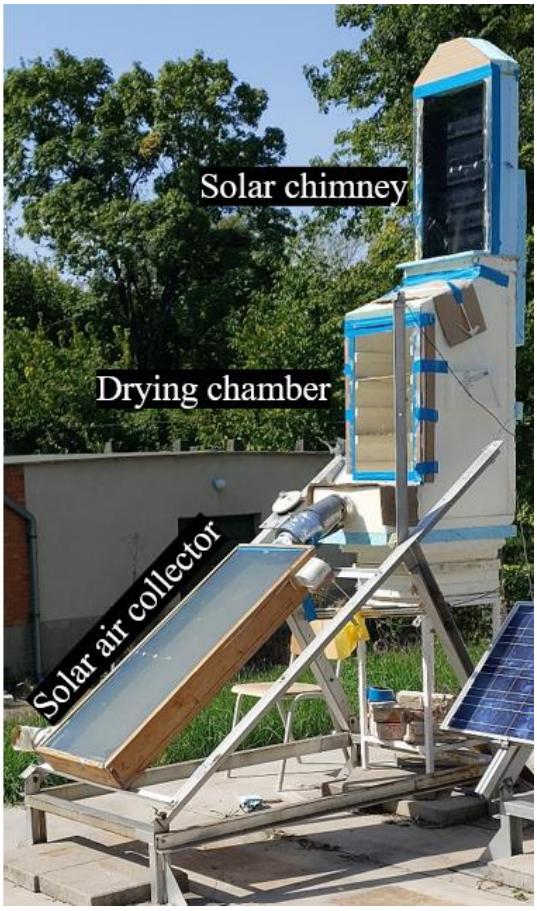

Fig. 3.2. Complete view of a novel ISD with vertical solar chimney

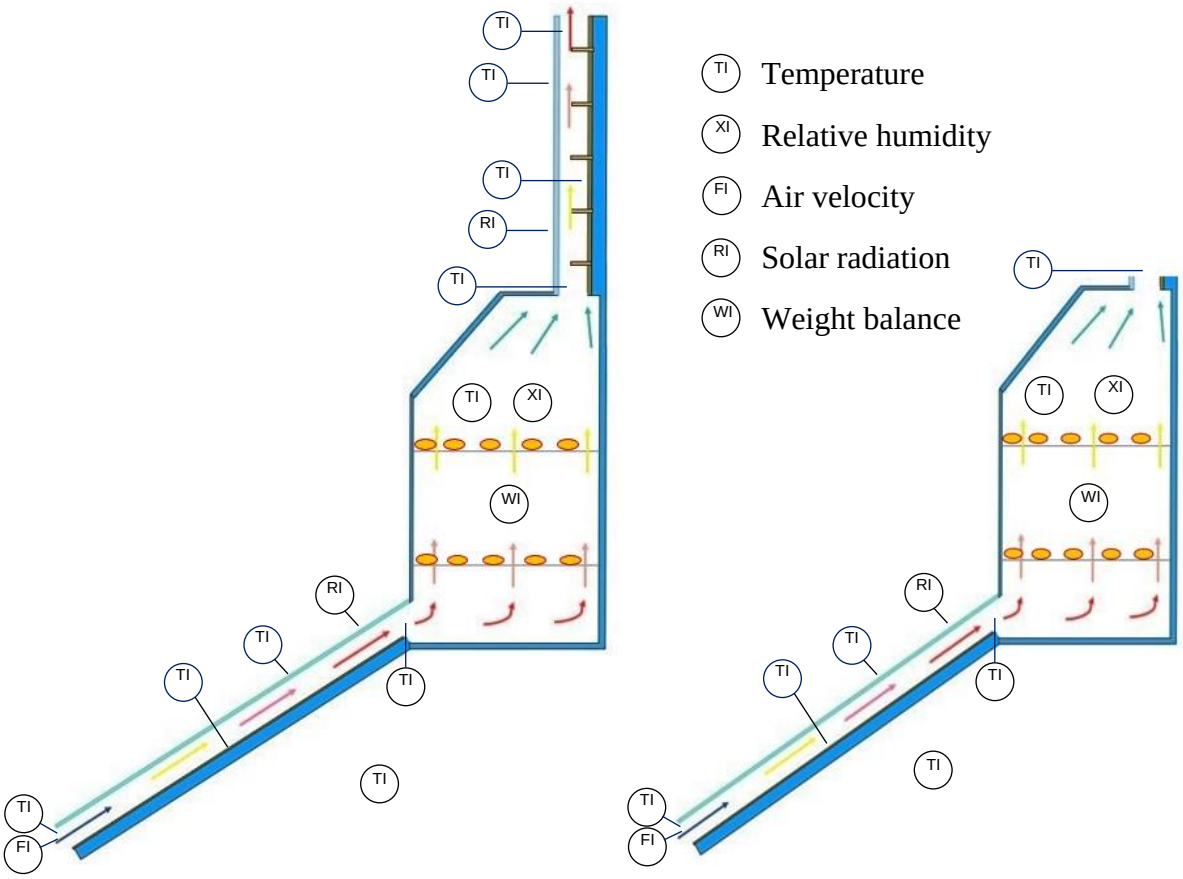

Fig. 3.3. Schematic diagram of novel and conventional dryers with all measuring instruments

3.2.1. Single-pass solar collector

Most solar energy systems have solar collectors. They are the most important part of a solar dryers, as they are built to meet the specific temperature requirements for various end-uses. According to the Bassey (1986) report, a single air passage solar collector is better suited for passive convective solar dryers than a double pass collector due to their simplicity in design and generally higher temperatures. consequently, a single pass solar collector was chosen for this research work. The sun's radiation is absorbed by the collector and converted into thermal energy. This thermal energy can then be used to dry the food product in the dryer. A single-pass solar air collector (SAC) was fabricated, using available materials. It consists of a rectangular box made of plywood, a copper absorber plate, a glass cover, and insulation material.

A 4 mm thick plexiglass was used as a transparent diathermanous material to transmit as much as 90% of the incoming shortwave solar radiation to the plate and was incapable of transmitting long-wave emitted outward by the absorber plate (Bahrehmand and Ameri, 2015). Thus, the solar radiation is trapped in a collector. To prevent heat loss from the backside, a 50 mm polystyrene sheet was provided. A 1.2 mm thick copper plate was used for absorbing the short-wavelength radiation to increase the temperature of the collector plate. This plate was selectively painted with enamel paint so that the surface absorptivity would be enhanced. The width and length of the absorber surface are 0.460 and 1.226 m (Ac ≅ 0.564 m^2), respectively.

The dimension of the inlet duct was kept the same (0.012 m^2). The channel gap between the absorber plate and the glazing cover is 10.8 mm. The drying chamber was connected to the outlet of the solar air collector through a PVC duct. Fig. 3.4 shows the schematic diagram of a single-pass solar air collector.

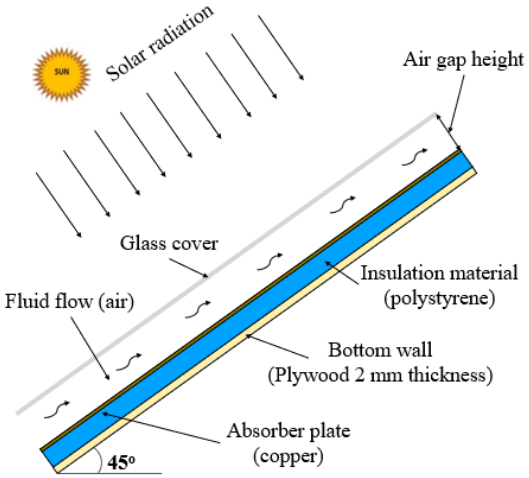

Fig. 3.4. Single-pass solar air collector

3.2.2. Drying chamber

The drying chamber, where the food to be dried is placed, is the second important component of the drying unit. It is made of 0.5 m thick expanded polystyrene (EPS) and has a rectangular box as shown in Fig. 3.5. On basis of this volume, the dimension of the drying chamber is 0.5 m length, 0.5 m width, and 1.0 m height equipped with two drying trays of size 0.38 m by 0.40 m made from the plastic net and these trays mounted inside the chamber. Sliding trays have been kept inside the chamber to make it easier to remove them during product loading or uploading. All sides of the drying chamber, except the front side with Plexiglas, are covered with EPS sheets.

Fig. 3.5. Drying chamber with tray (Al-Neama, 2018)

The roof of the drying chamber is inclined to form a tent dryer effect for smooth airflow. During the operation, the drying chamber was considered as adiabatic wherein drying sample and trays

have negligible heat capacity. The heat loss via the chamber's wall was insignificant. The SAC was attached to the drying chamber's bottom aperture, while the chamber's upper opening held the SC.

3.2.3. Solar chimney

The use of solar chimneys for generation electricity requires tall structures to acquire a reasonable amount of energy. However, solar chimneys can be employed to dry agricultural products with reduced dimensions (Ferreira et al., 2008). The characteristics of the solar chimney (SC), in addition to factors like solar radiation, air temperature, wind speed, humidity, and so on, are crucial for promoting air flow and enhancing the efficiency of the natural type of solar dryer. Solar chimneys work on the same principles as solar collectors but are mounted vertically. Fig. 3.6 shows the construction details a proposed solar chimney. The chimney is rectangular in shape with openings on either end; one end is connected to the drying chamber, and the other end is exposed to the surrounding.

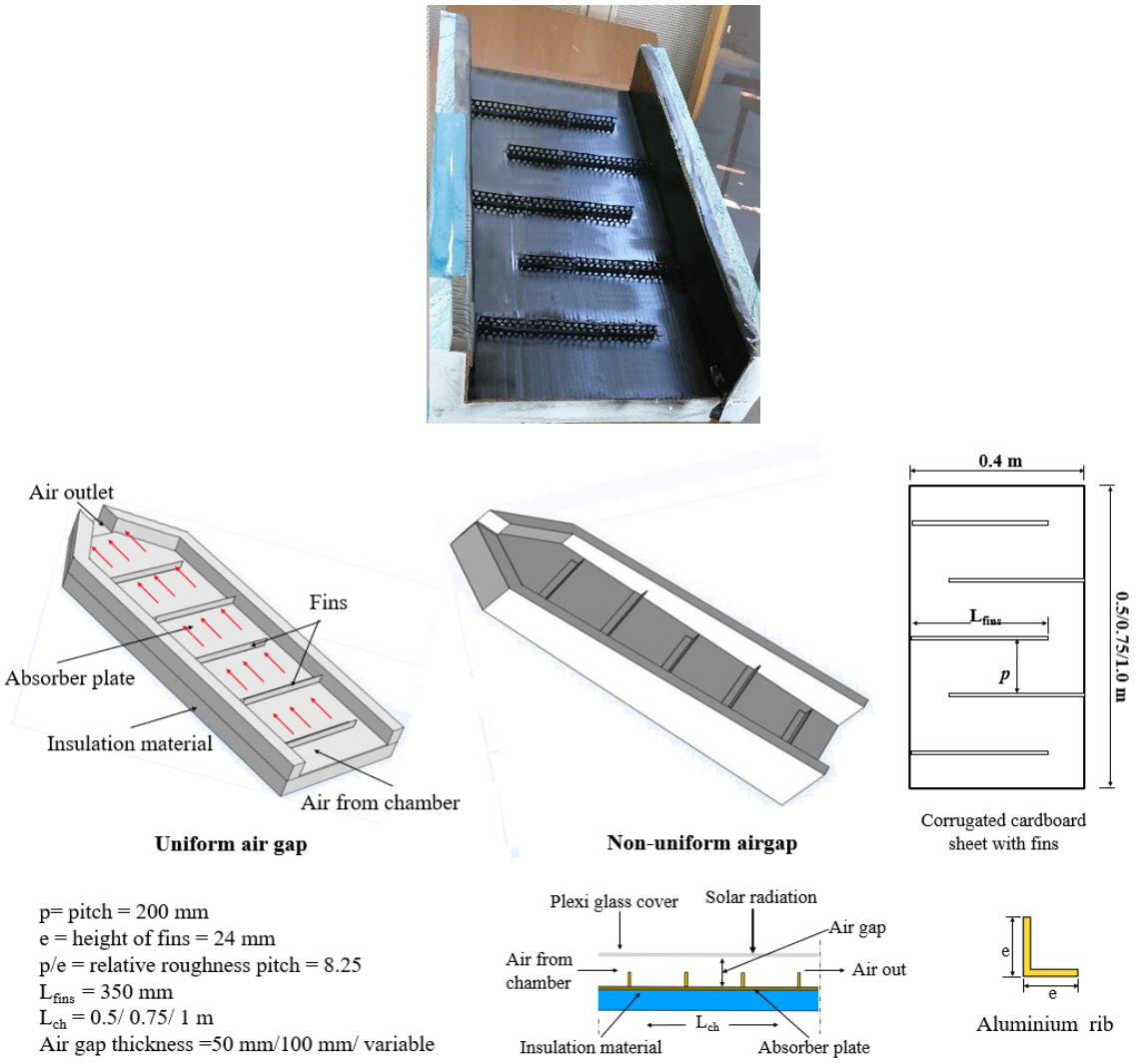

Fig. 3.6. Proposed solar chimney design

Plexiglas was used on the south-facing front side of the chimney to transmit high-temperature short-wave radiation to the absorber plate while blocking low-temperature long-wavelength

radiation from escaping to the surrounding atmosphere. The translucent Plexiglas is 4 mm thick and has a low thermal conductivity (0.19 $W.m^{-1}. K^{-1}$). The solar chimney's two side and back walls are composed of 50 mm thick expanded polystyrene (EPS), which reduces heat loss through conduction. As an absorber plate, a 5 mm thick double-face corrugated cardboard sheet with a back matt coating on the upper side was used. In order to improve energy and exergy efficiency, L-shaped Aluminium ribs were attached to the exposed surface of the absorber that is perpendicular to the direction of air flow (Bahrehmand and Ameri, 2015). The selected rib models have the following roughness parameters: rib's height (e), longitudinal pitch (p), which is the distance between two successive ribs in the flow direction, and attack angle (α), which is the angle between the rib and flow directions. The rib's parameters *e*, *p*, and *α* have values of, 24 mm, 200 mm, and 0°, respectively. The relative roughness pitch is 8.25 and the rib is 300 mm long. Table 3.1 shows the number of fins attached to the absorber in relation to the chimney height. The air flow channel is formed by the glass cover and absorber plate, and the absorbed solar energy on the absorber plate heats the air. Solar radiation is captured by the chimney plate, which warms the moist air entering the channel from the drying chamber. Due to high temperature inside the chimney, the moist air in the chamber rises up under buoyancy, causing a natural movement. As the moist air moves through the solar chimney from the inlet to the outlet, its temperature rises. The glass cover is assumed to gain heat energy uniformly from the absorber plate through thermal radiation.

3.3. Instrumentations

Throughout the trials, various operating parameters were measured using different measuring devices. Pyranometer (model: Kipp and Zonen MM11, Delft, the Netherlands; accuracy: ±0.1 $W.m^{-2}$; range: 1– 4000 $W.m^{-2}$) was installed along the collector position and used for measuring solar irradiance on a collector surface, while the solarimeter (model: KIMO SL200, France; accuracy: ±1 $W.m^{-2}$; range: 1–1300 $W.m^{-2}$) was installed along the chimney position to measure solar irradiance on chimney surface. The air temperature at the inlet and outlet section of SAC, the temperature in each tray, inlet and outlet air temperature of the SC, temperature of glass cover and absorber plates of both the SAC and SC is measured with 10 calibrated thermocouples (type: T-type, TT-T22S, UK; accuracy: ±1 °C; range: -270–370 °C). During the drying process, the temperatures (T-type) and solar radiation (Pyranometer) were recorded every 1 min intervals by using the ADAM data Acquisition (model: ADAM 4018 Advantech, Taipei, Taiwan; accuracy: ±0.1%). The ADAM data acquisition system converts sensor voltage or current (±20 mA, 4~20 mA) into digital data using a 16-bit microprocessor-controlled sigma-delta A/D converter. After that, the digital data is converted to engineering units. The module provides data to the host computer via a conventional RS-485 interface when requested by the host computer.

The air mass flow rate in the ISD is measured with Testo anemometer was placed in the SAC inlet port (model: Testo 405i, Germany; accuracy: ±0.1 m s^{-1}, range: 0–30 m s^{-1}). Thermo-hygrometer (model: Gove H5075, Shenzhen, China; temperature accuracy: ±0.32 °C; RH range: 0–99% with accuracy of ±3%) was used to measure the relative humidity inside the drying chamber. Additionally, a smart hygrometer (model type: ORIA, China; temperature accuracy: ±0.5 °C; RH range: 0–99% with accuracy of ± 5%) was used to measure the ambient

temperature and relative humidity around the dryer. This sensor was placed behind the solar air collector and protected from direct irradiance according to the standard ASHRAE (RA91). An electronic moisture analyzer (model: Sartorius MA 30, accuracy: ±0.05% MC, range: 0–100%MC) was used to estimate the initial moisture content of the apple slices and a digital balance (model: APTP457, CGOLDENWALL, accuracy: ±0.1 g; range: 0–5 kg) was used to record the moisture loss of the sample. The measurements were taken for eight hours each day. The samples were immediately returned to the drying chamber after the moisture loss was measured at each interval to ensure that the drying process proceeded. The temperature measurements of various components of solar dryer's collector, drying chamber, and solar chimney were monitored at regular time intervals throughout the experimental period. Appendix 4 lists the equipment used to measure thermal characteristics.

3.4. Experimentation procedure

In this research work, seven detachable solar chimneys of various designs were selected as shown in Table 3.1. Additionally, for purposes of comparison, conventional ISD and OSD were employed. It should be noted that a total of 17 tests were conducted, both with and without loads.

Table 3.1. Proposed solar chimney design

Chimney configuration	**Chimney width (m)**	**Chimney stack height (m)**	**[1]Chimney air gap (mm)**	**Number of fins**
Case_1	0.5	1	50	5
Case_2	0.5	0.75	50	4
Case_3	0.5	0.5	50	3
Case_4	0.5	1	100	5
Case_5	0.5	0.75	100	4
Case_6	0.5	0.5	100	3
Case_7	0.5	1	[2]Non-uniform	5
Case_8	Convectional ISD			
OSD				

Note: [1]Chimney air gap thickness is the distance between the glass cover and the absorber plate, [2]non-uniform: cross-sectional area changes with SC height (decreases towards the SC outlet) and glass cover tilted 86° from vertical.

In these experimental trails, solar radiation intensity, airflow velocity, relative humidity outside and inside the drying unit, temperature at each location were measured and recorded. The measurements were taken for eight hours starting from 09:00 until 17:00. Based on the experimental results, the following parameters were used to evaluate and compare each setup: energy and exergy(2E) analysis, drying efficiency, energy consumption to remove water from dried product (SEC), and sample moisture loss. There were no modifications to the solar air collector (SAC) or drying chamber over the whole experimental evaluation period. The data

were collected for 8-hour steady-state periods. Average values for these periods were used to even out environmental fluctuations. During under-load conditions tests, the product's moisture loss was measured every 2 hours. The measurements were taken for eight hours each day. The samples were immediately returned to the drying chamber after the moisture loss was measured at each interval to ensure that the drying process proceeded. The temperature measurements of various components of solar dryer's collector, drying chamber, and solar chimney were monitored at regular time intervals throughout the experimental period.

3.5. Thermal performance analysis

In this section, the parameters used to evaluate the ISD's performance are discussed in detail. The amount of solar radiation reflected on collection and chimney surfaces, as well as energy efficiency, exergy efficiency, drying efficiency, and energy required to dried products, are all factors to consider.

3.5.1. Global solar radiation incident on collector and chimney surfaces

The amount of total solar radiation impacting the collector's surface is one of the main parameters that affect efficiency. The total solar (I_T) radiation incident on a south-facing collector tilted surface can be determined by summing up the beam radiation, diffused radiation, and ground reflected radiation (Fig. 3.7) using Liu and Jordan's model (Liu and Jordan, 1963) as:

$$I_T = I_b R_b + I_d \frac{(1+\cos\beta)}{2} + I_h \rho_r \frac{(1-\cos\beta)}{2}, \quad (3.1)$$

where, ($I_h = I_b + I_d$) and the tilt angle β is positive for due south and negative for due north and zero for horizon. It is to be noted here that $\frac{(1+\cos\beta)}{2}$ and $\frac{(1-\cos\beta)}{2}$ are the radiation shape factors with respect to a tilted surface and the surrounding ground, respectively. Moreover, the ground reflectance (albedo), which is the fraction of solar radiation incident on the ground that is reflected, is assumed to be the value of 0.2.

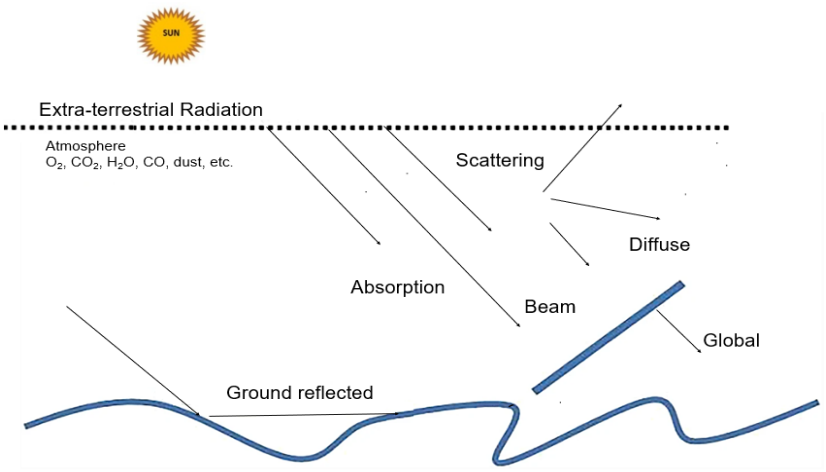

Fig. 3.7. The general components of solar radiation (Emeksiz, 2020)

For vertical chimney orientation when $\beta = 90°$, Eq. 3.1 can be rewritten as follows:

$$I_T = I_b R_b + \frac{I_d}{2} + \frac{I_h \rho_r}{2}. \quad (3.2)$$

The beam radiation conversion coefficient, R_b, could be calculated as follows:

$$R_b = \frac{\cos(\varphi - \beta)\cos\delta\sin\omega + \left(\frac{\pi}{180}\right)\omega\sin\delta\sin(\varphi - \beta)}{\cos\delta\cos\varphi\sin\omega_s + \left(\frac{\pi}{180}\right)\omega_s\sin\varphi\sin\delta}, \quad (3.3)$$

where φ is the geographic latitude of the study, β is the SAC tilted angle (Fig. 3.8), ω is the sunset angle, ω_s is the sunset angle toward the sloped surface, and δ is the sun declination angle (Eq. 3.4).

$$\delta = 23.45 \sin\left(360\frac{284 + n}{365}\right). \quad (3.4)$$

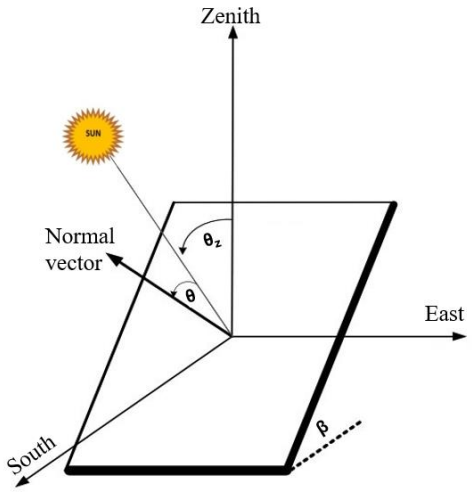

Fig. 3.8. Geometry description of south-facing solar air collector and solar chimney

The monthly average solar radiation absorbed by the SAC glass cover, S_1, is computed as (Cao et al., 2013):

$$S_1 = \bar{I}_b R_b \alpha_b + \bar{I}_d \alpha_d \frac{(1 + \cos\beta)}{2} + \bar{I}_h \rho_r \alpha_r \frac{(1 - \cos\beta)}{2}. \quad (3.5)$$

The monthly average solar radiation transmitted through the glass cover and absorbed by the absorber plate S_2, is:

$$S_2 = \bar{I}_b R_b(\tau\alpha)_b + \bar{I}_d(\tau\alpha)_d \frac{(1 + \cos\beta)}{2} + \bar{I}_h \rho_r(\tau\alpha)_r \frac{(1 - \cos\beta)}{2}. \quad (3.6)$$

3.5.2. Airflow and solar chimney

Airflow rate inside the collector/chimney under given solar radiation intensity and size based on the assumption of uniform air temperature and small density differences along the collector/chimney height is given by:

$$I_T\, H\, W = \dot{V}\, \rho\, C_P\left(T_{avg} - T_a\right), \tag{3.7}$$

where, $\dot{V}$ is the airflow rate ($m^3\, s^{-1}$), H is the height (m), W is width (m), and $T_{avg} = \frac{1}{2}(T_o + T_i)$ is the average air temperature inside the collector/ chimney.

For a vertical solar chimney, the pressure difference created in the solar chimney is (Ekechukwu and Norton, 1997):

$$\Delta P_{ch} = g\, H_{ch}(\rho_a - \rho_o). \tag{3.8}$$

The pressure difference between the SAC inlet and outlet is computed as (Cao et al., 2013):

$$\Delta P_c = \int_i^o g\left(\rho_a - \rho(z)\right)dz, \tag{3.9}$$

where, z is the SAC height and $\rho(z)$ is the density variation and calculated as:

$$\rho(z) = \rho_a + \frac{(\rho_o - \rho_a)}{H_c} z. \tag{3.10}$$

By integrating Eq. (3.9) with $\rho(z)$ from Eq. (3.10) and assuming $z = 0$ at the SAC inlet, the pressure difference generated in the SAC is:

$$\Delta P_c = \frac{(\rho_a - \rho_o)}{2} g\, H_c. \tag{3.11}$$

The total pressure difference ΔP_t, yielded due to buoyancy can be expressed as:

$$\Delta P_t = (\rho_a - \rho_o)\, g\left(H_{ch} + \frac{H_c}{2}\right) + \Delta P_{cha}. \tag{3.12}$$

3.5.3. Energetic and exergetic performance analysis

The available solar radiation, I_T, reaches the surface of the collector and solar chimney, crosses its transparent cover, but only a fraction is absorbed, causing an increase of the average temperature of the absorber. Due to the temperature difference between the absorber and the ambient air, heat is lost to the surrounding (Fig. 3.9). Heat loss in most commercial solar collectors occurs due to convective and radiative loss from the absorber surface. To improve collector efficiency, these losses from front and back surfaces must be reduced to minimum.

Energy and exergy analysis, which are based on the fundamental laws of thermodynamics, are necessary for any thermal system, such as a solar collector or solar chimney, in order to understand the basic design and performance evaluation.

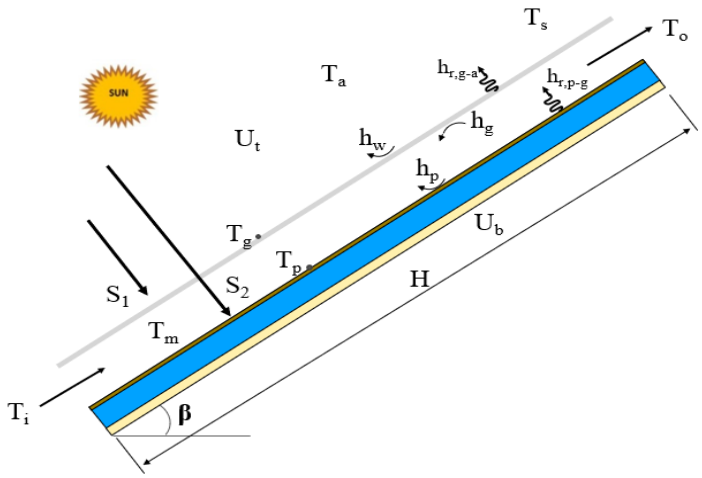

Fig. 3.9. Basic illustration and energy flows of a solar air collector

3.5.3.1. Energetic analysis

Based on the first law of thermodynamics, the useful heat gain, Q_u, from the collector was determined by applying the measured data from the experiment conducted under steady-state conditions and from the application of the Hottel-Whillier equation, Q_u expressed as (Chabane et al., 2013; Duffie and Beckman, 2013):

$$\mathrm{Q_u = \dot{m}_a\, C_p(T_o - T_i) = A_c\, F_R\,[I_T(\tau\alpha) - U_o(T_i - T_a)]}, \tag{3.13}$$

where, the term 'F_R' refers to the relationship between a collector's actual useful heat gain (useful heat gain sometimes used) and the useful heat gain if the entire collector's surface was at the fluid inlet temperature. U_o is the collector's overall heat loss coefficient. The total heat loss coefficient of the collector or chimney, U_o, is the sum of the top U_t, bottom U_b, and edges U_e of the collector. Edge losses can be neglected if proper insulation material is used.

$$\mathrm{F_R = \frac{\dot{m}_a\, C_p}{A_c\, U_0}\left[1 - \exp\left(-F\, U_o\, A_c/\dot{m}_a\, C_p\right)\right]}. \tag{3.14}$$

The top heat loss coefficient U_t, from the glass cover to the surrounding has been computed as follows (Duffie and Beckman, 2013):

$$\mathrm{U_t = \left[\frac{1}{(2.8+3V_w)+\varepsilon_g\,\sigma\left(T_p^2+T_s^2\right)\left(T_p+T_s\right)} + \frac{1}{\mathrm{Nu}\,\frac{\lambda}{L_{p-g}}+\frac{\sigma\,(T_p^2+T_g^2)(T_p-T_g)}{\left(\frac{1}{\varepsilon_g}+\frac{1}{\varepsilon_p}-1\right)}}\right]^{-1}}, \tag{3.15}$$

where, Nusselt number, N_u, of the air between absorber plate and the glass cover can be computed as follows (Duffie and Beckman, 2013):

$$\mathrm{Nu} = 1 + 1.44\left[1 - \frac{1708\,(\sin 1.8\beta)^{1.6}}{\mathrm{Ra}\cos\beta}\right]\left[1 - \frac{1708}{\mathrm{Ra}\cos\beta}\right]^{+} + \left[\left(\frac{\mathrm{Ra}\cos\beta}{5830}\right)^{1/3} - 1\right]^{+}. \quad (3.16)$$

The +, exponent in Equation 3.16 indicates that only the positive values of the terms are to be utilized and zero value is to be used for negative value.

The Rayleigh number, Ra, is given by (Duffie and Beckman, 2013):

$$\mathrm{Ra} = \mathrm{Gr}\ \mathrm{Pr} = \frac{\mathrm{g}\,\beta'\,\Delta\mathrm{T}\,\mathrm{L}^3}{\nu\,\alpha'}, \quad (3.17)$$

where:

$$\beta' = \frac{1}{\frac{(\mathrm{T_p}+\mathrm{T_g})}{2}+273}. \quad (3.18)$$

The bottom heat loss coefficient U_b, has been calculated by the basic conduction heat transfer resistance. For insulation layer with thickness t_b and material thermal conductivity λ_b (Ong and Chow, 2003):

$$\mathrm{U_b} = \frac{\lambda_\mathrm{b}}{\mathrm{t_b}}. \quad (3.19)$$

Then the energy efficiency of the SAC (η_I) or SC ($\eta_\mathrm{I,ch}$) according to ASHRAE (Abdelkader et al., 2020) is:

$$\eta_\mathrm{I} = \frac{\dot{m}_\mathrm{a}\,\mathrm{C_p}\,(\mathrm{T_o}-\mathrm{T_i})}{\mathrm{A_c}\,\mathrm{I_T}} = \mathrm{F_R}(\overline{\tau\alpha}) - \mathrm{F_R U_o}\left(\frac{\mathrm{T_i}-\mathrm{T_a}}{\mathrm{I_T}}\right). \quad (3.20)$$

From experimental data, Eq. 3.20 can be used to plot the energy efficiency curve versus $(\mathrm{T_i} - \mathrm{T_a})/\mathrm{I_T}$. Furthermore, if the terms $\left(\mathrm{F_R}(\overline{\tau\alpha})\right)$ and $(-\mathrm{F_R U_o})$ are taken to be constant, then Eq. 3.20 can be written as $Y = mx + b$, where b is the y-axis intercept and m is the slope. The slope of the line depends on the overall heat loss coefficient, where $m = -F_R U_o$. The intercept of the line depends on the transmissivity-absorptivity of the glazing and absorber plate, where $b = F_R(\overline{\tau\alpha})$ (optical gain coefficient). $(\overline{\tau\alpha}) \cong 1.01\tau\alpha$ can be approximated for most solar collectors (Duffie and Beckman, 2013). However, U_o, is not constant since it varies with the SAC and ambient air temperatures.

The outlet temperature of air in terms F_R of can be determined by:

$$\mathrm{T_o} = \mathrm{T_i} + \mathrm{F_R}\left(\frac{\mathrm{I_T}(\tau\alpha) - \mathrm{U_o}(\mathrm{T_i}-\mathrm{T_a})}{\dot{m}_\mathrm{a}\,\mathrm{C_p}}\right). \quad (3.21)$$

3.5.3.2. Exergetic analysis of the solar air collector

Exergy is a measure of energy quality that can be destroyed within a system due to its irreversibility. Due to irreversibility, some of the energy entering the collector or drying

chamber or solar chimney is destroyed within the system. The exergy of the SAC determined by the flowing air is exhibited by Eq. 3.22 (Bahrehmand and Ameri, 2015).

$$\mathrm{Ex_u} = \dot{m}_a C_p \left[(T_o - T_i) - T_a \left(\ln\left(\frac{T_o}{T_i}\right)\right)\right]. \tag{3.22}$$

The input exergy of the solar radiation is expressed by Eq. 3.23:

$$\mathrm{Ex_i} = I_T\, A_c \left[1 - \frac{T_a}{T_s}\right], \tag{3.23}$$

where T_s represent the photosphere temperature of sun and assumed to be 5600 K. The exergy efficiency of the SAC is articulated by the Eq. 3.24 (Park et al., 2014):

$$\eta_{II} = \frac{\mathrm{Ex}_u}{\mathrm{Ex_i}}. \tag{3.24}$$

The distinct physical properties of air as a function of temperature are expressed according to the following expressions (Bhushan and Singh, 2012; Ong and Chow, 2003):

$$C_p = 1006 \left(\frac{T_m}{293}\right)^{0.0155}, \tag{3.25}$$

$$\mu = 1.81 \cdot 10^{-5} \left(\frac{T_m}{293}\right)^{0.735}, \tag{3.26}$$

$$\lambda = 0.0275 \left(\frac{T_m}{293}\right)^{0.086}, \tag{3.27}$$

$$\rho = 1.1614 - 0.00353\,(T_m - 300). \tag{3.28}$$

3.6. Apple fruit preparation

The apple fruit, which accounts about 60% of all fruit grown in the country, is one of the most important fruits in Hungary (Felfoldi et al., 2011). The harvesting time of apples are from mid of September to end of October. Golden Delicious apples that were used in this study were purchased from the market. The samples of uniform size of about 60 mm in diameter were selected, cleaned with tap water, and then sliced into slices vertical to their axes before loading them into the drying chamber. The thickness of the apple slices was determined to be 4±1 mm using vernier caliper. Using a moisture analyser (Sartorius MA 30) set to 105 °C, the initial moisture content of apple slices was determined. This was done replicated three time at each experimental time to obtain a reasonable average. The initial moisture content (MC_i) of the samples was found to be about 85.6% (wet basis) with a maximum error of 0.12% and is computed using Eq. 3.30. Similar result has been reported by Rajasheker and Chandramohan (2017). The acceptable final moisture content of apple is 24% (Sharma et al., 2009). A single layer of apple slices was placed on the tray, which could accommodate around 457 g of apple slices. Two trays were with a combined sample mass of 915± 1 g were placed in the drying chamber as seen in Fig 3.10. The same amount of mass of apple slices were also dried in the

open environment for OSD. The apple slices were taken out of the drying chamber, weighed and recorded at one and a half hours intervals during the drying process.

The instantaneous moisture content of the samples during the drying time can be estimated as:

$$\mathrm{MC(t)} = \frac{\mathrm{m(t)} - \mathrm{m_{dry}}}{\mathrm{m}_{dry}}, \tag{3.29}$$

where $m(t)$ is the mass of the product at instant *t* in kg; m_{dry} is the dry weight in kg.

Fig. 3.10. Apple slices placed in trays before drying starts

3.7. Performance of the drying chamber

The study of the drying kinetics and represented them by mathematical models allows them to know their behaviour during drying. The experimentally obtained data were expressed as moisture ratio (MR):

$$\mathrm{MR} = \frac{\mathrm{MC(t)}}{\mathrm{MC}_i}. \tag{3.30}$$

The values of the experimental MR versus the time of drying were adjusted by three models widely used to model the drying kinetics of apple slices (see Table 2.2). The moisture diffusivity, D_{eff}, can be determined by the following equation:

$$\mathrm{D}_{eff} = \mathrm{slope}\ \frac{4L^2}{\pi^2}, \tag{3.31}$$

where *L* is the samples half thickness (m). The slope is found when plotting of ln (MR) vs time of drying.

The coefficient of determination (R^2), chi square (χ^2) and the root mean square error (RMSE) was used as the criterion of the goodness of fit of the experimental data against the data predicted by the mathematical models. A low value of Chi-square means a better fit. RMSE

values provide information about the deviation of the experimental data against the predicted ones. The following equations were used for the statistical analysis.

$$\chi^2 = \frac{\sum_{i=1}^{n}\left(MR_{exp,i} - MR_{pre,i}\right)^2}{N-n}, \tag{3.32}$$

$$RMSE = \left[\frac{1}{N}\sum_{i=1}^{n}\left(MR_{pre,i} - MR_{exp,i}\right)^2\right]^{1/2}, \tag{3.33}$$

$$R^2 = 1 - \frac{\sum_{i=1}^{n}\left(MR_{exp,i} - MR_{pre,i}\right)^2}{\sum_{i=1}^{n}\left(MR_{exp,i} - MR_{avg\ exp,i}\right)^2}, \tag{3.34}$$

where $MR_{exp,i}$ is the value of the experimental MR, $MR_{pre,i}$ is the i^{th} value of predicted MR, $MR_{avgexp,i}$ is the mean value of the experimental MR, *N* is the number of data observed, and *n* is the number of constants in the model (Menges and Ertekin, 2006).

The specific energy consumption (SEC) of the ISD system, which is the energy required for removing one kg of water (moisture) from a wet agricultural product during the drying process. It is defined as the ratio of the total useful energy input to the drying system (Q_u) to the amount of moisture removed from the dried product. The energy supplied to the chamber is the total od the energy received from the solar radiation incident on SAC. It is calculated by Eq. 3.35 (Moradi et al., 2020; Fudholi et al., 2013):

$$\mathrm{SEC} = \frac{Q_u}{m_w}. \tag{3.35}$$

The drying efficiency (η_d) is the ratio of energy required to evaporate the water content from the products to the total energy supplied to the dried product (Vijayan et al., 2020). Therefore,

$$\eta_d = \frac{m_w\, h_{fg}}{Q_u}, \tag{3.36}$$

where h_{fg} is the latent heat of water vapor in (kJ.kg^{-1}), m_w is the amount of water removed from the dried product and determined by Eq. 3.37:

$$m_w = m_p \frac{(MC_i - MC_f)}{100 - MC_f}, \tag{3.37}$$

where m_p is the mass of the sample (kg) at t = 0; MC_i is the moisture content at t = 0, and MC_f is the moisture content ($g_{water}/g_{wet\ matter}$) of drying samples at the end of the drying experiment.

4. RESULTS

The performance of an indirect passive convection solar dryer integrated with various solar chimney configurations was investigated using theoretical and experimental observations, and the results, together with commentaries that highlight the novel scientific findings, are presented in this chapter. There are three main sections in this chapter: no-load testing, product load testing, and new scientific findings.

4.1. Calculations on operating parameters

As a sample of calculations, the recorded measurements of a 0.75 m stack height with a 100 mm air gap thickness of SC attached to an ISD are as follows:

T_a = 27 °C	$T_{i,\,ch}$ = 48 °C	I_{Tc} = 945 W.m^{-2}	M_p = 0.915 kg
$T_{i,\,c}$ = 28 °C	$T_{o,\,ch}$ = 53 °C	I_{Tch} = 740 W.m^{-2}	MC_i = 85.6%
$T_{c,\,o}$ = 58 °C	A_c = 0.564 m^2	$A_{duct,c}$ = 0.012 m^2	MC_f = 25.09%
ρ = 1.2 kg.m^{-3}	A_{ch} = 0.375 m^2	$A_{duct,ch}$ = 0.04 m^2	h_{fg} = 2.27 MJ.kg^{-1}
C_p = 1005 J.kg^{-1}.K^{-1}	V = 0.88 m. s^{-1}	T_s = 5600 K	

- Calculations of energy efficiency

The mass flow rate of air at collector:

$$\dot{m}_c = \rho\, V\, A_{duct,c} = 0.0127 \text{ kg}.s^{-1}$$

The mass flow rate of air at chimney:

$$\dot{m}_{ch} = \rho\, V\, A_{duct,ch} = 0.0163 \text{ kg}.s^{-1}$$

The instantaneous useful heat gain of solar air collectors (Eq. 3.13):

$$Q_{u,c} = 0.0127 \cdot 1005 \cdot 23.5 = 300 \text{ W}$$

The instantaneous useful heat gain of solar chimneys (Eq. 3.13):

$$Q_{u,ch} = 0.0163 \cdot 1005 \cdot 4.9 = 80.37 \text{ W}$$

The instantaneous energy efficiency of the solar air collector (Eq. 3.20):

$$\eta_{I,c} = 100\ \frac{300}{974.7 \cdot 0.563} = 54.66\%$$

The instantaneous energy efficiency of the solar chimney (Eq. 3.20):

$$\eta_{I,ch} = 100\ \frac{80.37}{740 \cdot 0.375} = 28.96\%$$

- Calculations of exergy efficiency

The instantaneous exergy of flowing air, exergy input, and exergy efficiency of the SAC (According to Eq. 3.22, 3.23, and 3.24):

$$Ex_u = \dot{m}_a\ C_p \left[(T_o - T_i) - T_a \left(\ln\left(\frac{T_o}{T_i}\right)\right)\right] = 187.07\ W$$

$$Ex_i = I_T\ A_c \left[1 - \frac{T_a}{T_s}\right] = 503.03\ W$$

$$\eta_{II} = \frac{Ex_u}{Ex_i} = 37.24\%$$

- Calculation of drying efficiency

8.5 MJ of useful heat (Q_u) is required for the removal of 0.733 kg of water from 0.915 kg of dried product. The overall drying efficiency of the ISD is calculated as (Eq. 3.33):

$$\eta_d = \frac{m_w\ h_{fg}}{Q_u} = 100\ \frac{0.733 \cdot 2.27}{8.5} = 19.58\%$$

Where, m_w is the mass of water removed (kg), h_{fg} is the latent heat of evaporation of water ($MJ.kg^{-1}$).

4.2. Effect of solar radiation and ambient temperature on dryer performance

The performance of any solar dryer is influenced by local environmental parameters such as sun radiation, wind speed, ambient temperature, and relative humidity. These facts guided the choice of the summer season for the experiments. This period is characterized by strong solar radiation intensity and soaring ambient temperatures. Despite the unpredictable weather in Gödöllő, each experimental setup was carried out repeatedly until clear or less cloudy days were found for analysis.

Hourly variation of solar radiation at collector and chimney surfaces and ambient temperature are exemplified in Figs 4.1-4.3 for both under no-load and load conditions. It should be emphasized that data on solar radiation and ambient temperature were continuously collected. However, the data in these figures only represents the experimentation's days. The figures depict the fluctuation of solar radiation at collector and chimney surfaces as a function of the time of day. It has been observed that both profiles almost have a parabolic shape. Both gradually increased in the morning, peaked near at noon, and then began to decease in the afternoon, during all the experimental days. The trend and magnitude of the instantaneous solar radiation is the key input parameter to determine the performance of the solar dryer, all other derived parameters like collector inlet and outlet air temperature, air drying temperature, air inlet and outlet temperatures in the chimney, and the corresponding energy efficiency also

exhibit a similar pattern. The maximum solar intensity was observed between 11:50 and 12:30 h and was in the range of 920–1083 W.m^{-2} for solar radiation on collector surface (Fig 4.1). The maximum solar radiation intensity of 1083 W.m^{-2} was reported for Case_3, while Case_1 had the lowest (920 W.m^{-2}) in this time ranges. As noted in the figure, wind speed and cloud cover during the trial days caused a slight fluctuation in solar radiation. The ranges of the solar radiation at collector surface for each trial were close to each other, with Case_1 showing slight deviation, with a mean average deviation of 31.8 W.m^{-2}. For under load conditions, the peak value of the solar radiation that was reached on collector surface was 973, 944, 1045, 986, 1011, 1029, 1078, and 861 W.m^{-2} for case_1 to case_8, respectively while their corresponding averages solar radiation for all cases were 772. 711, 756, 793, 770, 697, 821, and 689 W.m^{-2}, respectively. Case_7 recorded the highest average sun radiations, whereas Case_8 recorded the lowest solar radiation.

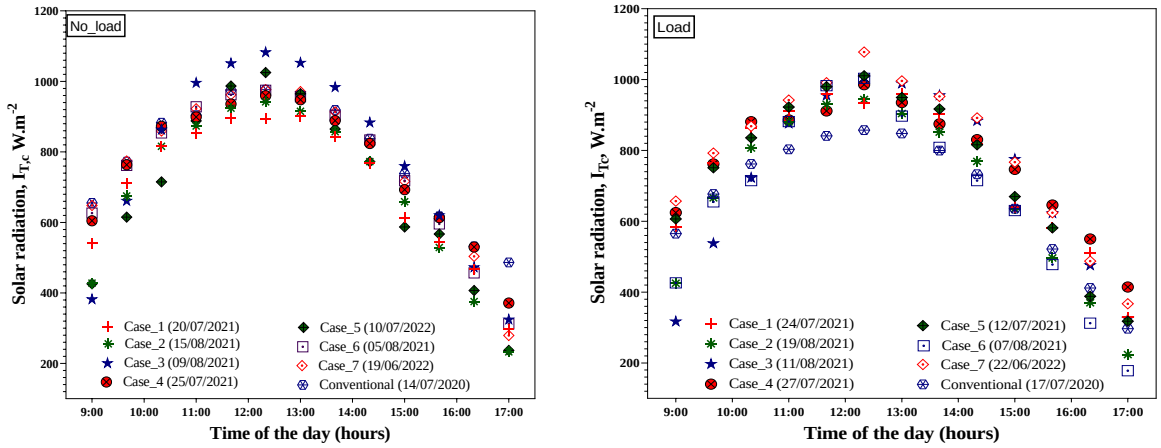

Fig. 4.1. Variation of solar radiation at collector surface under no load and load conditions

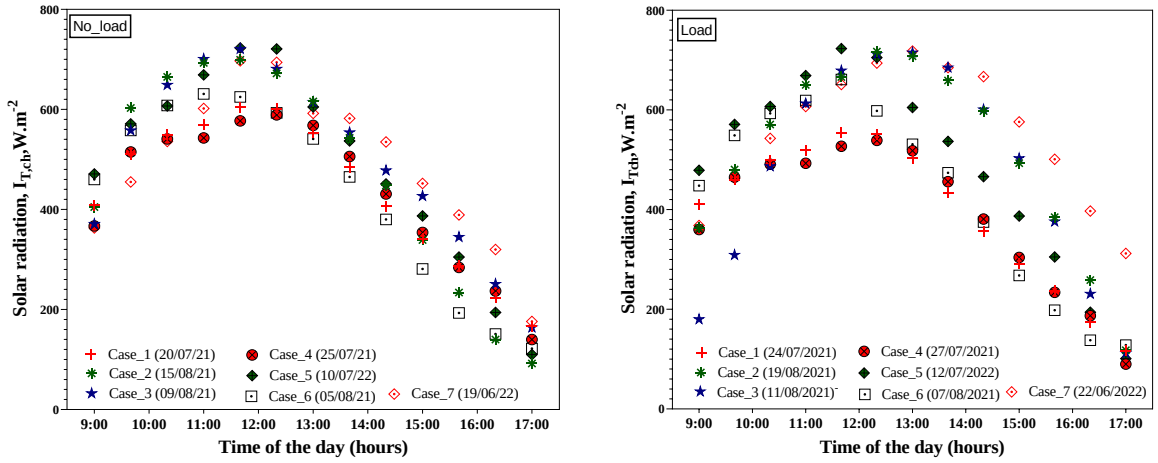

Fig. 4.2. Variation of solar radiation at chimney surface under no load and load conditions

Fig. 4.2 shows the variation of solar radiation on the surface of the SC for all scenarios as a function of the time of day. The solar intensity is much lower on the chimney surface than on the collector surface, which has an average solar intensity of about 37%, as a result of the surface orientation. Cloud cover and wind speed during various experiment days were the main contributors to variations in solar radiation and ambient temperatures. The performance of the

SACs and SCs were highly influenced by the environment, which involves many parameters like wind velocity, humidity, ambient temperature, etc. As plotted in the figure the solar radiation intensity ranged from 117 to 563 with an average of 402 $W.m^{-2}$ for Case_ 1, from 117 to 727 with an average of 535 $W. m^{-2}$ for Case_2, from 112 to 718 with an average of 499 $W.m^{-2}$ for Case_3, from 90 to 543 with an average of 399 $W.m^{-2}$ for Case_4, from 101 to 740 with an average of 502 $W. m^{-2}$ for Case_5, from 128 to 661 with an average of 437 $W. m^{-2}$ for Case_6, and from 312 to 723 with an average of 567 $W. m^{-2}$ for Case_7 while the standard deviation ranged between 120 and 169 respectively which shows the solar radiation ranges were rather close to one another. A model for forecasting the solar radiation received on solar chimney can be created based on the solar radiation data collecting conducted between June to August of 2020 to 2021. This model could reduce the number of solar meters employed on the experimental period (in this work two solar meters were used). In order to create the model data of solar radiation received on collector and chimney for each month were selected. The SAC was positioned 45° from the horizontal while the SC was facing vertically. The number of days for each month randomly selected. Seven days for each month and between 10:00 to 16:00 hours of measurements applied. The variation of solar radiation ranged between 400 to 1000 Wm^{-2} with ambient temperature ranged from 18.7 to 37.4 °C. Therefore, the developed models for month June to August were found in Eq. 4.1 to 4.3:

$$I_{SC} = 0.955\ I_{SAC} - 276.2, \tag{4.1}$$

$$I_{SC} = 0.471\ I_{SAC} + 158, \tag{4.2}$$

$$I_{SC} = 0.513\ I_{SAC} + 165. \tag{4.3}$$

During the approximation the correlation coefficient was 0.99, 0.849, and 0.988 for June, July, and August, respectively along with the standard deviation of 17%, 10%, and 14%.

Fig. 4.3 depicts the variation of ambient temperature throughout the experimental days for both no load and load condition. The maximum ambient temperature was measured 2–3 h after the peak sunshine hours. The ambient temperatures ranged from 26 to 34 with an average of 31 °C for Case_1, from 25 to 35 with an average of 32 °C for Case_2, from 19 to 32 with an average of 28 °C for Case_3, from 26 to 35 with an average of 32 °C for Case_4, from 21 to 33 with an average of 29 °C for Case_5, from 23 to 32.6 with an average of 29 °C for Case_6, from 22 to 30 with an average 27 °C for Case_7 and from 28 to 37 with an average of 35 °C for Case_8. The maximum ambient temperature was recorded for Case_8 (conventional dryer) whereas the lowest recorded was for Case_3 (19 °C). A solar meter was installed along with the SC's orientation to measure the amount of solar radiation hitting the vertical surface of the SC surfaces.

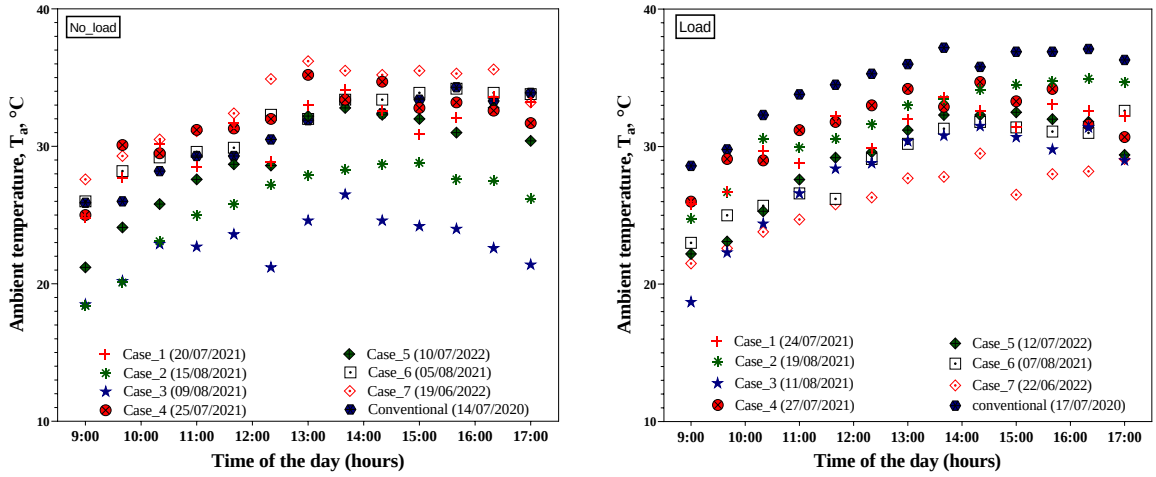

Fig. 4.3. Variation of ambient temperature under no load and load conditions

The environment, which includes several variables such as ambient temperature, ambient relative humidity, solar radiation, and wind speed, among others, had a significant impact on the effectiveness of the solar dryers. The outlet air temperature of the SAC was influenced by both solar radiation and the surrounding temperature. For the most part, the experimentation days' solar intensity values followed a consistent pattern.

With the same procedures followed to model the solar radiation received by solar chimney, a model can be developed for ambient temperatures based on the solar radiation received by SAC collector and it was found as depicted in Eq. 4.4 to Eq. 4.6 for June, July, and August respectively:

$$T_a = 0.018\, I_{SAC} + 12.1, \tag{4.4}$$

$$T_a = 0.020\, I_{SAC} + 12.5, \tag{4.5}$$

$$T_a = 0.014\, I_{SAC} + 15.1. \tag{4.6}$$

During the approximation the correlation coefficient was 0.785, 0.859, and 0.881 for June, July, and August, respectively along with the standard deviation of 8%, 8%, and 8.9%. It can be observed from the developed model, the coefficient of determination was lower in case of modelling the ambient temperature. This may be attributed to the fact that the maximum radiation on collector surface and the highest ambient temperature did not occurred at the same time.

Based on data on solar radiation and air temperature collected throughout the summer months of June through August, it was discovered that July had the greatest ambient temperature, while June had the highest solar intensity. Thus, it was determined that the average ambient temperature for July was 1.1 °C and 2.8 °C higher than for June and August, respectively. Moreover, are presented in Table 4.1 a) and b) presented only the minimum and maximum ambient temperature and solar radiation for all setups under no-load. The ranges of the solar radiation and ambient temperature of each trial were close to each other.

Table 4.1a. Summary of ambient temperature and solar intensity for Case_1 to Case_4

Description	**Case_1**	**Case_2**	**Case_3**	**Case_4**
Experimental date	20/07/2021	15/08/2021	09/08/2021	25/07/2021
Minimum ambient temperature, $T_{a,i}$ (°C)	25	18	19	25
Maximum ambient temperature, $T_{a,i}$ (°C)	34	30	31	36
Standard deviation (°C)	2.2	3.1	3.2	2.3
Minimum solar intensity, $I_{T,c}$ (W.m^{-2})	297	233	325	372
Maximum solar intensity, $I_{T,c}$ (W.m^{-2})	919	942	1084	974
Standard deviation (W.m^{-2})	178	205	237	169

Table 4.1b. Summary of ambient temperature and solar intensity for Case_5 to Case_8

Description	**Case_5**	**Case_6**	**Case_7**	**Case_8**
Experimental date	10/07/2022	05/08/2021	19/06/2022	14/07/2020
Minimum ambient temperature, $T_{a,i}$ (°C)	21	26	28	26
Maximum ambient temperature, $T_{a,i}$ (°C)	34	35	37	35
Standard deviation (°C)	3.6	2.5	2.6	2.8
Minimum solar intensity, $I_{T,c}$ (Wm^{-2})	237	312	211	487
Maximum solar intensity, $I_{T,c}$ (Wm^{-2})	1029	986	977	1014
Standard deviation (Wm^{-2})	221	188	192	158

4.3. Evaluation of solar chimney with finned absorber

In this section, a solar chimney (SC) was experimentally tested in August 2020 using the following configurations: a solar chimney without absorber; a solar chimney with absorber but without fins; a solar chimney with absorber and fins. The variations of solar radiation (I_T), ambient temperature (T_a), SC inlet ($T_{ch,i}$) and outlet temperature ($T_{ch,o}$), absorber (wall) temperature ($T_{ch,p}$), and glass temperature (T_g) for the three SC proposed are shown in Fig. 4.4. As solar radiation rises, temperatures in different locations of the SC rise from morning to peak between 12:00 and 13:00. The average value of the inlet and outlet temperature of the SC were 40 and 42 °C, 45 and 48 °C, 46 and 51 °C respectively for SC without absorber, SC without and with fins. While their corresponding average values of solar radiation and ambient temperature were 512 W m^{-2} and 30 °C, 497 W m^{-2} and 31 °C, 533 W m^{-2} and 30 °C, respectively. The mean highest absorber temperature (71 °C) was found for a SC with finned absorber. In comparison to a SC without fins and a SC without absorber, it was found that a SC with fins raised the outlet air temperature by more than 2 °C and 7 °C, respectively.

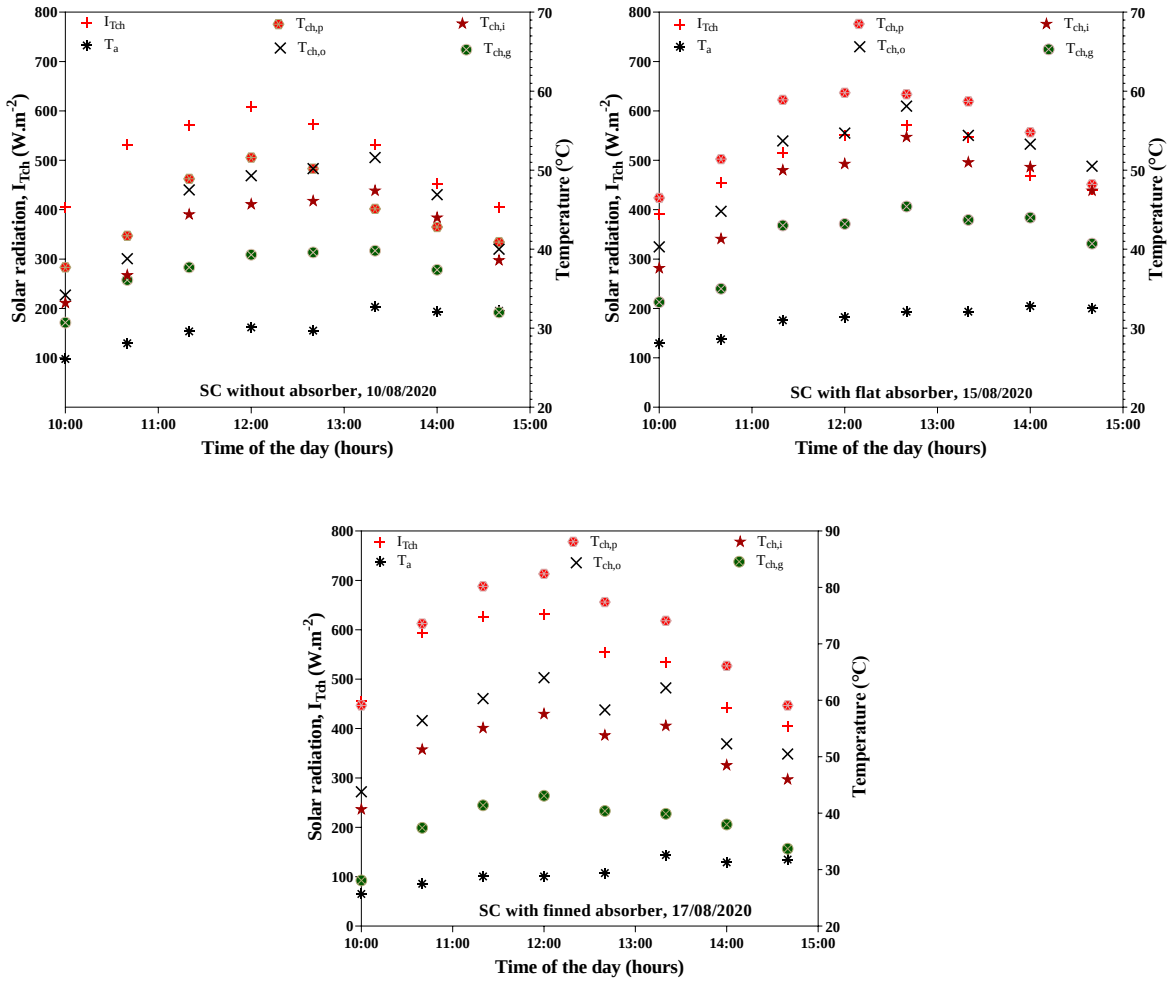

Fig. 4.4. Comparison between SC without absorber, SC with and without fins

In addition, the temperature difference between the mean air temperature inside the SC and the ambient temperature was 11, 15, and 19 °C for a SC without absorber, without fins and with fins, respectively. These temperature variations create a buoyancy effect in the chimney that causes air to flow. These results revealed that the SC performed better when a finned absorber was used. Therefore, all proposed solar chimneys have a finned absorber.

4.4. Effect of type of solar chimney under no-load conditions

The ISDs were subjected to a no-load test to fully explain the trends in various operating parameters related to drying time. It's also vital to consider how operational and environmental conditions affect the dryer's performance. The effects of the various solar chimney configurations described in section 3 on drying process are deduced and discussed while comparing the results with one another.

4.4.1. Temperature in solar air collector and solar chimney at various chimney setups

Fig 4.5 shows the temperature profile of novel ISD of 0.75 m stack height and 50 mm air gap thickness (Case_2) in SAC, and a conventional dryer. Other SC setups temperature profile can be found in Appendix A5. The average inlet and outlet air temperature of the collector, mean

plate temperature, mean glass temperature, and solar insolation during the day of trials. This observation was consistent with Arunsandeep et al. (2018). The temperature of the SAC outlet ranged between 50 to 60 °C. After passing through collector, air temperature was reduced to 45 to 52 °C in the drying chamber. The ambient temperature, solar radiation at SAC and SC were in the range of 18–37 °C, 233–1083 Wm^{-2} and 92–740 Wm^{-2}, respectively. During the experiment periods, the behavior of solar radiation had a significant effect on the thermal performance of the SAC and SC.

As solar radiation increased, the temperature inside the ISD also increased and followed a similar pattern. The maximum outlet air temperature in the collector was attained at 12:50. The highest absorber plate temperature was 87 °C at 1000 Wm^{-2} of solar radiation while the lowest temperature was 41 °C at 17:00 at 233 Wm^{-2} of solar radiation. It's evidence that the SAC outlet temperature raised the temperature of the surrounding air by about 5 °C during low radiation compared to 20 °C during high radiation hours.

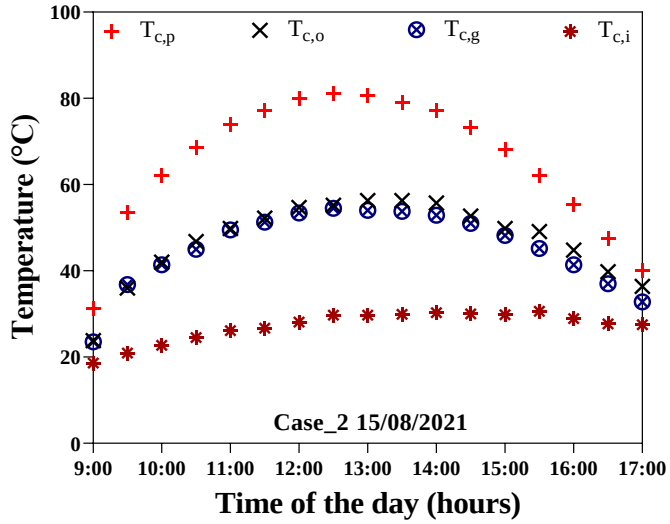

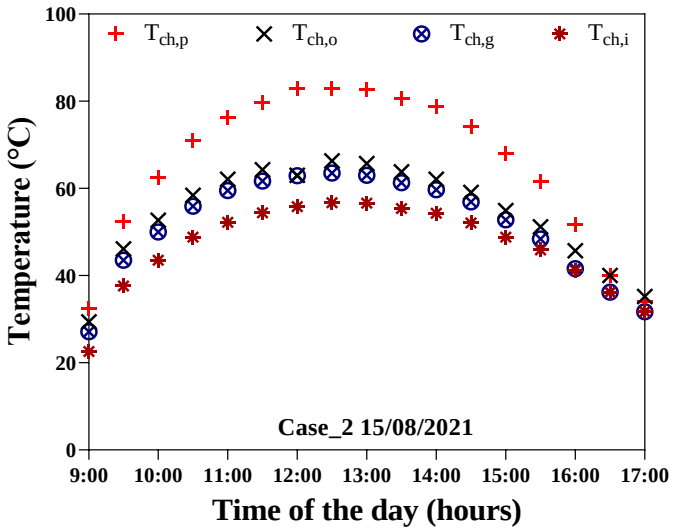

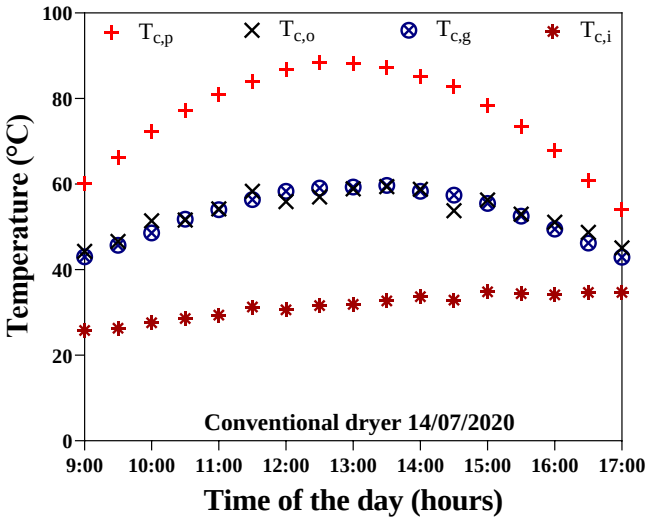

Fig. 4.5. Temperature profile at different locations for Case_2 and conventional dryer

The temperatures inside the dryer increased with the daytime and begins to fall in the afternoon hours. This trend is similar to the solar radiation trends. While the minimum temperature was 41 °C at 17:00 when the radiation was 233 Wm^{-2}, the maximum output temperature and plate temperature in the collector were found to be 67 °C in the traditional dryer and 92 °C in Case_2. It is also important to mention that the SAC increased the ambient temperature in low radiation times by around 5 °C against 20 °C for high radiation times.

4.4.2. Effect of type of solar chimney on temperature rise in solar chimney and collector

The air gap between the cover glass and the absorber plate as well as the collector length are two crucial design factors for solar air collectors or chimneys. Due to their effect on the rate of heat transfer from the absorber plate to the heated air, these parameters are significant. As the air gap thickness increases, buoyancy forces overcome friction forces, increasing the mass flow rate in the air gap channel. With change of the heat transfer coefficient, heat transfer rate to the air flow and consequently energy efficiency will change. However, the outlet temperature of air flow is decreased as the air gap thickness is increased.

The effect of air gap and stack height of SC on the air temperature difference in solar chimney, ($\Delta T_{ch} = T_{ch,o} - T_{ch,i}$) are illustrated in Fig. 4.6 a) to c). Similar trend of all profiles of the studied solar chimney heights was observed. The air temperature difference increased with increasing the solar intensity. The average ΔT_{ch} for Cases 1 to 7 was 6.7, 7.6, 4.7, 5.7, 6.8, 3.6, and 7.4 °C, respectively (Fig. 4.6). As can be seen in Fig 4.6. a), a SC configuration of 0.75 m height (Case_2) had 0.1 to 1.4 °C and 0.8 to 3.2 °C higher temperature as compared to a SC configuration of 1 m (Case_1) and 0.5 (Case_3) stack height respectively. Moreover, the temperature rises in the SC rose by more than 1.5 °C as the air gap thickness reduced from 100 to 50 mm. The same result was observed in Fig. 4.6 b), where a SC configuration with a 0.75 m height is superior to those with a 0.5 m and 1 m height. When compared to Cases 1 and 4, which have the same SC height, Case7's air temperature differential is greater due to Case7's SC tilt Fig. 4.6 c). The air temperature differential is greater in Case_7 than it is in Case_1 or Case_4, despite the identical SC height, since Case_7 has its glass cover tilted to the horizontal.

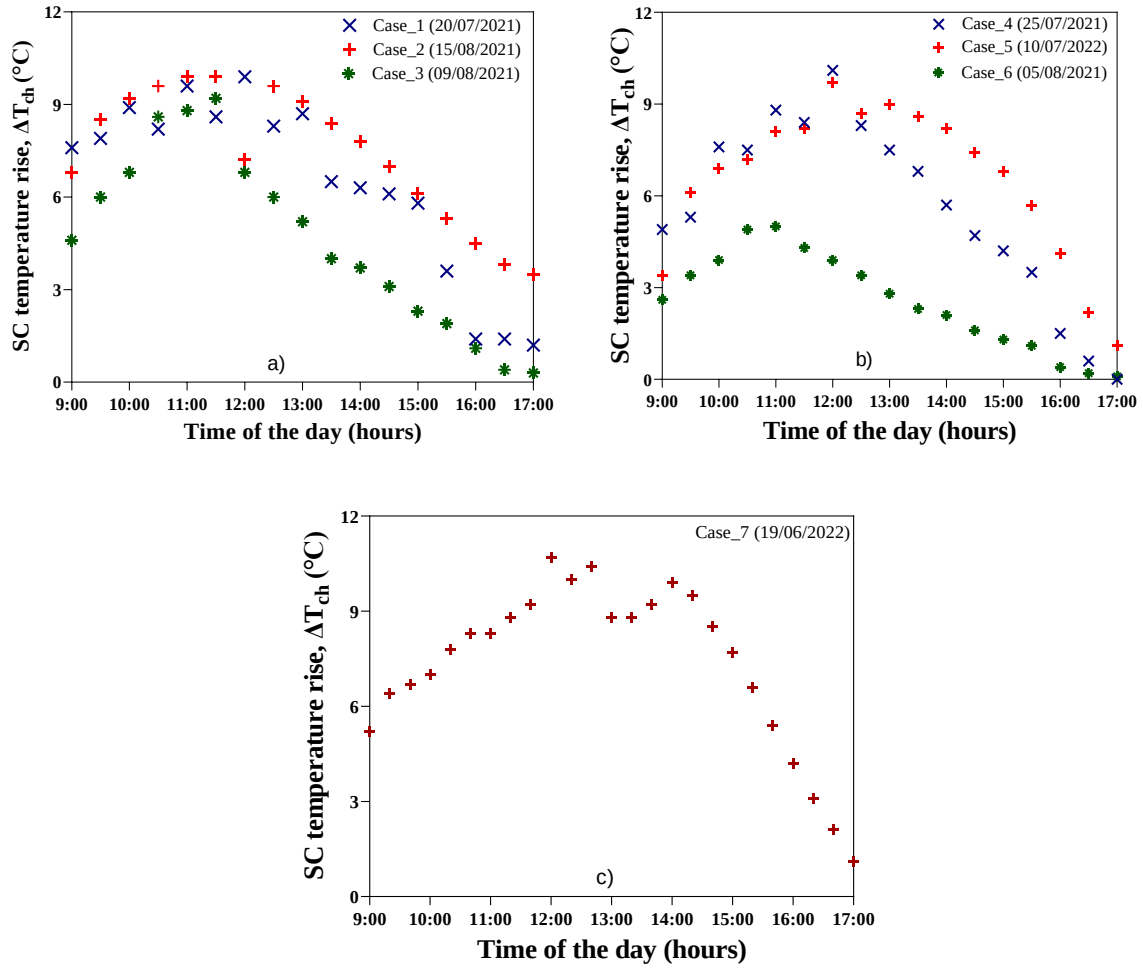

Fig. 4.6. Comparison of the SC air temperature difference for; a) 50 mm air gap, b) 100 mm air gap, and c) a non-uniform air gap

According to Fig. 4.6, it has been observed that 50 mm air gap thickness had a temperature difference that was between 0.9 and 1.1 °C higher than the 100 mm air gap thickness. This can be explained that small air volume for the narrow air gap led to a higher temperature for the air leaving the SC. Similar result was reported by Dheyab et al. (2019). Due to the low solar intensity and thermal characteristics of the SC absorber, the effect of the SC is ineffective after 16:00 h. The collector with the smallest air gap would be heated up more than the ones with wider air gaps, if all the suggested designs were subjected to the same amount of solar intensity value. This finding pointed out that Case_2 (50 mm air gap and 0.75 m stack height) and Case_7 (1 m stack height with non-uniform air gap thickness) were shown to have the best SC setups.

The impact of stack height on temperature rise in the SAC is also depicted in Fig. 4.7. According to the figure, the maximum and average air temperature rises were 26 and 18 °C, 27 and 21 °C, 32 and 25 °C, 25 and 16 °C, 24 and 18 °C, 25.7 and 19 °C, 27 and 18 °C, for Case_1 through 7, respectively. As seen from the figure, the temperature rises in the SAC rose by about 7.5 °C as the air gap thickness reduced from 100 to 50 mm. Moreover, as the stack height increases from the 0.5 m to 1 m the effect of air gap thickness becomes negligible.

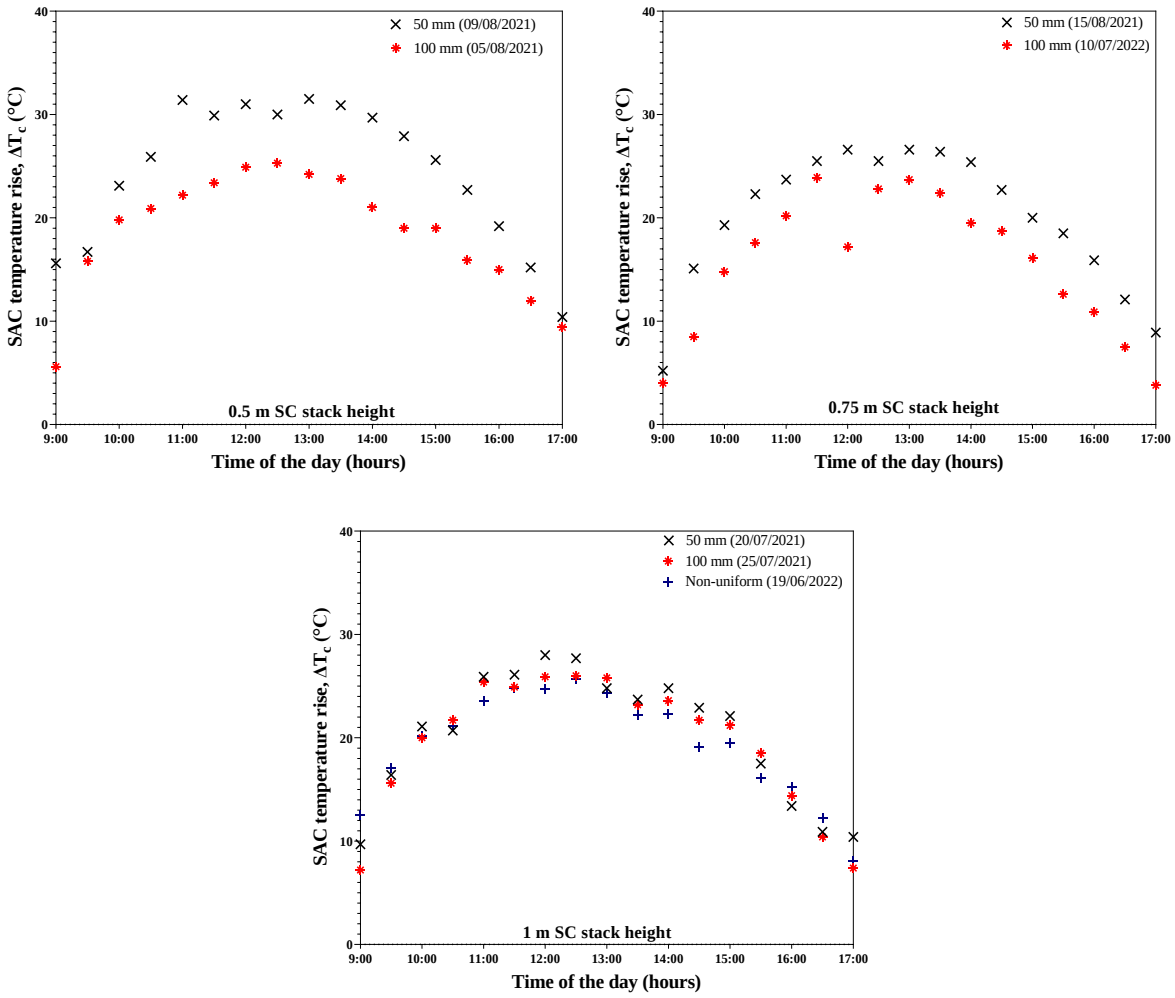

Fig. 4.7. Comparison of the SAC air temperature rise based on SC stack height

4.4.3. Temperature variation on drying chamber

The variation of drying chamber air temperature versus the time of day at different setups is demonstrated in Fig. 4.8. shows the average hourly variation of the drying temperature inside the drying chamber for various setups, under no-load conditions. According to the figure, for Cases 1 through 7 and conventional dryer, the hourly air temperature inside the drying chamber varied from 34 to 63.5 °C, 39 to 68.5 °C, 40 to 70 °C, 40 to 59 °C, 42 to 66 °C, 44 to 67 °C, 33 to 58 °C, and 43.5 to 61 °C, respectively, with corresponding relative standard deviations of 17.6, 18.2, 12.6, 17.4, 17.1, 12.1, 10.0, and 14.3%. These variations on air temperature can be explained due to the variation of solar insolation in each trial as well as the outlet temperature of the SACs.

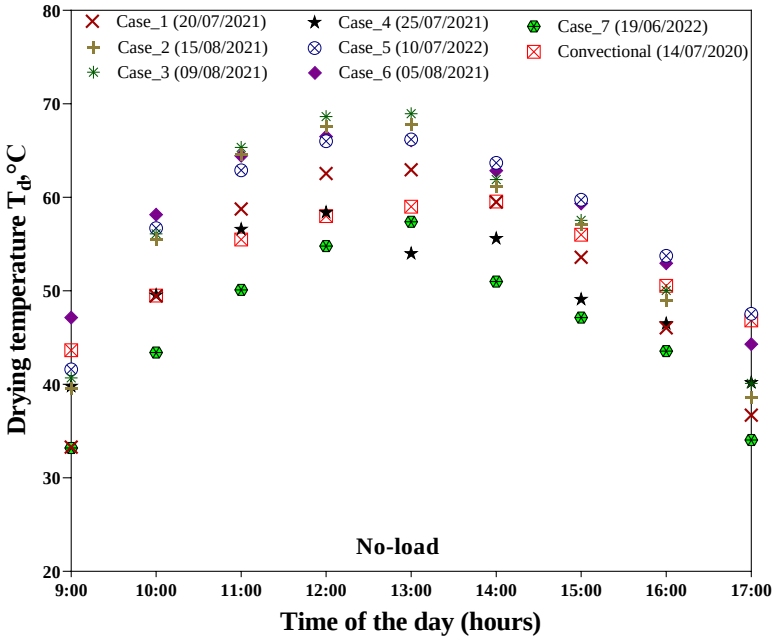

Fig 4.8. Variation of hourly average drying temperature for all setups

It clearly indicates that the drying chamber air temperature profiles of the various setups follow a decreasing and increasing trend that is directly related to the amount of solar insolation during the day. The highest drying air temperatures recorded between 12:10 and 13:50 in all experimental periods. According to the results, the average drying air temperatures for novel ISDs (Case_1 through Case_7) and conventional dryer were 53 °C, 57.5 °C, 58 °C, 51 °C, 59 °C, 59.5 °C, 47 °C, and 54 °C, respectively. Fig. 4.8 clearly shows that the drying air temperature above 45 °C was achieved in each configuration between 10:00 and 16:00, with the exception in some configurations due to cloudiness. A temperature range of 40 to 60 °C inside the drying chamber is appropriate for drying agricultural products (Bennamoun and Belhamri, 2003).

4.5. Effects of type of solar chimney under full load conditions

The variations of collector inlet air temperature, collector outlet air temperature, collector glass temperature, collector absorber temperature, chamber air temperature, chimney inlet air temperature, chimney outlet air temperature, chimney glass temperature and chimney absorber temperature, solar radiation and relative humidity of the surrounding and inside the drying temperature and moisture loss of the dried product for each setup during the drying period for drying apple slices and used to compare and evaluate the performance of the ISD. During the experimentation days, the ambient temperature, solar radiation at SAC and SC were in the range of 19–37 °C, 224–1078 Wm^{-2} and 90–740 Wm^{-2}, respectively.

4.5.1. Solar air collector and chimney temperatures for different chimney setups

Fig. 4.9 shows the variation of change of temperatures recorded as a function of time in SAC and SC for Case_2, while appendix A6 provided temperature changes for other configurations. As can be seen from the figure, the variation pattern was similar for all configurations except for the inlet air temperature, follow the same general pattern as the solar radiation curve. They followed a parabolic form with lower values in the early morning and late afternoon while the

peak occurred between 12:00 and 13:20 since solar radiation was at its highest at this time. The behavior of the air temperature at the collector outlet was consistent with the findings of the previous study (Lingayat et al., 2020a). From the figure, the average values of the collector's inlet air, outlet air and absorber temperatures were 32, 52, and 74 °C for Case_1, 33, 54.5, and 78 °C for Case_2, 29, 51 and 68 °C for Case_3, 33, 51.5 and 72 °C for Case_4, 28, 46.5, and 63 °C for Case_5, 31, 57, and 72 °C for Case_6, 28, 49, and 68 °C for Case_7 and it was 36, 56.5, and 75.5 °C for conventional dryer (Case_8), respectively. The inlet air temperature depended on the surrounding environment.

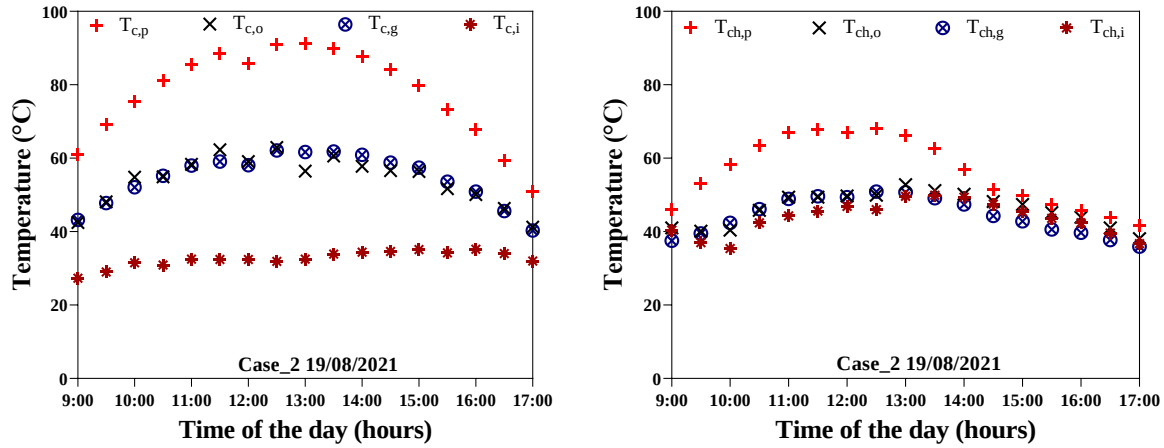

Fig. 4.9. Temperature profile in SAC and SC of Case_2 under load conditions

The wind velocity, which was a significant factor affecting the collector inlet air temperature, was the cause of the changes on some days of the experiment. As can be seen in the figure, the temperature difference between the air temperature at the collector's outlet and the ambient air was determined to be between 17.5 and 28 °C. The experimental data also reveals that there was an average temperature difference of more than 20 °C between SAC's outlet and inlet temperature. The figures in appendix A.6. c) also show that during the experimentation day, the outlet air temperature remained within the range that is useful for drying purposes. In the later part of the day, when the solar intensity is lower, heat that has been absorbed by the collector plate is released to the flowing air, keeping the temperature of the outlet air high. Karim and Hawlader (2006b) also reported similar results.

Table 4.2 a) and b) provides a summary of the minimum, maximum, and standard deviation of the collector's temperatures. As can be seen from the Tables, with an increase in inlet air temperature, the values of outlet air temperature and absorber temperatures also increased. This finding demonstrates that the inlet air temperature and solar radiation are the main determinants of the temperature of the collector's outlet air and absorber. The temperature of the inlet was affected by the state of the surrounding environment. It can be noted that higher absorber temperatures, however, result in large thermal losses.

Table 4.2a. Summary of collector's temperatures for Case_1 to Case_4

Description	**Case_1**	**Case_2**	**Case_3**	**Case_4**
Experimental date	24/07/2021	19/08/2021	11/08/2021	27/07/2021
Minimum inlet temperature, $T_{c,i}$ (°C)	27.4	27.3	17.7	27.0
Maximum inlet temperature, $T_{c,i}$ (°C)	34.5	35.5	32.9	36.3
Standard deviation (°C)	2.1	2.1	3.6	2.3
Minimum outlet air temperature, $T_{c,o}$ (°C)	43.3	41.2	30.3	38.0
Maximum outlet temperature, $T_{c,o}$ (°C)	61.7	62.9	61.1	61.2
Standard deviation (°C)	4.6	5.8	7.8	6.4
Minimum absorber temperature, $T_{c,p}$ (°C)	51.6	50.8	24.6	43.3
Maximum absorber temperature, $T_{c,p}$ (°C)	86.8	91.9	83.1	86.8
Standard deviation (°C)	11.1	11.3	14.7	11.2

Table 4.2b. Summary of collector's temperatures for Case_5 to Case_8

Description	**Case_5**	**Case_6**	**Case_7**	**Case_8**
Experimental date	12/07/2022	07/08/2021	22/06/2022	17/07/2020
Minimum inlet temperature, $T_{c,i}$ (°C)	19.7	23.2	22.2	28.0
Maximum inlet temperature, $T_{c,i}$ (°C)	33.0	35.0	31.1	41.0
Standard deviation (°C)	3.7	3.2	2.4	3.1
Minimum outlet temperature, $T_{c,o}$ (°C)	32.0	37.0	35.0	45.2
Maximum outlet temperature, $T_{c,o}$ (°C)	55.7	70.0	57.6	67.4
Standard deviation (°C)	7.3	6.1	6.0	5.2
Minimum absorber temperature, $T_{c,p}$ (°C)	32.0	37.0	48.0	55.6
Maximum absorber temperature, $T_{c,p}$ (°C)	79.4	85.5	81.8	86.5
Standard deviation (°C)	14.3	11.5	10.8	9.4

4.5.2. Type of solar chimney impact on collector air temperature rise and mass flow rate

The heat losses of the solar collector or solar chimney are significantly influenced by natural convection in the air space between the absorber and the glass cover. Fig. 4.10 shows the impact of chimney air gap on the collector performance (difference between outlet and inlet air temperature) for all ISD setups. In all setups, the temperature difference increased from morning to reach its maximum at noon and then slowly decreased from 13:00 to 17:00 in a similar pattern as the solar radiation. The solar intensity and air temperature difference showed a strong correlation, and as the solar intensity increased, so did the air temperature difference.

As shown in the figure, ΔT_c was greater for 0.5 m stack height and 50 mm SC air gap (Case_3) followed by Case_2, which was 35 and 31 °C respectively whereas a 1 m stack height and 50 mm air gap (Case_1) was the lowest record (19.7 °C). This is due to the high SC height and large air gap, which causes an increase in airflow rate and a drop in ΔT_c. Considering same air gap of 50 mm, it was found that Case_3 had a temperature difference of 5.5 °C and 7 °C higher than Case_1 and Case_2 respectively. A 50 mm air gap indicates a temperature rise of between 1 and 4 °C greater when compared to the temperature rise of a 100 mm air gap thickness. The summary of the temperature rise (ΔT_c) of a SAC for all setups shown in Table 4.3.

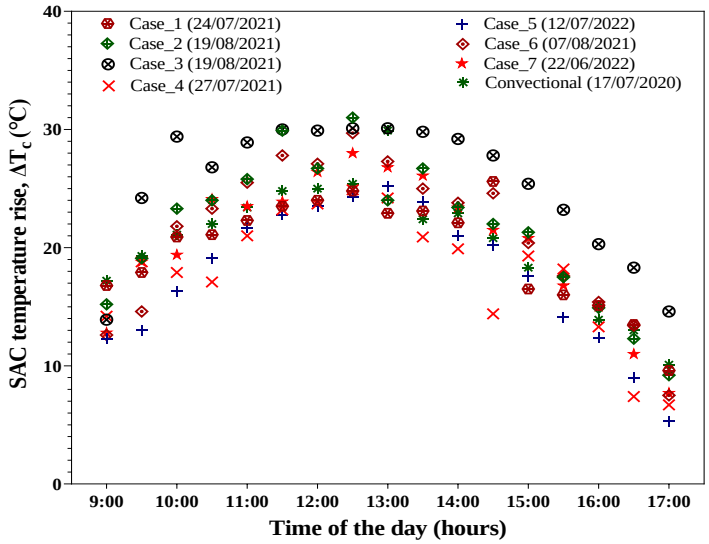

Fig. 4.10. Temperature difference versus time of the day for SAC for all experimental setups

Table 4.3. Minimum, maximum, average of temperature rises and mass flow rate for all cases

Setup	ΔT_c (°C)			$\dot{m}_a$ (kgs^{-1})		
	Min	Max	Average	Min	Max	Average
Case_1	10	30	20	0.0086	0.018	0.014
Case_2	9	31	22	0.0068	0.016	0.013
Case_3	14	35	26	0.0045	0.014	0.011
Case_4	7	26.5	18	0.0088	0.021	0.016
Case_5	5	25	18	0.011	0.018	0.014
Case_6	7.5	30	21.5	0.0034	0.016	0.012
Case_7	8	29	21	0.0098	0.021	0.017
Conventional	10	30	20.5	0.0043	0.008	0.007

Table 4.3 also shows the effect of types of SC configurations on mass flow rate of the dryer unit. The maximum and average mass flow rates were found to be 0.018 and 0.014 kg s^{-1}, 0.016 and 0.013 kg s^{-1}, 0.014 and 0.011 kg s^{-1}, 0.021 and 0.016 kg s^{-1}, 0.018 and 0.014 kg s^{-1}, 0.016 and 0.012 kg s^{-1}, 0.021 and 0.017 kg s^{-1}, and 0.008 and 0.007 kg s^{-1}, for novel ISD configurations and conventional dryer, respectively. It is reasonable to expect that a higher SAC temperature rise will result in a lower air mass flow rate. According to the result, a non-uniform SC configuration was found to produce the maximum air flow rate compared to the other settings. This can be explained by the fact that the front wall (glass) of this configuration was inclined to the horizontal, receiving more solar radiation than the other setups. Moreover, the air flow rate was found low for a 50 mm air gap thickness. The air flow rate increased by 31% as the height of the SC stack raised from 0.5 to 1 m and a 3.72 °C decrease in temperature rise. It has been noted that SC stack height and air gap thickness both have an impact on the air flow rate and temperature rise in the SAC. The amount of solar radiation that the collector receives is one of the factors that affects the air mass flow rate and SAC's outlet air temperature. Therefore, based on the data collection, this effect can be modelled for future use for predicting the air mass flow as well as the collector' outlet temperature. The operating solar radiation range of 500 to 950 W m^{-2} and collector inlet air temperature ranged from 19.8 to 36.4 °C were

considered in this model. Based on the experimental finding, the developed model for both air mass flow and collector's outlet temperature presented in Eq. 4.7 and Eq. 4.8.

$$\dot{m}_a = 0.535 + 0.00163 \cdot 10^{-2}\, I_{Tc}. \quad (4.7)$$

During the approximation, the correlation coefficient was 0.95 along with standard deviation of 0.118 kg s^{-1}. It should be noted that this model operated between 0.008 and 0.021 kg s^{-1}. The correlation between solar radiation and collector's outlet air temperature was also developed with the same input range of solar radiation and inlet air temperature. It was determined as:

$$T_{c,o} = 29.3 + 0.0487\, I_{Tc}. \quad (4.8)$$

The correlation coefficient was 0.96 along with standard deviation of 2.014 °C.

Based on the experimental data and with the help of least squares method, a linear equation was developed that can relate SAC air temperature difference (ΔT_c) between inlet and outlet and solar intensity which is shown in Fig. 4.11. Table 4.4 presented the standard deviation and the correlation coefficient of each setup. The scatter of the data was noticed closely clustered as the ΔT_c increased in all cases. It has been observed that ΔT_c increased as the solar intensity increases. According to the figure, the average air temperature rise was about 20 °C above ambient air temperature.

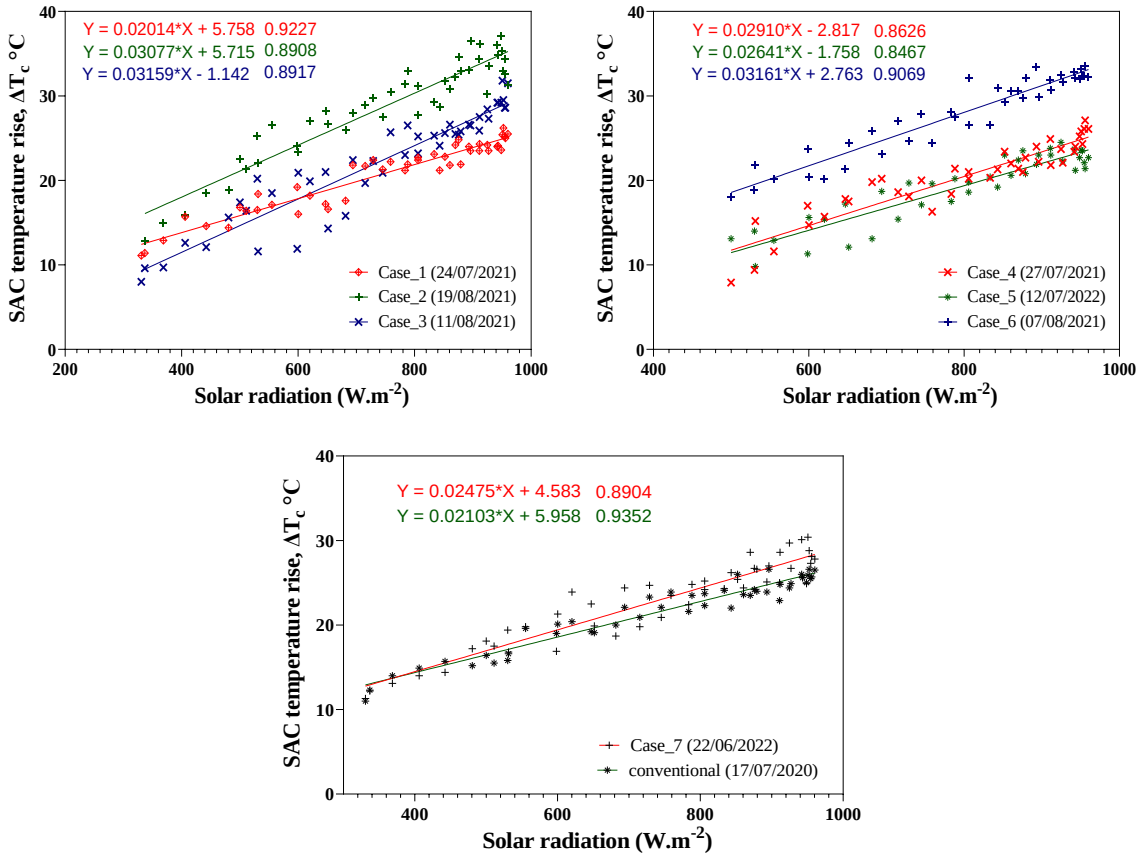

Fig. 4.11. Correlation between SAC's air temperature rise and solar intensity for all experimental setups

Table 4.4. The theoretical model for each setup

Description	Equations	SD	R^2
Case_1	$\Delta T_c = 0.0206\, I_T + 4.842$	1.049	$R^2 = 0.933$
Case_2	$\Delta T_c = 0.0266\, I_T + 10.040$	1.879	$R^2 = 0.904$
Case_3	$\Delta T_c = 0.0276\, I_T + 1.437$	1.819	$R^2 = 0.926$
Case_4	$\Delta T_c = 0.0328\, I_T - 6.203$	1.464	$R^2 = 0.927$
Case_5	$\Delta T_c = 0.0270\, I_T - 3.304$	1.738	$R^2 = 0.908$
Case_6	$\Delta T_c = 0.0198\, I_T + 14.070$	1.424	$R^2 = 0.910$
Case_7	$\Delta T_c = 0.0271\, I_T + 0.247$	1.375	$R^2 = 0.936$
Case_8	$\Delta T_c = 0.0248\, I_T + 4.438$	1.128	$R^2 = 0.928$

4.5.3. Impact of solar chimney type on energy efficiency

Understanding the fundamental design and performance of any thermal system requires the use of energy and exergy (2E) analysis. The anticipated fluctuation in solar air collector efficiency was depended on the time of day, solar irradiation, ambient air temperature, air velocity and mean temperature of the absorber plate.

An energy analysis of the drying system was done to ascertain the effect of the solar chimney type on the system's performance. The useful heat gain for each dryer setups was calculated using Eq. (3.13). The energy efficiency of the SAC (η_I) was computed using Eq. (3.20) and the results are plotted in Fig. 4.12. Fig. 4.13 shows the variation of useful heat gain ($\dot{Q}_u$) and thermal efficiencies (η_I) for setups. According to the figure, the hourly variation of useful heat gain and instantaneous efficiencies were proportional to solar radiation falling on SAC, as previously discussed for all setups.

Additionally, the interval between 10:30 and 15:00 found the highest values of the $\dot{Q}_u$ for the novel ISD. The variation of $\dot{Q}_u$ ranged from 129.96 to 408.13 W for Case_1, 131.79 to 479.81 W for Case_2, 57.79 to 449.92 W for Case_3, 130.09 to 370.46 W for Case_4, 103.26 to 411.05 W for Case_5, 75.03 to 356.19 W for Case_6, 147.64 to 429.15 W for Case_7, and it varied between 60.01 and 228.87 W for conventional dryer, (about 75% of the total useful energy found between 10:00 to 14:00), whereas the corresponding average energy efficiency was 60.12, 63.53, 59.84, 55.52, 61.96, 50.11, 59.98, and 37.82 for Case_1 to 8 and conventional dryer, respectively.

The result showed that the highest efficiency was achieved by Case_2, followed by Case_1 (1 m height and 50 mm air gap) and Case_5 (0.75 m height and 100 mm air gap), while conventional dryer had the lowest efficiency. The SC with a 0.75 m height and 50 mm air gap arrangement is therefore the best configuration. The results revealed that the energy efficiency of the novel dryer was increased by 32.5% to 68% when it was compared with the conventional dryer. This result is in good agreement with the result obtained by Russon et al. (2009). Furthermore, results showed that increasing the SC height up to a definite point and decreasing the air gap was favorable.

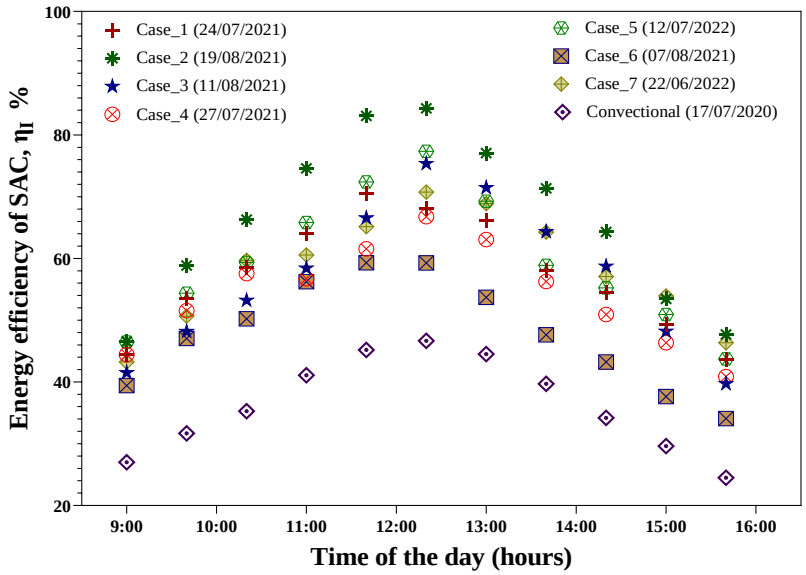

Fig. 4.12. SAC efficiency comparison for various setups

A SC with a small air gap performed better overall than one with a larger air gap, which represented an improvement of an average of 13% in performance. It has been found that enhancing collector efficiency depends on both solar intensity and ambient temperature (Appendix A7). To boost the efficiency, both the solar intensity and ambient temperature should be higher.

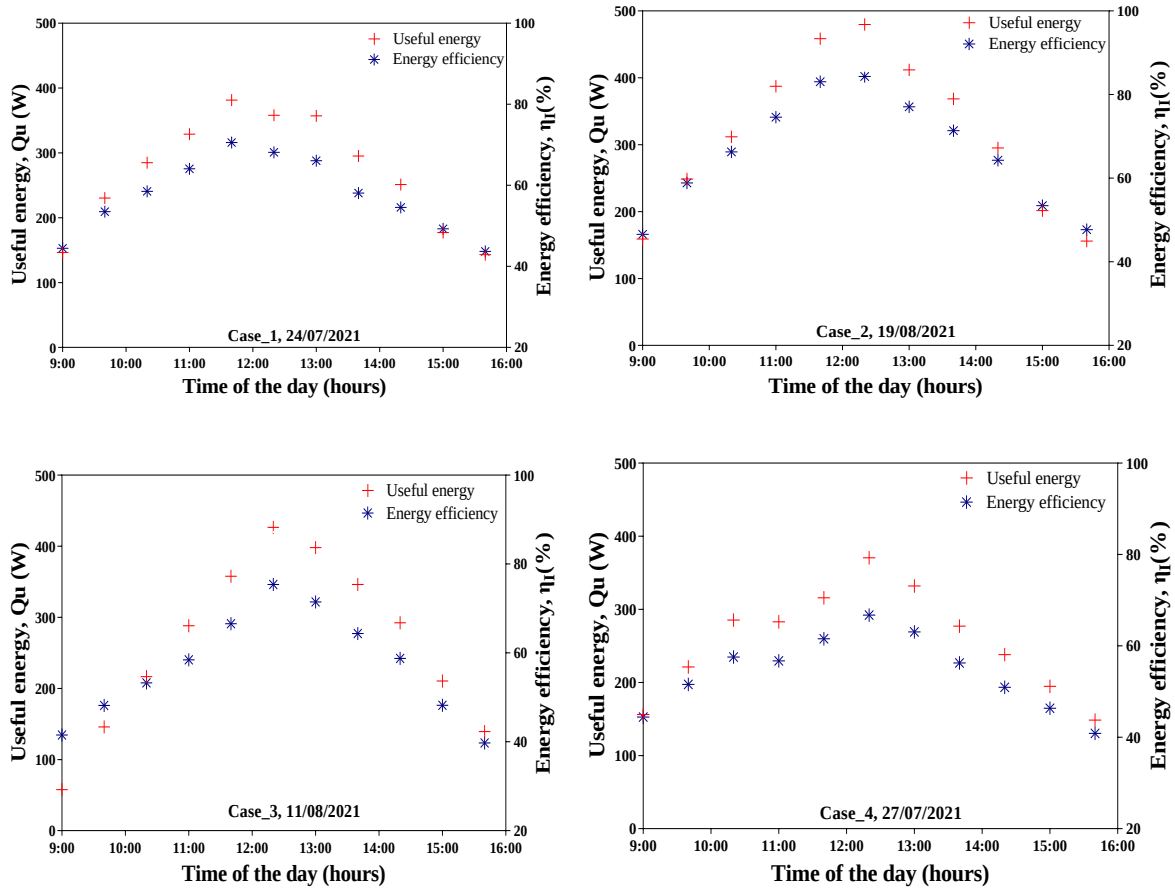

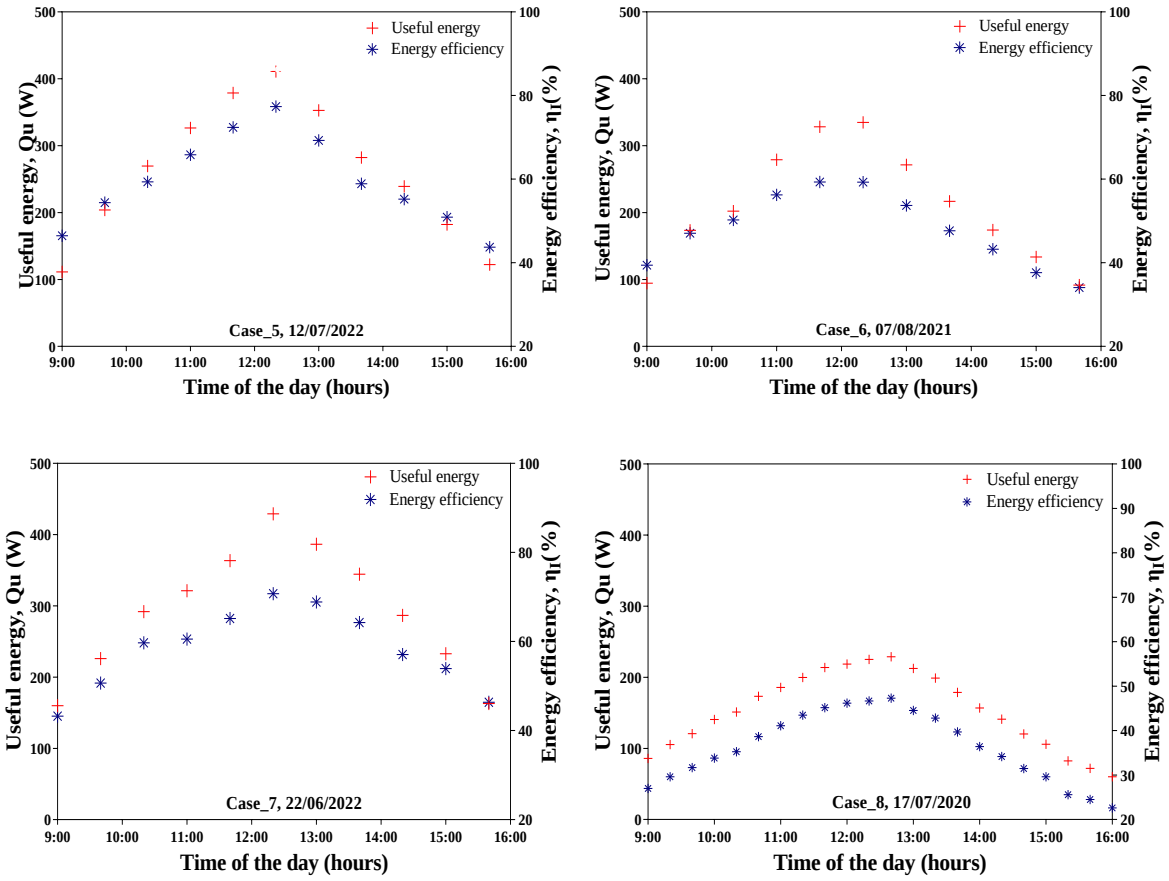

Fig. 4.13. Average useful heat gain and energy efficiency of SAC by different type SC setup

Using the trapezoidal rules, the daily total useful heat gain ranged from 1.1 to 2.26 kWh as shown in Fig. 4.14. It can be observed that Case_2 had the maximum heat gain whereas the conventional dryer had the lowest.

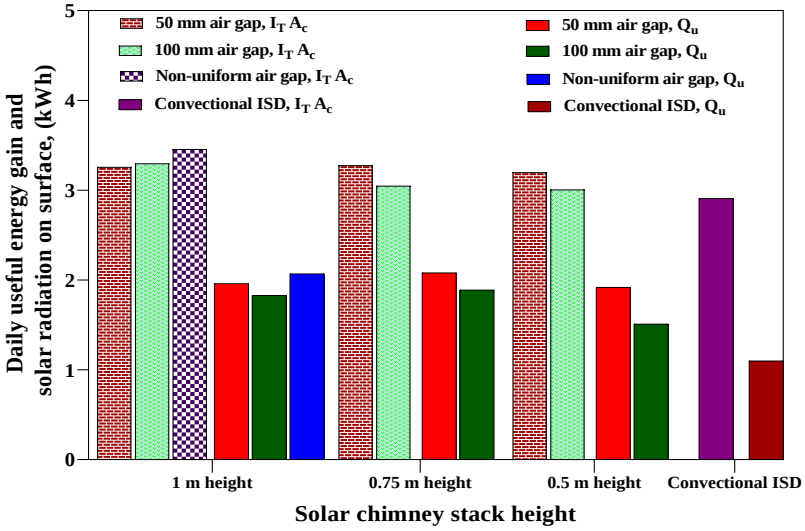

Fig. 4.14. Average daily heat input and useful heat gain for all setups

For the same SC height, a small air gap thickness outperformed one with a big air gap, while for the same SC air gap thickness, a medium SC height outperformed both large and small stack heights (Fig 4.15). This is because air flow rate higher for small air gaps. Another finding showed that a SC with non-uniform cross-section setup shows higher value of heat gain than those with constant air gap SC (2.07 kWh against 1.96 and 1.83 kWh).

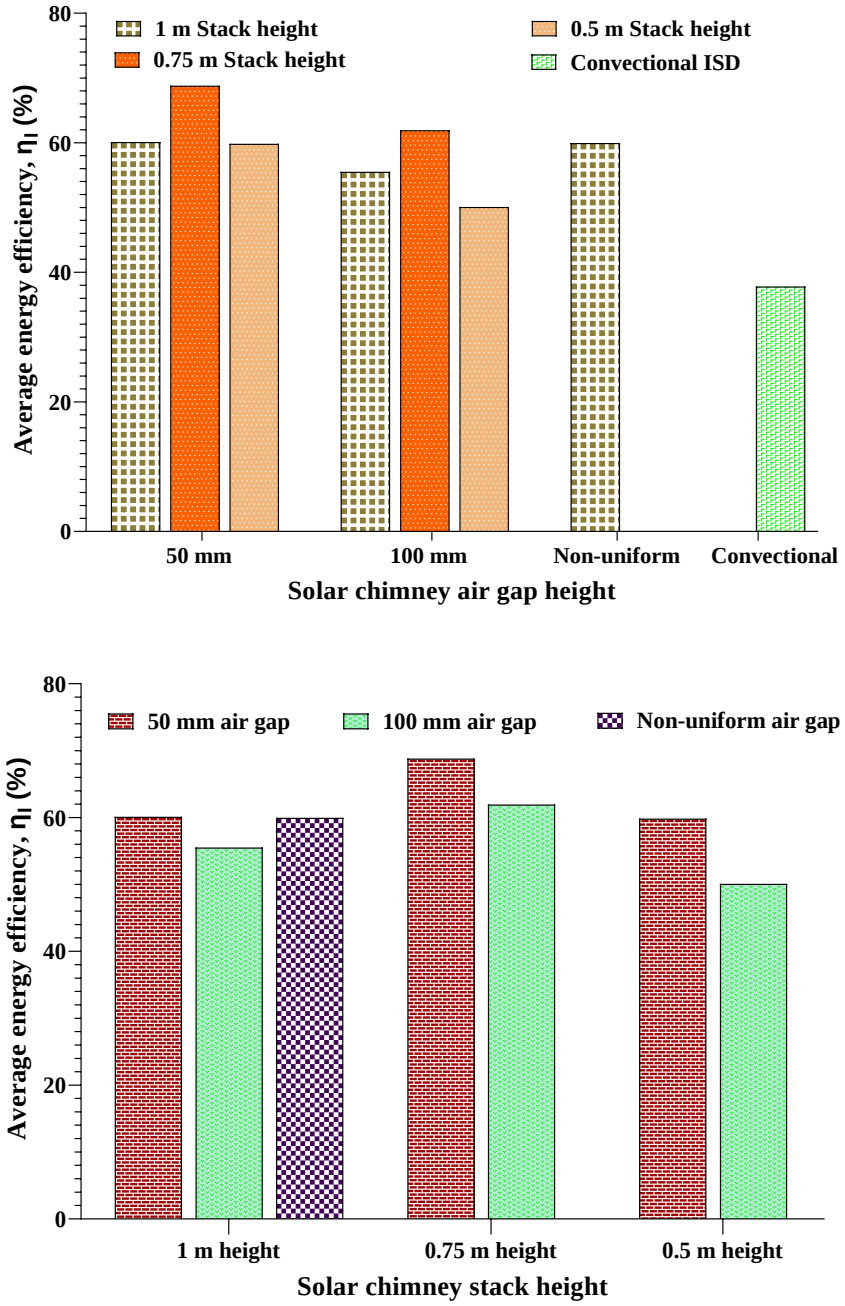

Fig. 4.15. Comparison of average collector efficiency versus: SC air gap height; stack height

The most important parameter to evaluate the efficiency of the SAC is the performance curve $(T_i - T_a)/I_T$. Therefore, based on the experimental data of inlet air temperature, ambient temperature and solar radiation and the calculated energy efficiency, an empirical correlation of energy efficiency against performance curve can be developed. This relation can be seen in Fig. 4.16 for all the setups. The variation in angle of incidence, wind speed, and the dependence

of the heat loss on plate temperature are the main causes of the data's scatter around the straight line. From the figure, it can be observed that a negative correlation was discovered.

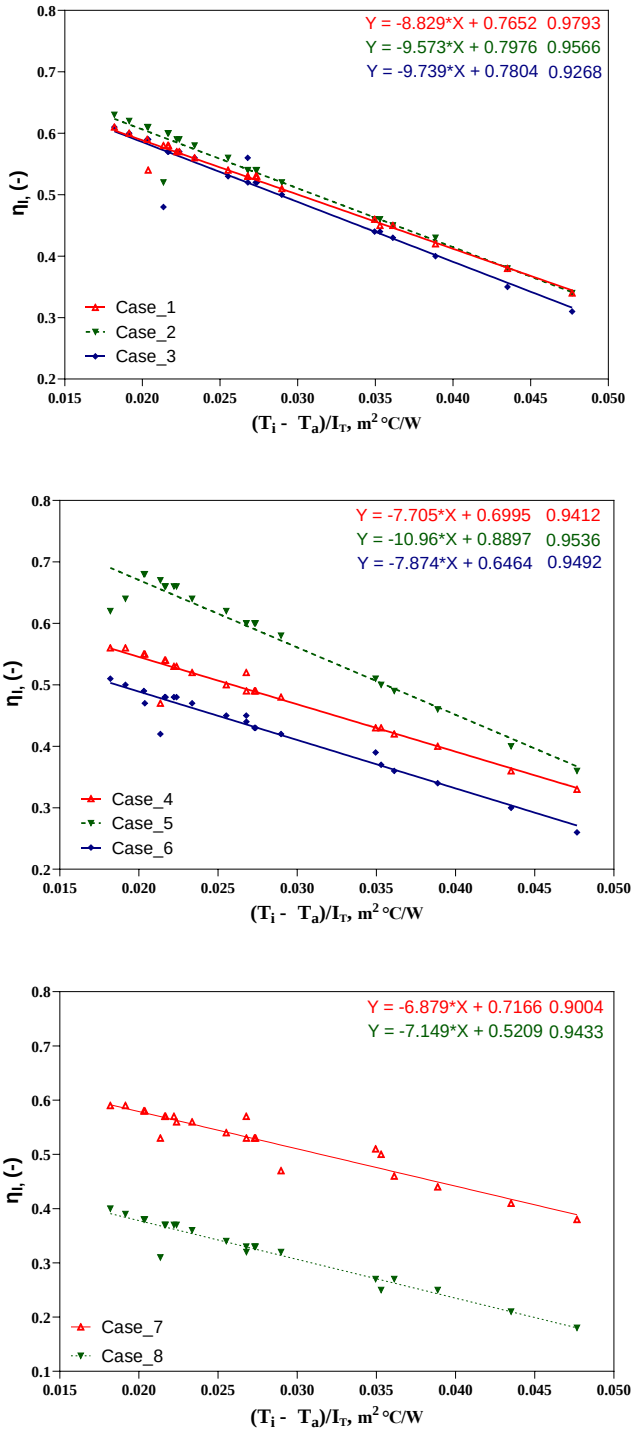

Fig. 4.16. Correlation between collector efficiency with $(T_i - T_a)/I_T$

Table 4.5 depicted the effective optical efficiency and effective heat loss coefficient for each setup. It is expected that the slope with the highest mass flow rate is anticipated to be less steep than those with the lowest mass flow rate. A similar result was found by Chabane and Moummi (2014). From this experimental result, the highest effective optical efficiency that can be achieved with SC setup that has an air gap thickness of 100 mm and a stack height of 0.75 m.

This is due to the fact that, when compared to other set ups, this SC setup obtained a better mass flow rate and temperature rise (see section 4.5.3). However, due to the higher temperature rise the heat loss to the ambient is more.

Table 4.5. Effective optical efficiency and effective heat loss coefficient for various setup

Description	$\mathbf{F_R(\tau\alpha)}$	$\mathbf{F_R U_o}$
Case_1	0.7652	8.829
Case_2	0.7976	9.573
Case_3	0.7804	9.739
Case_4	0.6995	7.705
Case_5	0.8897	10.960
Case_6	0.6464	7.874
Case_7	0.7166	6.879
Case_8	0.5209	7.149

When the air inlet temperature equals the ambient temperature ($T_i = T_a$), the SAC efficiency (optical efficiency) reached its peak. For this condition, the $(T_i - T_a)/I_T$ value is zero and the intercept is $F_R(\tau\alpha)$. The intercept with the $(T_i - T_a)/I_T$ axis is other interesting point. This point of interest can be reached when the SAC no longer removes useful energy, which can occur if air flow through the SAC is stopped.

The variation of average energy efficiency of SAC with SC stack height is depicted in Fig. 4.17 for 50 mm and 100 mm air gap thickness. The average efficiency is shown to increase with SC height; however, the figure demonstrates that this is not always the case. It has been found that the SC's stack height and its air gap thickness both have an impact on energy efficiency. Therefore, a SAC's energy efficiency can be calculated using the chimney's height-to-air gap ratio. It is evidence that while the SAC temperature differential reduces, the mass flow rate increases with the SC height. This demonstrates that optimum mass flow rate and temperature differential for greater efficiency exist at a certain threshold. As a result, the optimal design for greater energy efficiency was a 0.75 m SC height with a 50 mm air gap thickness.

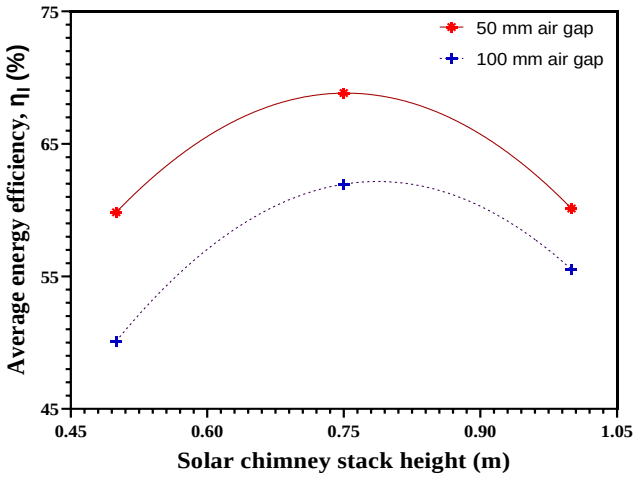

Fig. 4.17. Average efficiency values of SC stack height for different air gap thicknesses

Fig. 4.18 demonstrates the energy diagram of a SAC for SC configuration of 0.75 m stack height and 50 mm air gap thickness. From this diagram one can calculated the overall heat loss coefficient of a SAC and SC with known values of transmissivity–absorptivity product of glass and absorber plate, mean absorber and ambient temperatures. The average overall heat loss coefficients for novel dryers (Case_1 through 7) and conventional dryer were determined to be 4.03, 3.60, 4.61, 5.33, 4.69, 5.12, 4.50, and 6.35 $Wm^{-2}K^{-1}$, respectively. The conventional dryer had the highest overall heat loss coefficient followed by Case_3 and 5. This can be explained by the fact that there the SAC of these configurations had low airflow rates, which caused the absorber plate temperature to rise and increased heat losses to the surroundings.

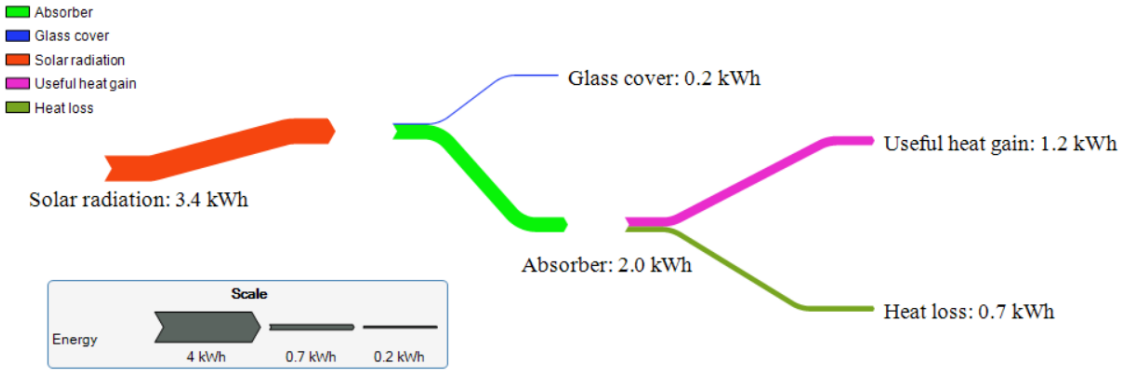

Fig. 4.18. Energy flow diagram of a SC configuration of 0.75 m height and 50 mm air gap

Fig. 4.19 shows the average energy efficiency for SC for various configurations. As can be seen from the figure, the average efficiencies of Case_1 through 7 were found to be 12.5, 24.57, 24.81, 10.98, 25.42, 22.61, and 12.64%, respectively and the corresponding overall heat loss coefficients were 6.33, 7.22, 6.38, 6.87, 5.96, 6.55 and 7.41 $Wm^{-2}K^{-1}$, respectively. It has been observed that Case 5 (0.75 m stack height with 100 mm air gap) has a modest advantage over other configurations followed by Case_2 and Case_3 while the lowest energy efficiency was found for SC stack height of 1 m. The figure revealed that while SC stack height exhibits a considerable influence on boosting SC performance, air gap thickness had no discernible effect on SC performance.

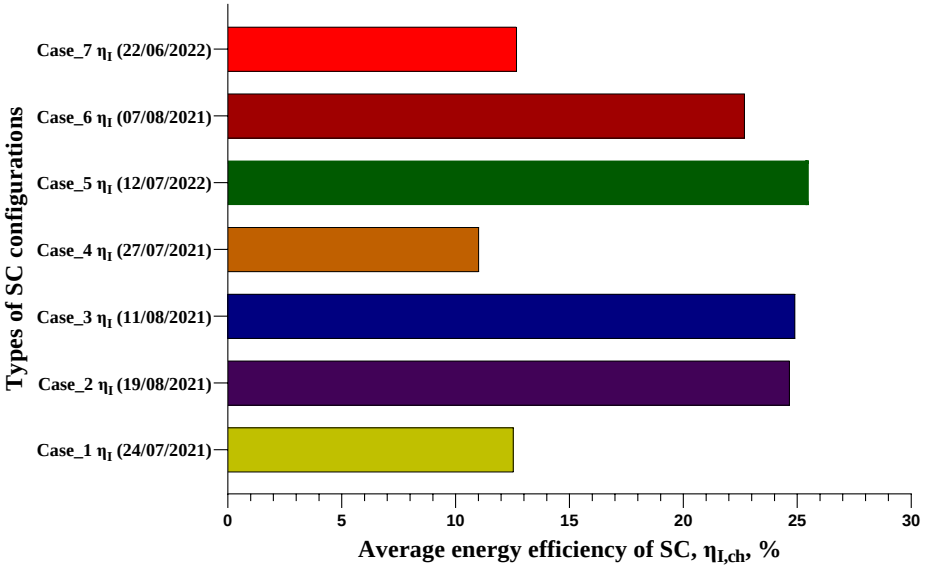

Fig. 4.19. Average energy efficiency of a solar chimney for all setups

4.5.4. Impact of solar chimney type on exergy efficiency

The exergy destruction, exergy input and instantaneous exergy efficiencies of SAC were computed for various SC arrangements of the novel and conventional dryer. According to the results, the novel dryers' average SAC exergy efficiency for Case_1 through 7 was 27.57%, 31.47%, 27.25%, 25.54%, 28.69%, 22.86%, and 28.02%, respectively, while the conventional dryer achieved its average exergy efficiency of 17.02%. The maximum value was reached with a stack height of 0.75 m and an air gap thickness of 50 mm in a SC arrangement.

The novel dryer outperformed the conventional dryer in terms of daily exergy efficiency by 34.3 to 85%. It was observed that the SAC's energy efficiency increased along with the increase in solar intensity. The highest energy efficiency coincided with the highest time of day for sunshine. The highest exergy efficiency was found between 12:00 to 12:40 in all setups. The maximum exergy efficiency along with maximum solar radiation were 35.26% and 973 Wm^{-2}, 40.16% and 1011 Wm^{-2}, 36.5% and 1045 Wm^{-2}, 31.51% and 985.6 Wm^{-2}, 37.24% and 944 Wm^{-2}, 29.65% and 1022 Wm^{-2}, 34.07% and 1078 Wm^{-2}, 22.15% and 859.2 Wm^{-2} for Case_1 through 7 and conventional dryer, respectively. A 50 mm air gap performed better than a 100 mm air gap thickness when compared. Results showed that mass flow rate has a greater effect on energy efficiency than solar radiation.

Additionally, the outcomes demonstrated that the exergy efficiency of SC is significantly influenced by the stack height and air gap thickness. The ranges for solar radiation, air temperature, exergy in moving air, exergy destruction, and SAC exergy efficiency is shown in Table 4.6 for all configurations. Fig. 4.20 illustrates the effect of solar radiation on the exergy efficiency of the SAC for all setups. This figure demonstrated that exergy efficiency rises linearly as solar radiation increases.

Table 4.6. Range of solar radiation, ambient temperature, exergy flow, exergy destruction and exergy efficiency of SAC

Set ups	**Solar radiation**	**Ambient temperature**	**Exergy flow**	**Exergy destruction**	**Exergy efficiency**
	(W m^{-2})	**(°C)**	**(W)**	**(W)**	**(%)**
Case_1	541.5 – 973	27 – 35	58 – 183	230 – 351	20 – 35.3
Case_2	521.7 – 1011	20 – 33	59 – 216	218 – 324	21 – 40
Case_3	247 – 1045	18 – 33	27 – 203	105 – 353	18 – 36.5
Case_4	605 – 986	27 – 36	58 – 165	262 – 359	18 – 31.5
Case_5	425 – 944	27 – 35	47 – 187	175 – 325	20 – 37
Case_6	412 – 1022	23 – 35	33.5 – 161	184 – 383	15 – 30
Case_7	578 – 1078	22 – 31	67 – 196	241 – 379	21 – 34
Conventional	471 – 859	28 – 41	26 – 101	224 – 357	10.5 – 22

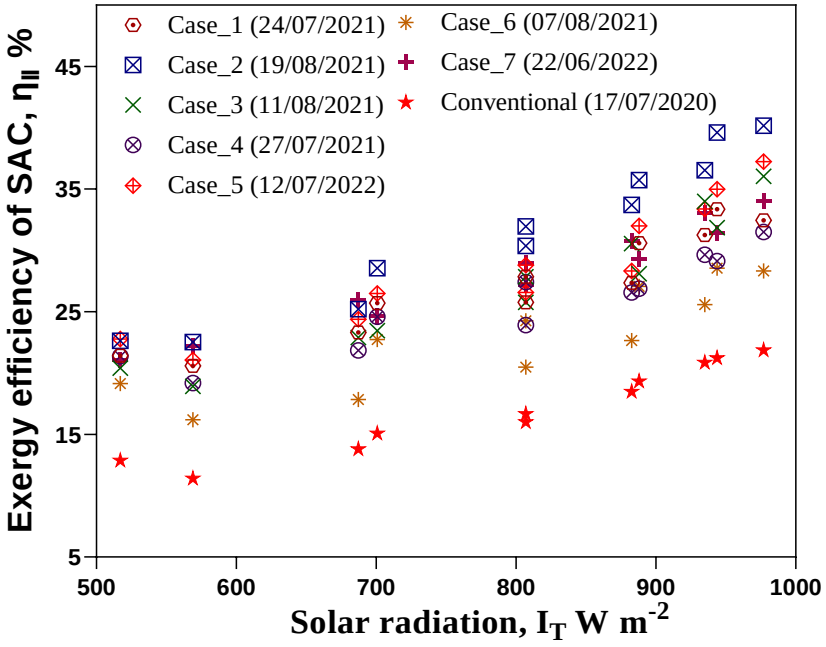

Fig. 4.20. Effect of solar radiation on exergy efficiency

It can be summarized that the effect of both SC stack height and air gap on energy and exergy efficiency has been observed. It was also observed that the SC stack height increases both efficiencies were increased until some points and then started to decrease. In addition, as the air gap thickness reduced from 100 to the 50 mm, both efficiencies increased. Therefore, based on the experimental results, a mathematical model could be developed that can related efficiency with the change in SC stack heigh and airgap thickness. The model for energy and exergy efficiency shown in Eq. 4.9 and Eq. 4.10:

$$\eta_I = -0.1785\left(\frac{H_{ch}}{t_{ch}}\right)^2 + 5.124\left(\frac{H_{ch}}{t_{ch}}\right) + 62.80, \tag{4.9}$$

$$\eta_{II} = -0.0875\left(\frac{H_{ch}}{t_{ch}}\right)^2 + 2.481\left(\frac{H_{ch}}{t_{ch}}\right) + 13.52. \tag{4.10}$$

It was found that a second order polynomial model was obtained with the correlation coefficient of 0.8912 and 0.8654 for energy and exergy efficiency, respectively. It should be noted that the regression model's plausible range for the energy and exergy efficiencies falls between 45.5% to 70% and 20% to 35% with the corresponding SC's stack height and air gap thickness in the ranges of 0.5 m to 1 m, and 50 mm to 100 mm, respectively. Additionally, these models could operate a solar radiation between 500 to 950 W m^{-2}, air mass flow rate between 0.008 to 0.021 kg s^{-1} and the overall heat loss coefficient should not be greater than 6.35 $Wm^{-2}K^{-1}$.

4.5.5. Effect of solar chimney on drying temperature

During the trial periods, the ambient temperature and relative humidity varied from 21.5 to 35 °C and 35% to 63%, respectively, with corresponding average values of 28.8 °C and 37.8%.

Fig. 4.21 shows the daily mean air temperature and relative humidity values for several ISD settings inside the drying chamber. The drying air temperatures gradually increased, reaching their maximum values between 12:30 and 13:30, while the relative humidity decreased to its lowest point at this time. It was observed that the pattern of the drying temperature was found to be similar to the trend of solar radiation. The drying temperatures are generally higher due to higher solar radiation, as would be expected. The drying air temperatures for lower solar intensities are occasionally very near to or even higher than those for higher intensities, despite the fact that the solar radiations for each comparison are quite different. This tendency can be related to the variation of solar radiation during the trials.

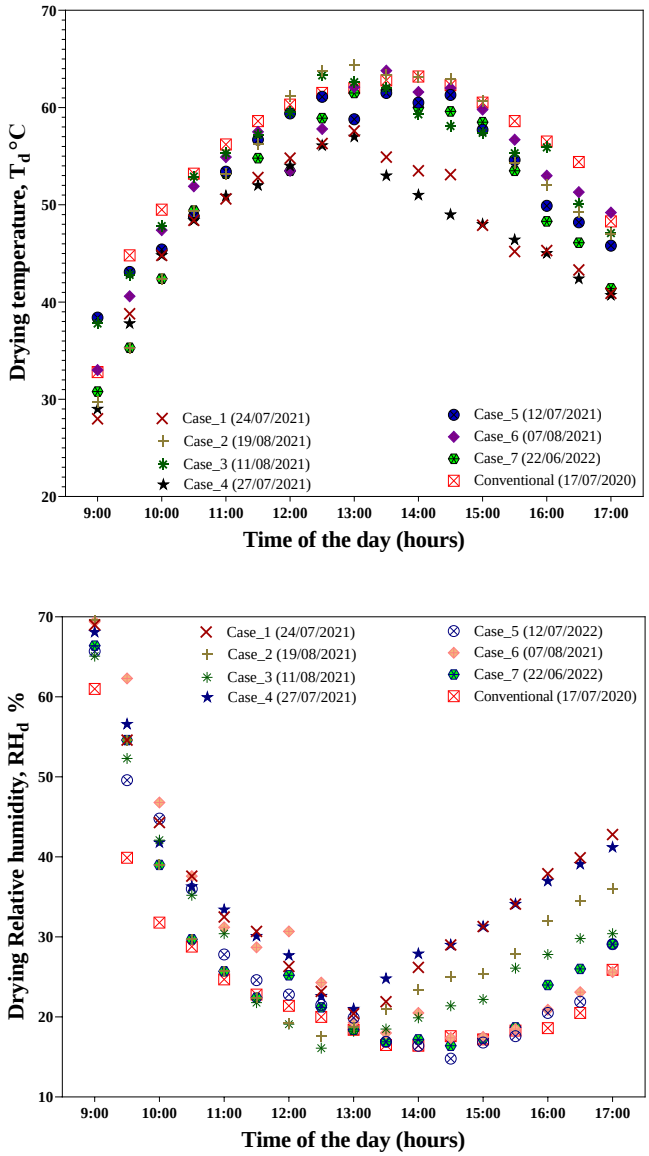

Fig. 4.21. Comparison of drying temperature and relative humidity inside drying chamber for different setups

According to the figure, the conventional ISD's drying temperature ranged from 32.8 to 63.5 °C, whereas the novel ISD's ranged from 28 to 65 °C, with Case_2 configuration the highest record. This is because Case_2 obtained the highest useful heat gain from the SAC. For Cases_1 through 8, the average drying temperatures were 48.5, 54, 55, 48, 53.5, 54, 52, and 56

°C, with a 6% deviation from mean. Convectional dryer had an average drying temperature that was 4 °C higher than novel ISD since air flow rate of this dryer is low. The drying air temperatures under load are dropped by around 3.5 °C to 6 °C when compared to the drying temperature under no load conditions. The drop in temperature drying chamber was because of the product load. It was observed that the drying chamber's temperatures was roughly 19 to 27.5 °C higher than the ambient temperature during experimentation period. This temperature differential between dry air temperature in the chamber and ambient temperature was sufficient for the drying process. This observation corroborated Das and Akpinar (2020) and Hegde et al. (2015).

The average relative humidity (RHs) for Case_1 though 8 were 34.5, 29.5, 28, 35, 26.5, 29.5, 26.5, and 24%, with a 7% deviation from mean. It was evident that when the drying air temperature in the chamber was high, RH decreased. The lowest RH and maximum drying temperature record were discovered for the conventional dryer. When compared to the novel dryer, the convectional dryer's RH value drops by roughly 3 to 11%. With regard to the novel ISD setup, a SC with large stack height, aside from Case_7, exhibited a higher RH, whilst a SC with a small stack height found a lower record. A second order negative correlation between drying temperature and relative humidity was discovered using the least squares approach, and the results are displayed in appendix A8. It is noted that when air flow rate increases, the vapor pressure drops, resulting in less resistance to water evaporation from the product. It has been observed that drying time is shortened as drying rate increases with rising drying air temperature and decreasing relative humidity. As the air temperature rises, the thermal gradient of the dried product rises, increasing the rate of water evaporation During the drying process, consideration should be given to the maximum solar intensity, the maximum energy efficiency, and the lowest possible ambient humidity. Additionally, a drying chamber's data of a high flow rate and high drying air temperature show that the dried product dries more quickly.

4.5.6. Effect of type of solar chimney on moisture reduction

The amount of moisture extracted from the products throughout the drying process has been taken into account when evaluating the performance of the novel ISD with various SC configurations. The product moisture reduction for each experimental setup is shown in Fig. 4.22. After 8 hours drying period, the product's final weights for novel ISD of Case_1 through 7, conventional dryer and OSD were determined to be 199, 185, 205, 208, 182, 194, 197, 225, and 251 g, respectively. The corresponding moisture content was found to be 33.8, 28.8, 35.7, 36.7, 27.6, 32.1, 33, 37, and 45.3% (w.b.), respectively. The total amount of water removed from the sample for each setup was determined using Eq. 3.37 to be 0.716, 0.730, 0.710, 0.707, 0.733, 0.721, 0.718, 0.69, and 0.664 kg for Case_1 through 7, conventional dryer, and OSD, respectively. According to the data, about 93.4% of the initial moisture content removed in Cases_2 and 5 after 8 hours drying time. According to the results, a novel ISD with a 0.75 m stack height arrangement removed water from the sample more effectively than a conventional dryer and an OSD by about 3.85% and 8.75%, respectively. At the initial stages of drying (the first two hours of drying), drying was faster in Case_1, 4, 7 and OSD drying compared to other setup due to better air velocity, however their performance become slow at later stages of drying. At later stage, the apple slices need more time to remove the water trapped inside the pores of the sample where higher air temperature required.

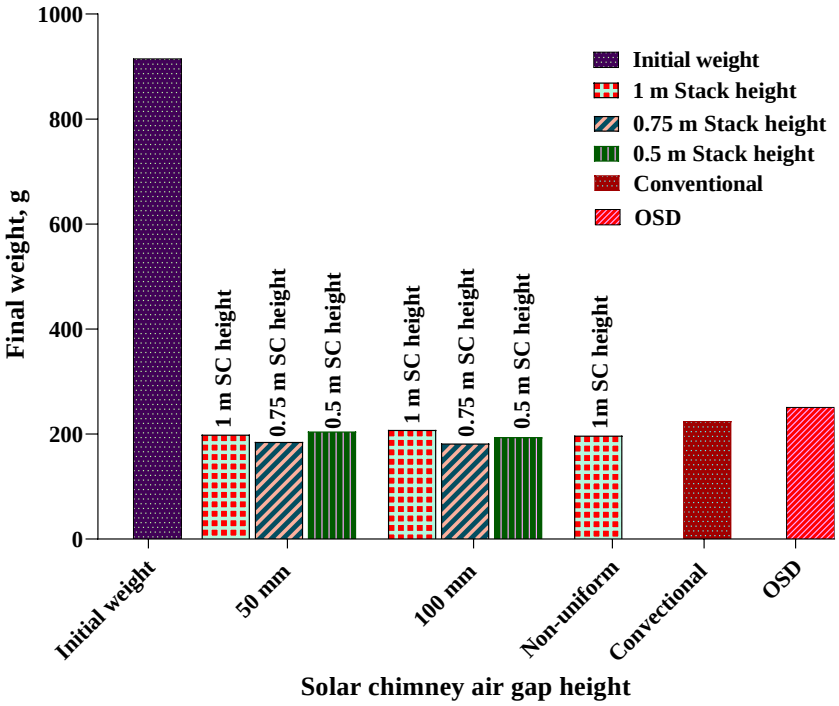

Fig. 4.22. Final measured weight of apple slices for each experimental setup

The size and shape of the dried apple slices after the end of drying period are depicted in Fig. 4.23. The amount of energy being absorbed by the air from the collector increased, which sped up the drying process in the dryer. It was observed that the rate at which moisture was removed from the sample increased as the Solar's intensity rose. Doymaz, (2009) made a similar observation with the green apple.

Fig. 4.23. Sample photograph apple slices after eight hours of drying process

In order to study the effect of stack height and air gap thickness on moisture removal a two-way ANOVA performed in excel and the result was depicted in Table 4.6. The *P*-value for stack height is less than our significance level, this factor is statistically significant. On the other hand, the air gap thickness effect is not significant because its *P*-value (0.5598) is greater than our significance level which is Alpha = 0.05. Another way of explaining the significance, the value of *F*-statistic, which is the ratio of variation between sample means to variation within samples. If the *F*-value greater than the *F*-critical then we reject the null hypothesis.

Table 4.6. Summary of statistical result

Source of Variation	*SS*	*df*	*MS*	*F*	*P-value*	*F crit*
Air gap	4.167	1	4.167	0.481	0.5598	18.513
Stack height	532	2	266	30.692	0.0316	19
Error	17.333	2	8.667			
Total	553.5	5				

4.5.7. Modeling of apple slices

Based on the literature four mathematical model were identified for apple slices drying for best fit: Modified page, Midilli and Kucuk, Logarithmic and Verma et al (see Table 2.2). These models were used to evaluate to predict the moisture ratio (MR) obtained from the experimental data. In this research work, a novel dryer with a 0.75 m stack height and 100 mm air gap was selected to develop a mathematical model for apple slices. Conventional dryer and OSD were also modelled for comparison. Fig. 4.24 shows the moisture ratio versus drying time for both experimental and predicted value for novel, conventional and OSD, which represents the typical characteristic drying curve of apple slices during thin-layer drying operation. After 8 hours drying period, it was observed that the moisture ratio for novel, conventional and OSD were found to be 0.07, 0.11, and 0.14, respectively.

Table 4.7 presented the models parameters and the details of the statistical analysis of the four thin layer drying models for the novel ISD. It was found that Verma et al model gave better predicitions for moisture ratio of the apple slices than the other models. This is in agreement with the report of Dissa et al. (2009) for mango slices, Menges and Ertekin, (2006) for Golden apples, and Rayaguru and Routray, (2012) for Apple slices. It can be concluded that the models can be used to predict moisture loss during drying, improve process control and produce products of high quality.

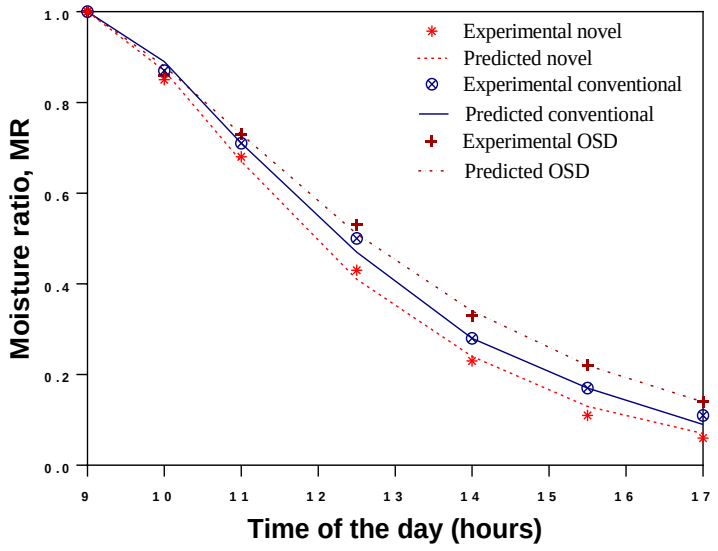

Fig. 4.24. Measured and predicted moisture ratio of apple slices

Table 4.7. Parameters and statistical analysis for novel ISD

Model	Model constants	RMSE	χ^2	R^2
Modified page	k = 0.04135, n = 0.10508	0.06126	0.00525	0.96818
Midilli and Kucuk	k = 0.00104, n = 1.26796, a = 1.02604, b = 0.00012	0.02112	0.00105	0.99622
Logarithmic	k = 0.00464, a = 1.06298, c = 0.00021	0.05402	0.00511	0.97525
Verma et al.	k = 0.00786, a = 3.81475, g = 0.001036	0.01334	0.00031	0.99849

Fig. 4.25 shows the variation of the logarithm of moisture ratio with time of drying. The slope found in this figure can be used to calculate the moisture diffusivity of apple slices. Based on Eq. 3.31, the computed moisture diffusivities for the dried apple slices for novel ISD, conventional dryer and OSD were 9.75683, 8.42992, and $6.80878 \cdot 10^{-9}$ $m^2.s^{-1}$. These moisture diffusivities between the 10^{-12} and 10^{-8} which is reported for drying of agricultural products (Komolafe et al., 2018). As can be observed, the novel dryer the moisture diffusivity value was 15.73% and 43.3% greater than that of a conventional dryer and OSD, respectively.

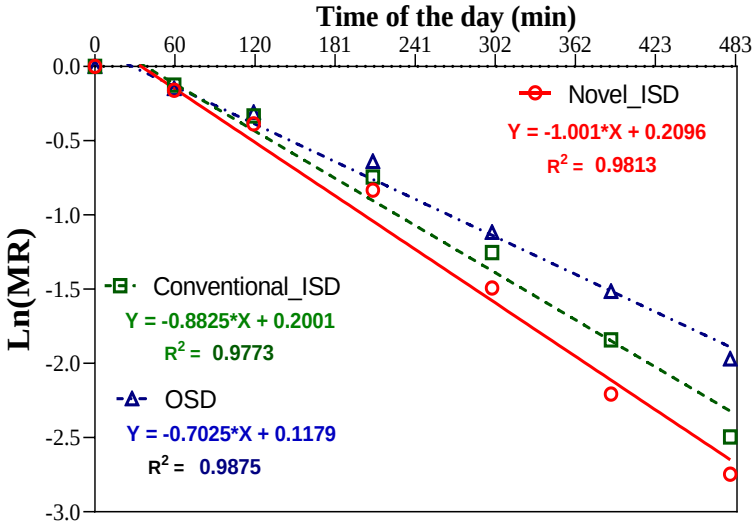

Fig. 4.25. Variation of logarithm of moisture ratio with time of drying

4.5.8. Effect of type of solar chimney on energy consumption and drying efficiency

Table 4.8 shows the overall value of the amount of water removed from the dryer, specific energy consumption and the drying efficiency for the eight drying experiments. The effectiveness of the energy utilization was defined in the overall specific energy consumption (SEC). During the 8 h drying process, the ISD with a SC consumed 6.78 MJ to 10.15 MJ of useful energy to remove 0.707 to 0.733 kg of water, whereas the conventional dryer required 4.96 MJ of energy to expel 0.690 kg of water during the same drying hours. However, it should be noted that bad weather conditions during the experiment also have effects in varying the results mentioned above. The amount of water removed from dried products in each setup for 8 hours of drying has been mentioned in previous section. The effectiveness of the energy utilization was defined in the overall specific energy consumption (see Eq. 3.34) which was obtained as 2.50, 2.36, 2.47, 2.37, 2.81, 1.91, 2.64, and 1.46 $kWh.kg^{-1}$, for Case_1 to Case_8

respectively. This result indicated the effective utilization of energy by Case_8 (conventional dryer) than others. Comparison between the ISD with a SC, Case_6 exhibited lower energy consumption (SEC) than the others ISD with a SC while the highest value was obtained in Case_5. This result indicated the effect of mass flow rate on energy utilization. High mass flow rates improve useful heat gains, which rises the energy required to remove water from the food products. According to the findings, the novel ISD consumed 0.45 to 1.35 kWh more energy to dry 1 kg of dried product than that of conventional dryer. This is due to the fact that dryers with highest energy efficiency use more energy to dry product than those with the lowest energy efficiency. The calculated SEC in each case was lower than the result reported by Ndukwu et al. (2017), which ranged from 3.34 to 5.92 $kWh.kg^{-1}$.

The drying efficiency was calculated using Eq. 3.35 and the calculated results were presented in Table 4.8. The table clearly shown that the drying efficiency values were similar for all SC configurations, with Case_6 showing a slight improvement. Case_4 exhibted higher drying efficiency than Case_1 and Case_7 while the lower values were obtained in Case_7 for the same SC height. After eight hours of drying, the value of the drying efficiency a conventional dryer was estimated to be 8 to 16% more than the value obtained by the novel ISDs. It can be concluded that the amount energy supplied from collector (useful heat gain) to dried product is the parameter that affecting both drying efficiency and water removal from the product. The drying time can be reduced when more energy supplied to the product to be dried.

There was no significance difference between SEC and drying effeciency at same stack height and air gap thickness between Case_1, 2, 3, 4, 5, 6 and Case_7 (0.05 level of significance). However, there is a considerable difference in SEC and drying efficiency between novel and conventional dryers. A further finding of the study was that the value of the SEC decreases as drying and energy efficiencies increase.

Table 4.8. Comparison on water removed, SEC and drying efficiencies of present setups

Model	**Chimney gap (mm)**	**Total mass of water removed (kg)**	**SEC (kWh. kg^{-1})**	**Drying efficiency, η_d (%)**
Case_1	50	0.716	2.50	19.37
Case_2		0.730	2.36	20.40
Case_3		0.710	2.47	19.54
Case_4	100	0.707	2.37	20.51
Case_5		0.733	2.81	17.15
Case_6		0.721	1.91	25.25
Case_7	Non-uniform air gap	0.718	2.64	18.31
Case_8	Conventional dryer	0.690	1.46	32.98
OSD	-	0.664	-	-

4.6. New scientific results

This section presents the new scientific findings from this research work as follows:

1. *Correlation between the solar intensity on solar chimney and solar air collector surface, and ambient temperature*

Based on experimental results, I have developed a linear model to estimate relation between the amount of solar insolation received by solar chimney (SC) and solar air collector (SAC) surfaces in the operation range of 400 to 1000 Wm^{-2} and ambient temperature range from 18.7 to 37.4 °C for experimentally for the most applicable months: June, July, and August:

$$I_{SC} = 0.955\ I_{SAC} - 276.2,\ R^2 = 0.990,\ \text{for June}$$

$$I_{SC} = 0.471\ I_{SAC} + 158,\ R^2 = 0.849,\ \text{for July}$$

$$I_{SC} = 0.513\ I_{SAC} + 165,\ R^2 = 0.988,\ \text{for August}$$

During the approximation the standard deviation was 17%, 10% and 14% for June, July, and August, respectively.

Additionally, I have developed a correlation between the intensity on SAC and the ambient temperature (T_a) for each month:

$$T_a = 0.018\ I_{SAC} + 12.1,\ R^2 = 0.785\ \text{for June}$$

$$T_a = 0.020\ I_{SAC} + 12.5,\ R^2 = 0.859\ \text{for July}$$

$$T_a = 0.014\ I_{SAC} + 15.1,\ R^2 = 0.881\ \text{for August}$$

During the approximation the standard deviation was 8%, 8% and 8.9% for June, July and August, respectively. I have pointed out that the effect of SC on the dryer performance is ineffective when the intensity of solar radiation is below a certain threshold (200 $W.m^{-2}$).

Any location with a comparable climate can used these models.

2. Effect of solar chimney type on air flow rate and collector temperature rise

According to experimental results, I justified the increase of air mass flow rate ($\dot{m}_a$) with increase in solar radiation. For that purpose, I have developed a linear model to approximate the airflow rate and SAC outlet air temperature for solar radiation intensity range of 500 $W.m^{-2}$ and 950 $W.m^{-2}$.

$$\dot{m}_a = 0.535 + 0.00163 \cdot 10^{-2}\ I_{Tc}.$$

The correlation coefficient was 0.95 along with standard deviation of 0.118 $kg.s^{-1}$.

Additionally, I have developed a linear model to estimate SAC's outlet air temperature ($T_{c,o}$) in terms of solar radiation intensity for a range between 500 $W.m^{-2}$ and 950 $W.m^{-2}$ and inlet air temperature range from 19.8 to 36.4 °C.

$$T_{c,o} = 29.3 + 0.0487 \cdot I_{Tc}.$$

The correlation coefficient was 0.96 along with standard deviation of 2.014 °C. I have proved that raising the stack height from 0.5 m to 1 m resulted in a 31% increase in airflow rate and a 3.72 °C decrease in temperature rise. Moreover, I have proven that the air gap does not have any significant correlation with SAC outlet temperature with stack height beyond 1 m.

3. Impact of solar chimney type on collector performance

I have pointed out that the SC stack height and air gap thickness have a significant impact on the energy and exergy efficiency of the SAC, and so based on the experimental findings and chimney height-to-gap ratio (H_{ch}/t_{ch}), I have developed a second order polynomial model in order to approximate the relation between the energy (η_I) and exergy (η_{II}) efficiency of the SAC versus the SC stack height-to gap ratio:

$$\eta_I = -0.1785\left(\frac{H_{ch}}{t_{ch}}\right)^2 + 5.124\left(\frac{H_{ch}}{t_{ch}}\right) + 62.80, \quad R^2 = 0.8912$$

$$\eta_{II} = -0.0875\left(\frac{H_{ch}}{t_{ch}}\right)^2 + 2.481\left(\frac{H_{ch}}{t_{ch}}\right) + 13.52, \quad R^2 = 0.8654$$

The regression model's plausible range for the energy and exergy efficiencies falls between 45.5% to 70% and 20% to 35% with the corresponding SC's stack height and air gap thickness within the ranges of 0.5 m to 1 m, and 50 mm to 100 mm respectively.

Comparing air gap thickness, I justified a SC with a 50 mm air gap thickness outperformed with a 100 mm air gap, a 13% boost in performance for solar radiation range of 500 $W.m^{-2}$ to 950 $W.m^{-2}$.

4. Moisture removal of apple slices

I have evaluated and justified the integration of a solar chimney on improving the solar drying process in terms of moisture removal from the product to be dried. I have determined that after 8 hours drying period about 93.4% of the product's initial moisture content removed when using a SC stack height of 0.75 m and an air gap of 50 and 100 mm.

Based on experimental results, I have proven the Verma et al. model found to best explain thin layer drying behavior of apple slices (Golden Delicious) as compared to other models for an initial moisture content of 85.6 % (w.b.) and apple thickness of 4 mm.

$$MR = a\ exp(-kt) + (1-a)\ exp(-gt).$$

The identified model parameters are k = 0.00786, a = 3.81475 and g = 0.00104 and the coefficient of determination was 0.9985.

5. Energy consumption and drying efficiency

I have justified that the quantity of total useful heat gain suppled from the solar collector determines the amount of energy required to remove moisture from the drying product and drying efficiency. I have proven that in terms of specific energy consumption (SEC), a novel solar dryer utilized between 22 and 53% more energy to remove 1 kg of dried product's moisture than a conventional dryer. I have elaborated that the drying efficiency rise by 38% when the SEC is reduced from 2.4 to 1.6 kWh kg^{-1}.

Additionally, I have pointed out that the quantity of SEC is dependent on the amount of moisture remaining in the product to be dried, with low moisture content requiring more SEC.

Based on the experimental findings, I have also pointed out that both stack height and air gap have a considerable impact on energy consumption for removal of moisture from the product.

5. CONCLUSION AND SUGGESTIONS

In conclusion, an experimental evaluation has been conducted to determine the performance of a novel natural indirect type solar dryer (ISD) using different solar chimney designs under no-load and load conditions. In this research work, the effect of solar chimney types has been evaluated by comparison between different SC stack heights and air gap thicknesses. Additionally, conventional dryer and OSD were also tested for comparison purposes. The SC uses cardboard sheet painted black and equipped with aluminium fins has showed a higher temperature than a SC without an absorber and fin.

During the experimental periods, the range of solar radiation and ambient temperature were between 213 to 1083 $W.m^{-2}$ and 18 to 37 °C with their corresponding average value of 751 $W.m^{-2}$ and 30 °C, respectively. It was found that July had the highest temperature. SC stack height and air gap thickness are played a significant effect to improve the drying process. It had been found that the solar chimney has no effect when the solar radiation intensity below 200 $W.m^{-2}$.

The no-load performance evaluation of the novel ISDs is crucial to understand the extent of the maximum temperature achieved by the ISD. Under-load evaluation, it was found that the SAC outlet temperature raised above the ambient temperature by about 5 °C at low radiation and reached 20 °C at higher radiation.

Under product load conditions, the collector temperature change was found to be higher by about 1 to 4 °C when using an air gap of 50 mm. The drying air temperature under load conditions was lower than a drying temperature under no load conditions because of the presence of product in case of under load conditions.

The parameters of the solar chimney play a vital role in improving the efficiency of SAC and the drying process, in addition to variables like wind speed, ambient temperature, and so on. The study showed that highest energy and exergy efficiency has been found when a 0.75 m and a 50 mm air gap SC was used. Compared to a conventional dryer, a dryer with a SC performed much better. A SC with non-uniform airgap worked better than 50 mm and 100 mm of the same SC stack height of 1 m. Increasing SC height up to a definite point and a decreasing air gap were favorable.

Based on moisture removal, energy utilization and drying efficiency, a 0.75 m stack height with 100 mm air gap solar chimney was the best configuration where the highest drying efficiency, lowest energy consumption (SEC) and more moisture removed obtained by this configuration.

There are numerous suggestions that might be made for future works to improve this one. The study's experience has shown that conducting an experiment to determine the impact of all pertinent parameters would be time-consuming. Specific aspects need to be scrutinized in future experimental activities. The next step should be analytical modeling and CFD simulations on passive indirect dryers utilizing actual inputs like those given in this paper, in order to understand how the dryers, operate under various circumstances. Such a technique would make it easier to identify areas that required additional testing, enhancing dryer designs.

6. SUMMARY

PERFORMANCE EVALUATION OF SOLAR CHIMNEY APPLIED FOR DRYING PROCESSES

A comprehensive experimental evaluation of the performance of a novel indirect type of natural convection solar dryer (ISD) for drying applications has been conducted in summer months, under the climatic conditions of Gödöllő, Hungary (47° 35' 39" N and 19º 21' 59" E). The novel dryer consists of three primary components: a single-pass solar air collector, a drying chamber, and a solar chimney (SC). These components were fabricated in the Solar energy laboratory at the Hungarian University of Agriculture and Life Sciences (MATE). To achieve the aim of the research, three SC stack height (0.5, 0.75 and 1 m) and three air gap thicknesses (50 mm, 100 mm, and non-uniform gap) were selected. In addition, conventional dryer and OSD were tested for comparison purposes. Therefore, a total of 17 experiments have been carried out under both no-load and load conditions. Solar radiation, ambient temperature, temperatures at different location of dryer, relative humidity and air flow rate were collected for evaluation purposes. Parameters utilized to evaluate and compare the proposed novel ISDs were energy and exergy (2E) analysis, product moisture loss, drying efficiency and specific energy consumption (SEC).

According to the findings, variation in solar radiation and ambient temperature influenced the performance of the novel dryer. The SAC temperature difference between inlet and outlet of an air gap of 50 mm greater than 1 to 4 °C when compared to a 100 mm air gap. It was found that as the SC height increased from 0.5 m to 1 m, the air flow rate increased by 31%, while the temperature reduced by 3.7 °C. The novel ISD's thermal and exergy efficiencies of SAC increased by 31.8 to 82% and 48.5 to 87%, respectively, as compared to the conventional ISD. The daily total useful heat gained by the novel ISDs and conventional ISD ranged from 1.1 to 2.26 kWh where the lowest useful heat gain obtained by conventional ISD. It was also found that SC with non-uniform air gap thickness performed better when compared to SC with 50 mm and 100 mm air gap of 1 m stack. Moreover, a SC with 0.75 m stack height and an air gap of 50 mm found to be the best configuration in terms of efficiency.

The drying air temperatures under load conditions have been found to be between 3.5 °C to 6 °C lower than the drying temperatures under no load conditions. Statistical results showed that SC stack height has a significant effect on product moisture loss than SC air gaps. After 8 hours drying period, about 93.4% of the product's initial moisture content removed when using a SC stack height of 0.75 m and an air gap of 50 and 100 mm. However, the amount of energy required to remove the moisture from the product was higher. The novel dryer consumed 0.45 to 1.35 kWh more energy (SEC) to dry 1 kg of dried product than conventional dryer. Moreover, there was no considerable difference on SEC and drying efficiency for SC stack heights and air gap thicknesses, with the exeption of a 0.5 m SC stack height.

In this research work, Verma et al. model found to best explain thin layer drying behavior of apple slices (Golden Delicious) as compared to other models.

According to the parameters used to evaluate the proposed novel ISD, the best configuration was a SC with 0.75 m stack height and a 50 mm air gap thickness.

7. ÖSSZEFOGLALÁS (SUMMARY IN HUNGARIAN)

SZÁRÍTÁSI FOLYAMATOKHOZ ALKALMAZOTT NAPENERGIÁS KÉMÉNY TELJESÍTMÉNYÉRTÉKELÉSE

Átfogó kísérleti vizsgálatok kerültek elvégzésre egy új típusú közvetett természetes konvekciós szoláris szárító teljesítményének értékelésére, a nyári hónapokban Magyarországon, Gödöllő (é. sz. 47° 35' 39" és k. h. 19° 21' 59") éghajlati viszonyai között. Az újszerű szárító három fő összetevőből áll: egyjáratú levegős napkollektorból, szárítókamrából és napenergiás kéményből. Ezek az alkatrészek a Magyar Agrár- és Élettudományi Egyetem (MATE) Napenergia laborjában kerültek elkészítésre. A kutatás céljának elérése érdekében három napenergiás kémény magasság (0,5, 0,75 és 1 m) és három légrés vastagság (50 mm, 100 mm és változó légrés) került kiválasztásra. Ezenkívül összehasonlítás céljából hagyományos szárítóval és napon történő szárítással is vizsgálatok kerültek elvégzésre. Ezért összesen 17 kísérlet került elvégezésre szárítandó termék nélkül és szárítandó termékkel. Kiértékelés céljából rögzítésre került a napsugárzás, a környezeti hőmérséklet, a szárító különböző helyeinek hőmérséklete, a relatív légnedvesség és a légáramlási sebesség. A javasolt újszerű közvetett természetes konvekciós szoláris szárítók értékeléséhez és összehasonlításához használt paraméterek az energia- és exergiaelemzés (2E), a termék nedvességvesztése, a szárítási hatékonyság és a fajlagos energiafogyasztás voltak.

Az 50 mm-es légrés bemeneti és kimeneti nyílása közötti levegős napkollektor hőmérsékletkülönbség 1–4 °C-nál nagyobb a 100 mm-es légréshez képest. Megállapítást nyert, hogy a szoláris kémény magasság 0,5 m-ről 1 m-re történő növelésével a levegő áramlási sebessége 31%-kal nőtt, míg a hőmérséklet 3,7 °C-kal csökkent. Az új közvetett természetes konvekciós szoláris szárító hő- és exergia hatékonysága 31,8-82%-kal, illetve 48,5-87%-kal nőtt a hagyományos közvetett természetes konvekciós szoláris szárítóhoz képest. Az újszerű- és a hagyományos közvetett természetes konvekciós szoláris szárítók által nyert napi hasznos hőmennyiség 1,1 és 2,26 kWh között mozgott, ahol a legkisebb hasznos hőnyereséget a hagyományos szárító érte el. Az is megállapítható, hogy a nem egyenletes légrésvastagságú szoláris kémény jobban teljesített, mint az 1 m magas 50 mm-es és 100 mm-es légrésvastagságú kémény. Ezen túlmenően a 0,75 m-es kéménymagassággal és 50 mm-es légréssel rendelkező szoláris kémény hatékonyság szempontjából a legjobb konfigurációnak bizonyult.

A szárítólevegő hőmérséklete termék szárítás során 3,5 °C és 6 °C között alacsonyabb volt, mint a szárítandó termék nélküli szárítási hőmérséklet. A statisztikai eredmények azt mutatták, hogy a szoláris kémény magasságnak jelentősebb hatása van a termék nedvességvesztésére, mint a kémény légréseknek. 8 órás száradási periódus után a termék kezdeti nedvességtartalmának körülbelül 93,4%-a eltávolítható 0,75 m napenergiás kémény magasság és 50 és 100 mm légrés esetén. A nedvesség termékből való eltávolításához szükséges energia mennyisége azonban magasabb volt. Az újszerű szárító 0,45-1,35 kWh-val több energiát fogyasztott 1 kg szárított termék szárításához, mint a hagyományos szárító. Ezenkívül nem volt jelentős különbség a fajlagos energia fogyasztás és a szárítási hatékonyság tekintetében a napenergiás kémény magasságok és a légrés vastagságok között, kivéve a 0,5 m-es kémény magasságot.

Ebben a kutatómunkában Verma et al. modellje magyarázta meg legjobban az almaszeletek (Golden Delicious) vékonyrétegű szárítási viselkedését a többi modellel összehasonlítva.

A javasolt újszerű indirekt természetes konvekciós szoláris szárító értékeléséhez használt paraméterek szerint a legjobb konfiguráció a 0,75 m magasságú és 50 mm légrésvastagságú napenergiás kémény volt.

8. APPENDICES

A1: Bibliography

1. Abdelkader, T.K., Fan, Q., Gaballah, E.S., Wang, S., and Zhang, Y., (2020): Energy and exergy analysis of a flat-plate solar air heater artificially roughened and coated with a novel solar selective coating. Energies, 13(4), pp. 997. *https://doi.org/10.3390/en13040997*
2. Afriyie, J.K., and Bart-Plange, A. (2012): Performance investigation of a chimney-dependent solar crop dryer for different inlet areas with a fixed outlet Area. International Scholarly Notices, Hindawi (2012), pp. 1–9. https://doi.org/10.5402/2012/194359
3. Afriyie, J.K., Nazha, M.A.A., Rajakaruna, H., and Forson, F.K. (2009). Experimental investigations of a chimney-dependent solar crop dryer. Renewable Energy, 34(1), 217–222. https://doi.org/10.1016/j.renene.2008.04.010
4. Afriyie, J.K., Rajakaruna, H., Nazha, M. A.A., and Forson, F.K. (2011). Simulation and optimization of the ventilation in a chimney-dependent solar crop dryer. Solar Energy. https://doi.org/10.1016/j.solener.2011.04.019
5. Afriyie, J.K., Rajakaruna, H., Nazha, M.A.A., and Forson, F.K. (2013): Mathematical modelling and validation of the drying process in a Chimney-Dependent Solar Crop Dryer. Energy Conversion and Management, 67, pp. 103–116. https://doi.org/10.1016/j.enconman.2012.11.007
6. Agrawal, A., and Sarviya, R.M. (2016). A review of research and development work on solar dryers with heat storage. International Journal of Sustainable Energy, 35(6), 583–605. https://doi.org/10.1080/14786451.2014.930464
7. Aissa, W., El-Sallak, M., Elhakem, A. (2014). Performance of solar dryer chamber used for convective drying of sponge-cotton. Thermal Science, 18(SUPPL.2), 451–462. https://doi.org/10.2298/TSCI110710084A
8. Ajam, H., Farahat, S., and Sarhaddi, F., (2005). Exergetic optimization of solar air heaters and comparison with energy analysis. International Journal of Thermal, 8(4), pp. 183–190.
9. Akpinar, E.K., and Kocyigit, F., (2010). Energy and exergy analysis of a new flat-plate solar air heater having different obstacles on absorber plates. Applied Energy, 87(11), pp. 3438–3450. https://doi.org/10.1016/j.apenergy.2010.05.017
10. Al-Neama, M.A., & Farkas, I. (2019). Energy efficiency of vertical and horizontal-finned solar collector integrated with forced air circulation dryer for Apple as a sample. Drying Technology, 37(5), 546–558. https://doi.org/10.1080/07373937.2018.1488260
11. Al-Neama M.A. (2018). Performance enhancement of solar air collectors applied for drying processes (Doctoral dissertation, Ph.D. Thesis, Szent Istvan University, Gödöllő)

12. Arunsandeep, G., Lingayat, A., Chandramohan, V.P., Raju, V.R.K., and Reddy, K S. (2018). A numerical model for drying of spherical object in an indirect type solar dryer and estimating the drying time at different moisture level and air temperature. International Journal of Green Energy, 15(3), 189–200. https://doi.org/10.1080/15435075.2018.1433181

13. Ayensu, A., and Asiedu-Bondzie, V. (1986). Solar drying with convective self-flow and energy storage. Solar and Wind Technology, 3(4), 273–279. https://doi.org/10.1016/0741-983X(86)90006-8

14. Babu, A.K., Kumaresan, G., Raj, V.A.A., and Velraj, R. (2018). Review of leaf drying mechanism and influencing parameters, drying methods, nutrient preservation, and mathematical models. Renewable and Sustainable Energy Reviews, 9, pp. 536–556. *https://doi.org/10.1016/j.rser.2018.04.002*

15. Bahrehmand, D. and Ameri, M., (2015): Energy and exergy analysis of different solar air collector systems with natural convection. Renewable Energy, 74, pp. 357–368. *https://doi.org/10.1016/j.renene.2014.08.028*

16. Baniasadi, E., Ranjbar, S., and Boostanipour, O. (2017). Experimental investigation of the performance of a mixed-mode solar dryer with thermal energy storage. Renewable Energy, 112, 143–150. https://doi.org/10.1016/j.renene.2017.05.043

17. Bassey, M.W. (1986). Interaction between temperatures, airflow and chimney design in indirect free convective solar dryers. *Proceedings of the international conference on research and development of renewable energy technologies in Africa*, held in Mauritius, 25-29 March 1985, Vol. 2. DOI:10.14217/9781848594098-2-en

18. Belessiotis, V., and Delyannis, E. (2011). Solar drying. Solar Energy, 85(8), 1665–1691. https://doi.org/10.1016/J.SOLENER.2009.10.001

19. Bena, B., and Fuller, R. J. (2002). Natural convection solar dryer with biomass back-up heater. Solar Energy, 72(1), 75–83. www.elsevier.com/locate/solener

20. Bennamoun, L., and Belhamri, A. (2003). Design and simulation of a solar dryer for agriculture products. Journal of Food Engineering, 59(2–3), 259–266. https://doi.org/10.1016/S0260-8774(02)00466-1

21. Bentley, R.W. (2002). Global oil and gas depletion: An overview. Energy Policy, 30(3). https://doi.org/10.1016/S0301-4215(01)00144-6

22. Bhardwaj, A.K., Kumar, R., Kumar, S., Goel, B., and Chauhan, R. (2021). Energy and exergy analyses of drying medicinal herb in a novel forced convection solar dryer integrated with SHSM and PMM. Sustainable Energy Technologies and Assessments, 45, 101119. https://doi.org/10.1016/J.SETA.2021.101119

23. Bhushan, B., and Singh, R. (2012). Thermal and thermohydraulic performance of roughened solar air heater having protruded absorber plate. Solar Energy, 86 (11), 3388–3396. https://doi.org/10.1016/j. solener.2012.09.004

24. Bolaji, B.O. (2005). Development and performance evaluation of box-type absorber solar air collector. Journal of Food Technology, Vol. 3, pp. 595–600.

25. Cao, F., Zhao, L., Li, H., and Guo, L. (2013). Performance analysis of conventional and sloped solar chimney power plants in China. Applied Thermal Engineering, 50(1), 582–592. https://doi.org/10.1016/j.applthermaleng.2012.06.038

26. Chabane, F., and Moummi, N. (2014). Heat transfer and energy analysis of a solar air collector with smooth plate. The European Physical Journal-Applied Physics, 66(1), 10901. doi:10.1051/epjap/2014130405

27. Chabane, F., Moummi, N., Benramache, S., Bensahal, D., and Belahssen, O. (2013). Collector efficiency by single pass of solar air heaters with and without using fins. Engineering Journal, 17(3), 43–55. https://doi.org/10.4186/ej.2013.17.3.43

28. Chakraverty, A., Mujumdar, A.S. and Ramaswamy, H.S. (2003). Handbook of postharvest technology: cereals, fruits, vegetables, tea, and spices. Vol. 93, Marcel Dekker Inc., New York. ISBN: 0-8247-0514-9

29. Chasiotis, V., Tzempelikos, D., and Filios, A. (2021). Evaluation of a moisture diffusion model for analyzing the convective drying kinetics of Lavandula x allardii Leaves. Computation, Vol. 9 (12), https://doi.org/10.3390/computation 9120141

30. Chaudhari, A.D., and Salve, S.P. (2014). A Review of Solar Dryer Technologies. International Journal of Research in Advent Technology, 2(2), 2321–9637.

31. Chauhan, P.S., Kumar, A., and Tekasakul, P., (2015): Applications of software in solar drying systems: A review. Renewable and Sustainable Energy Reviews, 51, pp. 1326–1337. https://doi.org/10.1016/j.rser.2015.07.025

32. Chauhan, Y.B., and Rathod, P.P., (2020): A comprehensive review of the solar dryer. International Journal of Ambient Energy, 41(3), pp. 348–367. Taylor and Francis Ltd. https://doi.org/10.1080/01430750.2018.1456960

33. Chen, W., and Qu, M., (2014): Analysis of the heat transfer and airflow in solar chimney drying system with porous absorber. Renewable Energy, 63, 511–518. https://doi.org/10.1016/j.renene.2013.10.006

34. Chen, Z.D., Bandopadhayay, P., Halldorsson, J., Byrjaisen, C., Heiselberg, P. and Li, Y., (2003): An experimental investigation of a solar chimney model with uniform wall heat flux. Building and Environment, 38(7), pp. 893–906. https://doi.org/10.1016/S0360-1323(03)00057-X

35. Chung, L.P., Ahmad, M.H., Ossen, D.R., and Hamid, M., (2015): Effective solar chimney cross section ventilation performance in Malaysia terraced house. Procedia - Social and Behavioral Sciences, 179, 276–289. https://doi.org/10.1016/j.sbspro.2015.02.431

36. Condorí, M., Duran, G., Echazú, R., and Altobelli, F., (2017): Semi-industrial drying of vegetables using an array of large solar air collectors. Energy for Sustainable Development, 37, 1–9. https://doi.org/10.1016/J.ESD.2016.11.004

37. Correia, A.F.K., Loro, A.C., Zanatta, S., Spoto, M.H.F., and Vieira, T.M.F.S., (2015): Effect of Temperature, Time, and Material Thickness on the Dehydration Process of Tomato. International Journal of Food Science, 2015, 1–7. https://dx.doi.org/10.1155/2015/970724

38. Corzo, O., Bracho, N., Pereira, A., and Vásquez, A., (2008): Weibull distribution for modeling air drying of coroba slices. LWT - Food Science and Technology, 41(10), pp. 2023–2028. https://doi.org/10.1016/j.lwt.2008.01.002

39. Da Silva, W.P., E-Silva, C.M., Gama, F.J., and Gomes, J.P., (2014): Mathematical models to describe thin-layer drying and to determine drying rate of whole bananas. Journal of the Saudi Society of Agricultural Sciences, 13(1), 67–74. https://doi.org/10.1016/j.jssas.2013.01.003

40. Das, M., and Akpinar, E.K. (2020). Determination of thermal and drying performances of the solar air dryer with solar tracking system: Apple drying test. Case Studies in Thermal Engineering, 21, 100731. https://doi.org/10.1016/J.CSITE.2020.100731

41. Das, S., and Kumar, Y. (1989). Design and performance of a solar dryer with vertical collector chimney suitable for rural application. Energy Conversion and Management, 29(2), 129–135. https://doi.org/10.1016/ 0196-8904(89)90021-6

42. Demir, V., Gunhan, T., and Yagcioglu, A.K. (2007). Mathematical modelling of convection drying of green table olives. Biosystems Engineering, 98(1), 47–53. https://doi.org/10.1016/j.biosystemseng.2007.06.011

43. Dhanushkodi, S., Wilson, V.H., and Sudhakar, K., (2017): Mathematical modeling of drying behavior of cashew in a solar biomass hybrid dryer. Resource-Efficient Technologies, 3(4), pp. 359–364. *https://doi.org/10.1016/j.reffit.2016.12.002*

44. Dheyab, H.S., Al-Jethelah, M.S.M., Yassen, T.A., and Ibrahim, T.K., (2019): Experimental study of the optimum air gap of a rectangular solar air heater. Journal of Advanced Research in Fluid Mechanics and Thermal Sciences, 59(2), pp. 318–329.

45. Dissa, A.O., Bathiebo, J., Kam, S., Savadogo, P.W., Desmorieux, H., and Koulidiati, J., (2009): Modelling and experimental validation of thin layer indirect solar drying of mango slices. Renewable Energy, 34(4), pp. 1000–1008. *https://doi.org/10.1016/j.renene.2008.08.006*

46. Doymaz, I. (2009): An experimental study on drying of green apples. Drying Technology, 27(3), pp. 478–485. *https://dx.doi.org/10.1080/07373930802686065*

47. Duffie, J.A., and Beckman, W.A., (2013): *Solar Engineering of Thermal Processes*, 4th ed. Wiley, Hoboken, NJ, USA. *ISBN: 9781118671603*

48. Ekechukwu, O.V., and Norton, B., (1999): Review of solar-energy drying systems II: an overview of solar drying technology. Energy Conversion and Management, 40(3), 216. *https://doi.org/10.1016/s0140-6701(99)97881-5*

49. Ekechukwu, O.V., (1999): Review of solar-energy drying systems I: An overview of drying principles and theory. Energy Conversion and Management, 40(6), 593–613. *https://doi.org/10.1016/S0196-8904(98)00092-2*

50. Ekechukwu, O.V., and Norton, B., (1997): Design and measured performance of a solar chimney for natural-circulation solar-energy dryers. Renewable Energy, 10(1), 81–90. *https://doi.org/10.1016/0960-1481(96)00005-5*

51. Ekka, J.P., Bala, K., Muthukumar, P., and Kanaujiya, D.K. (2020). Performance analysis of a forced convection mixed mode horizontal solar cabinet dryer for drying of black ginger (Kaempferia parviflora) using two successive air mass flow rates. Renewable Energy, 152, pp. 55–66. *https://doi.org/10.1016/j.renene.2020.01.035*

52. El Hage, H., Herez, A., Ramadan, M., Bazzi, H., and Khaled, M., (2018): An investigation on solar drying: A review with economic and environmental assessment. Energy, 157, pp. 815–829. *https://doi.org/10.1016/J.ENERGY.2018.05.197*

53. El-Sebaii, A.A., Aboul-Enein, S., Ramadan, M.R.I., and El-Gohary, H.G., (2002): Experimental investigation of an indirect type natural convection solar dryer. Energy Conversion and Management, 43(16), pp. 2251–2266. *https://doi.org/10.1016/S0196-8904(01)00152-2*

54. El-Sebaii, A.A., Al-Hazmi, F.S., Al-Ghamdi, A.A., and Yaghmour, S.J., (2010): Global, direct and diffuse solar radiation on horizontal and tilted surfaces in Jeddah, Saudi Arabia. Applied Energy, 87(2), pp. 568–576. *https://doi.org/10.1016/j.apenergy.2009.06.032*

55. El-Sebaii, A.A., and Shalaby, S.M., (2012): Solar drying of agricultural products: A review. Renewable and Sustainable Energy Reviews, 16(1), pp. 37–43. Elsevier Ltd. *https://doi.org/10.1016/j.rser.2011.07.134*

56. Eltawil, M.A., Azam, M.M., and Alghannam, A.O. (2018). Solar PV powered mixed-mode tunnel dryer for drying potato chips. Renewable Energy, 116, 594–605. https://doi.org/10.1016/J.RENENE.2017.10.007

57. Emeksiz, C., (2020): The estimation of diffuse solar radiation on tilted surface using created new approaches with rational function modeling. Indian Journal of Physics, 94(9), pp. 1311–1322. *https://doi.org/10.1007/s12648-019-01573-w*

58. Ertekin, C., and First, Z.M. (2017). A comprehensive review of thin-layer drying models used in agricultural products. Critical Reviews in Food Science and Nutrition, 57(4), 701–717. https://dx.doi.org/10.1080/10408398.2014.910493

59. Everitt, S.K. (1980). Solar food dryer (Patent No. US 4221059).

60. Farkas, I., (2008). Solar drying, Stewart Postharvest Review. 2(9), pp. 2–8.

61. Farkas, I., (2011). Application of solar drying technologies for biological products conservation. Environmental Engineering and Management Journal, 10(8), pp. 1207–1212.

62. Farkas, I., (2013). Integrated use of solar energy for crop drying. Drying Technology, 31(7), pp. 866–871. https://doi.org/10.1080/07373937.2013.790410

63. Felfoldi, J., Vanyi, N., Nyeki, J., Szabo, Z., and Soltesz, M., (2011). Economic figures of apple production at national level of Hungary. International Journal of Horticultural Science, 17(4-5), pp. 103–105.

64. Ferahta, F.Z., Bougoul, S., Medale, M., and Abid, C., (2012). Influence of the air gap layer thickness on heat transfer between the glass cover and the absorber of a solar collector. Fluid Dynamics and Materials Processing, 8(3), pp. 339–351. https://doi.org/10.3970/fdmp.2012.008.339

65. Ferreira, A.G., Maia, C.B., Cortez, M.F.B., and Valle, R.M. (2008). Technical feasibility assessment of a solar chimney for food drying. Solar Energy, 82(3), 198–205. https://doi.org/10.1016/j.solener.2007.08.002

66. Forson, F.K., Nazha, M.A.A., Akuffo, F.O., and Rajakaruna, H. (2007). Design of mixed-mode natural convection solar crop dryers: Application of principles and rules of thumb. Renewable Energy, 32(14), 2306–2319. https://doi.org/10.1016/j.renene.2006.12.003

67. Fudholi, A., Othman, M.Y., Ruslan, M.H., and Sopian, K. (2013): Drying of Malaysian Capsicum annuum L. (red chili) dried by open and solar drying. International Journal of Photoenergy, pp. 1–9. *https://doi.org/10.1155/2013/167895*

68. Fudholi, A., and Sopian, K. (2019). A review of solar air flat plate collector for drying application. Renewable and Sustainable Energy Reviews, 102, 333–345. https://doi.org/10.1016/J.RSER.2018.12.032

69. Fudholi, A., Sopian, K., Ruslan, M.H., Alghoul, M. A., and Sulaiman, M. Y. (2010). Review of solar dryers for agricultural and marine products. In Renewable and Sustainable Energy Reviews (Vol. 14, Issue 1, pp. 1–30). https://doi.org/10.1016/j.rser.2009.07.032

70. Getahun, E., Gabbiye, N., Delele, M.A., Fanta, S.W., and Vanierschot, M. (2021). Two-stage solar tunnel chili drying: Drying characteristics, performance, product quality, and carbon footprint analysis. Solar Energy, 230, 73–90. https://doi.org/10.1016/J.SOLENER.2021.10.016

71. Ghaffari, A., and Mehdipour, R. (2015). Modeling and improving the performance of cabinet solar dryer using computational fluid dynamics. International Journal of Food Engineering, 0(0). https://doi.org/10.1515/ijfe-2014-0266

72. Ghatrehsamani, and Zomorodian. (2012). Impacts of drying air temperature, bed depth and air flow rate on walnut drying rate in an indirect solar dryer. International Journal of Agriculture Sciences, 4(6), 253–256. https://doi.org/10.9735/0975-3710.4.6

73. Ghritlahre, H.K., and Sahu, P.K., (2020). A comprehensive review on energy and exergy analysis of solar air heaters. Archives of Thermodynamics, 41(3), pp. 183–222. https://doi.org/10.24425/ather.2020.134577

74. Gray, D.D., and Giorgini, A. (1976). The validity of the boussinesq approximation for liquids and gases. International Journal of Heat and Mass Transfer, 19(5), 545–551. https://doi.org/10.1016/0017-9310(76)90168-X

75. Gulcimen, F., Karakaya, H., and Durmus, A. (2016). Drying of sweet basil with solar air collectors. Renewable Energy, 93, 77–86. https://doi.org/10.1016/j.renene.2016.02.033

76. Gupta, M.K., and Kaushik, S.C., (2008). Exergetic performance evaluation and parametric studies of solar heater. Energy, 33(11), pp. 1691–1702

77. Gupta, V., Sunil, L., Sharma, A., and Sharma, N. (2012). Construction and performance analysis of an indirect solar dryer integrated with solar air heater. Procedia Engineering, 38, 3260–3269. https://doi.org/10.1016/j.proeng.2012.06.377

78. Hajar, E., Rachid, T., and Najib, B.M. (2017). Conception of a Solar Air Collector for an Indirect Solar Dryer. Pear Drying Test. Energy Procedia, 141, 29–33. https://doi.org/10.1016/j.egypro.2017.11.114

79. Habtay, G., Al-Neama, M.A., Buzas, J., and Farkas, I. (2021). Experimental performance of solar air heaters for drying applications. European Journal of Energy Research, 1(5), 4–10. https://doi.org/10.24018/ejenergy.2021.1.5.29

80. Hedayatizadeh, M., and Chaji, H. (2016). A review on plum drying. In Renewable and Sustainable Energy Reviews, 56, 362–367). https://doi.org/10.1016/j.rser.2015.11.087

81. Hegde, V.N., Hosur, V.S., Rathod, S.K., Harsoor, P.A., and Narayana, K.B. (2015). Design, fabrication and performance evaluation of solar dryer for banana. Energy, Sustainability and Society, 5(23), 1–12. https://doi.org/10.1186/s13705-015-0052-x

82. Henderson, S.M., and Pabis, S. (1961). Journal of Agricultural Engineering Research. Journal of Agricultural Engineering Research, 6, 169–174.

83. Hussain, F., Akhtar, I., Murtaza, G., Haider, U., Rukh, L. and Owais, M. (2021). Simulation and performance evaluation of solar tunnel dryer for apricot drying in northern Pakistan. International Journal of Applied Sciences and Engineering, 9(1), 1–5.

84. Ibrahim, Z., Ibarahim, Z., Yatim, B., and Ruslan, M.H. (2013). Energy efficiency of single-pass solar air collector. AIP Conference Proceedings, 1571, 90–94. https://doi.org/10.1063/1.4858635

85. Jangam, S.V., (2011). An overview of recent developments and some R and D challenges related to drying of foods. Drying Technology, 29(12), 1343–1357. https://doi.org/10.1080/07373937.2011.594378

86. Kafui, A.D., Seres, I., and Farkas, I. (2019). Efficiency Comparison of Different Photovoltaic Modules. Acta Technologica Agriculturae, 22(1), 5–11. https://doi.org/10.2478/ata-2019-0002

87. Kapadiya, S., and Desai, M.A. (2014). Solar Drying of Natural and Food Products: A Review. In International Journal of Agriculture and Food Science Technology (Vol. 5, Issue 6). http://www.ripublication.com/ijafst.htm

88. Karim, M.A., & Hawlader, M.N.A. (2004). Development of solar air collectors for drying applications. Energy Conversion and Management, 45(3), 329–344. https://doi.org/10.1016/S0196-8904(03)00158-4

89. Karim, M.A., and Hawlader, M.N.A. (2006a). Performance investigation of flat plate, v-corrugated and finned air collectors. Energy, 31(4), 452–470. https://doi.org/10.1016/j.energy.2005.03.007

90. Karim, M.A., and Hawlader, M.N.A. (2006b). Performance evaluation of a v-groove solar air collectors for drying applications. Applied Thermal Engineering, 26(1), 121–130. https://doi.org/10.1016/j.applthermaleng.2005.03.017

91. Kasaeian, A.B., Molana, S., Rahmani, K. and Wen, D., (2017): A review on solar chimney systems. Renewable and Sustainable Energy, 67, 954–987. *https://doi.org/10.1016/ j. rser.2016.09.081*

92. Khaldi, S., Korti, A.I.N., and Abboudi, S. (2017). Improving the Airflow Distribution Within an Indirect Solar Dryer by Modifications Based on Computational Fluid Dynamics. International Journal of Air-Conditioning and Refrigeration, 25(03), 1750022. *https://doi.org/10.1142/s2010132517500225*

93. Khama, R., Aissani, F., and Alkama, R. (2016). Design and performance testing of an industrial-scale indirect solar dryer. Journal of Engineering Science and Technology, 11(9), pp. 1263–1281.

94. Khanlari, A., Güler, H.Ö., Tuncer, A.D., Şirin, C., Bilge, Y.C., Yılmaz, Y., & Güngör, A. (2020). Experimental and numerical study of the effect of integrating plus-shaped perforated baffles to solar air collector in drying application. Renewable Energy, 145, pp. 1677–1692. *https://doi.org/10.1016/j.renene.2019.07.076*

95. Krishnananth, S.S., & Kalidasa Murugavel, K. (2013). Experimental study on double pass solar air heater with thermal energy storage. Journal of King Saud University - Engineering Sciences, 25(2), pp. 135–140. *https://doi.org/10.1016/j.jksues.2012.05.004*

96. Koyuncu, T. (2006). An investigation on the performance improvement of greenhouse-type agricultural dryers. Renewable Energy, 31(7), pp. 1055–1071. *https://doi.org/10.1016/j.renene.2005.05.014*

97. Kucuk, H., Midilli, A., Kilic, A., and Dincer, I., (2014): A review on thin-layer drying-curve equations. Drying Technology, 32(7), pp. 757–773. Taylor and Francis Inc. *https://doi.org/10.1080/07373937.2013.873047*

98. Kumar, N., and Sharma, H.K. (2022): 'Drying'. In Sharma, H. K., Kumar, N (eds) *Agro-Processing and Food Engineering:* operational and application aspects. Singapore: Springer Nature, pp. 147–215. *https://doi.org/10.1007/978-981-16-7289-7_5*

99. Kumar, A., Singh, R., Prakash, O., and Ashutosh., (2014): Review on global solar drying status. Agricultural Engineering International: CIGR Journal, 16(4), pp. 161–177.

100. Kumar, M., Sansaniwal, S.K., and Khatak, P., (2016): Progress in solar dryers for drying various commodities. Renewable and Sustainable Energy Reviews, (55), pp. 346–360. *https://doi.org/10.1016/j.rser.2015.10.158*

101. Kumar Nayak, P., Basumatary, B., Roy, M., Basumatary, D., Narzary, S., Deuri, U., Nayak, P.K., and Kumar, N. (2013). Design, Construction and Calibration of Low-Cost Solar Cabinet Dryer. International Journal of Environmental Engineering and Management, 4 (4), pp. 351–358. *http://www.ripublication.com/ijeem.htm*

102. Kumar, R., Goel, V., Singh, P., Saxena, A., Kashyap, A.S., Rai, A. (2019): Performance evaluation and optimization of solar assisted air heater with discrete multiple arc shaped ribs. Journal of Energy Storage, 26, pp. 100978. *https://doi.org/10.1016/j.est.2019.100978*

103. Leon, M.A., Kumar, S., and Bhattacharya, S.C., (2002): A comprehensive procedure for performance evaluation of solar food dryers. Renewable and Sustainable Energy Reviews, 6 (4), pp. 367–393. *https://doi.org/10.1016/S1364-0321(02)00005-9*

104. Lewis, W.K., (1921): The rate of drying of solid materials. Journal of Industrial and Engineering Chemistry, 13, pp. 427–432.

105. Lingayat, A.B., Chandramohan, V.P., and Raju, V.R.K. (2017): Design, development and performance of indirect type solar dryer for banana drying. Energy Procedia, 109, pp. 409–416. *https://doi.org/10.1016/j.egypro.2017.03.041*

106. Lingayat, A., Chandramohan, V.P. and Raju, V.R.K. (2020a): Energy and exergy analysis on drying of banana using indirect type natural convection solar dryer. Heat Transfer Engineering, 41(6-7), pp. 551–561.

107. Lingayat, A.B., Chandramohan, V.P., Raju, V.R.K. and Meda, V. (2020b): A review on indirect type solar dryers for agricultural crops–dryer setup, its performance, energy storage and important highlights. Applied Energy, 258(109), pp. 409–416. *https://doi.org/10.1016/j.apenergy.2019.114005*

108. Liu, B.Y.H., and Jordan, R.C., (1963): The long-term average performance of flat-plate solar-energy collectors. Solar Energy, 7(2), pp. 53–74.

109. Macedo, I.C., and Altemani, C.A.C., (1978): Experimental evaluation of natural convection solar air heaters. Solar Energy, 20(5), pp. 367–369. *https://doi.org/10.1016/0038-092X(78)90151-2*

110. Madhlopa, A., Jones, S.A., and Saka, J.K., (2002): A solar air heater with composite-absorber systems for food dehydration. Renewable Energy, 27(1), pp. 27–37. *https://doi.org/10.1016/S0960-1481(01)00174-4*

111. Mahapatra, A., and Tripathy, P.P., (2019). Thermal performance analysis of natural convection solar dryers under no load condition: experimental investigation and numerical simulation. International Journal of Green Energy, 16(15), pp. 1448–1464. *https://doi.org/10.1080/15435075.2019.1671417*

112. Menges, H.O., and Ertekin, C., (2006): Mathematical modeling of thin layer drying of Golden apples. Journal of Food Engineering, 77(1), pp. 119–125.

113. Moradi, M., Fallahi, M.A., and Mousavi Khaneghah, A., (2020): Kinetics and mathematical modeling of thin layer drying of mint leaves by a hot water recirculating solar dryer. Journal of Food Process Engineering, 43(1). *https://doi.org/10.1111/jfpe.13181*

114. Matavel, C.E., Hoffmann, H., Rybak, C., Hafner, J. M., Salavessa, J., Eshetu, S. B., and Sieber, S., (2021): Experimental evaluation of a passive indirect solar dryer for agricultural products in Central Mozambique. Journal of Food Processing and Preservation, 45(11), pp. 1–11. *https://doi.org/10.1111/jfpp.15975*

115. Meisami-Asl, E., Rafiee, S., Keyhani, A., and Tabatabaeefar, A., (2010): Determination of suitable thin layer drying curve model for apple slices (*variety-Golab*). Plant Omics Journal, 3(3), pp. 103–108.

116. Midilli, A., Kucuk, H., and Yapar, Z., (2002): A new model for single-layer drying. Drying Technology, 20(7), pp. 1503–1513. *https://doi.org/10.1081/DRT-120005864*

117. Mohana, Y., Mohanapriya, R., Anukiruthika, T., Yoha, K.S., Mose, J.A. and Anandharamakrishnan, C., (2020): Solar dryers for food applications: Concepts, designs, and recent advances. Solar Energy, 208, pp. 321–344. *https://doi.org/10.1016/j.solener.2020.07.098*

118. Morgan, C.A., Herman, N., White, P.A., and Vesey, G. (2006). Preservation of micro-organisms by drying; A review. In Journal of Microbiological Methods, 66(2), pp. 183–193. *https://doi.org/10.1016/j.mimet.2006.02.017*

119. Mujumdar, A.S., & Law, C.L., (2010): Drying Technology: Trends and Applications in Postharvest Processing. Food and Bioprocess Technology, 3(6), pp. 843–852. *https://doi.org/10.1007/s11947-010-0353-1*

120. Mustayen, A.G.M.B., Mekhilef, S., and Saidur, R., (2014): Performance study of different solar dryers: A review. Renewable and Sustainable Energy Reviews, 34, pp. 463–470. *https://doi.org/10.1016/j.rser.2014.03.020*

121. Nahar, N.M., and Gupta, M.P., (1989): Studies on gap spacing between absorber and cover glazing in flat plate solar collectors. International Journal of Energy Research, 13(6), pp. 727–732. *https://doi.org/10.1002/er.4440130611*

122. Naplopo. (2014): No title retrieved December 21, 2021, Hálózatra csatlakozó napelemes rendszerek. https://www.naplopo.hu/tudastar/szakcikkeink-hasznos-irasaink/231-napsugarzas-alapjai/.

123. Ndukwu, M.C., Bennamoun, L., Abam, F.I., Eke, A.B. and Ukoha, D., (2017): Energy and exergy analysis of a solar dryer integrated with sodium sulfate decahydrate and sodium chloride as thermal storage medium. Renewable Energy, 113, pp. 1182–1192. https://doi.org/10.1016/j.renene.2017.06.097

124. Noori, A.W., Royen, M.J., Haydary, J., (2021): Thi-layer mathematical modeling of apple slices drying using open sun and cabinet solar drying methods. International Journal of Innovative Research and Scientific Studies, 4(2), pp. 43–52.

125. Odewole, M.M., and Falua, K.J., (2021): Modelling of thin-layer drying of Osmo-Pretreated Red Bell Pepper. Acta Technologica Agriculturae, 24(2), pp. 67–71. *https://doi.org/10.2478/ata-2021-0011*

126. Omojaro, A.P., & Aldabbagh, L.B.Y., (2010): Experimental performance of single and double pass solar air heater with fins and steel wire mesh as absorber. Applied Energy, 87(12), pp. 3759–3765. *https://doi.org/10.1016/j.apenergy.2010.06.020*

127. Page, G., (1949): Factors influencing the maximum rates of air-drying shelled corn in thin layers. M.Sc. thesis, Purdue University, West Lafayette, Illinois, USA.

128. Pagukuman, B.N.D., and Ibrahim, M.K.W., (2021): A review of the significance effect of external factors of the solar dyer design to dried foods product quality. Journal of Engineering, Design and Technology, 19(5), https://doi.org/10.1108/jedt-01-2021-0033

129. Park, S.R., Pandey, A.K., Tyagi, V.V., and Tyagi, S.K., (2014): Energy and exergy analysis of typical renewable energy systems. Renewable and Sustainable energy Reviews, 30, pp. 105–123. *https://doi.org/10.1016/j.rser.2013.09.011*

130. Phadke, P.C., Walke, P.V., and Kriplani, V.M., (2015): A review on indirect solar dryers. ARPN Journal of Engineering and Applied Sciences. 10(8), pp. 3360–3371.

131. Prakash, O., Kumar, A., and Laguri, V., (2016). Performance of modified greenhouse dryer with thermal energy storage. Energy reports, 2, pp. 155–162. https://doi.org/10.1016/j.egyr.2016.06.003

132. Pramanik, R.N., Sahoo, S.S., Swain, R.K., Mohapatra, T.P., and Srivastava, A.K., (2017): Performance analysis of double pass solar air heater with bottom extended surface. Energy Procedia, 109, pp. 331–337. *https://doi.org/10.1016/j.egypro.2017.03.077*

133. Qasaimeh, A., (2012): Solar Energy Optimization through Seasons: Case Study in Jordan. Smart Grid and Renewable Energy, 03(04), pp. 275–281. *https://doi.org/10.4236/sgre.2012.34038*

134. Ong, K.S., and Chow, C.C., (2003): Performance of a solar chimney. Renewable Energy, 74(1), pp. 1–17. https://doi.org/10.1016/S0038-092X(03)00114-2

135. Öybek, B., and Dadali, G., (2007): Thin-layer drying characteristics and modelling of mint leaves undergoing microwave treatment. Journal of Food Engineering, 83(4), pp. 541–549. *https://doi.org/10.1016/j.jfoodeng.2007.04.004*

136. Ozturk, H.H., and Demirel, Y., (2004). Exergy-based performance analysis of packed-bed solar air heaters. International Journal of Energy, 28, pp. 423–432. https://doi.org/10.1002/er.974

137. Rajasheker, G., and Chandramohan, V.P., (2017): Estimation of initial moisture content of agricultural products by an ASTM experimental procedure. Indian Journal of Natural and Sciences, 8(43), pp. 12618–12622.

138. Rayaguru, K., and Routray, W., (2012): Mathematical modeling of thin layer drying kinetics of stone apple slices. International Food Research Journal, 19(4), pp. 1503–1510. *http://agris.upm.edu.my:8080/dspace/handle/0/11805*

139. Rusirawan, D. (2012): Energetic modelling of photovoltaic modules in grid-connected systems (Doctoral thesis, Szent István University, Gödöllő, Hungary). Retrieved from *https://archive2020.szie.hu/file/tti/archivum/Rusirawan_dissertation_final.pdf*.

140. Russon, J.K., Dunn, M.L., and Steele, F.M., (2009): Optimization of a convective air flow solar food dryer. International of Food Engineering, 5 (1). *https://doi.org/10.2202/1556-3758.1500*

141. Samimi, A.H., Arabhosseini, A., Kianmehr,M.H., (2016): Effective moisture diffusivity during hot air solar drying of tomato slices. Research in Agricultural Engineering, 62, pp. 15–23.

142. Sangamithra, A., Swamy, G.J., Prema, R.S., Priyavarshini, R., Chandrasekar, V., and Sasikala, S., (2014): An overview of a polyhouse dryer. Renewable and Sustainable Energy Reviews, 40, pp. 902–910. *https://doi.org/10.1016/j.rser.2014.08.007*

143. Saxena, A., Varun, and El-Sebaii, A.A., (2015): A thermodynamic review of solar air heaters. Renewable and Sustainable Energy Reviews, 43, pp. 863–890. Elsevier Ltd. *https://doi.org/10.1016/j.rser.2014.11.059*

144. Sekyere, C.K.K., Forson, F.K., and Adam, F.W. (2016). Experimental investigation of the drying characteristics of a mixed mode natural convection solar crop dryer with back up heater. Renewable Energy, 92, pp. 532–542. *https://doi.org/10.1016/j.renene.2016.02.020*

145. Sharma, A., Chen, C.R., and Nguyen, V.L., (2009): Solar-energy drying systems: A review. Renewable and Sustainable Energy Reviews, 13(6–7), pp. 1185–1210. *https://doi.org/10.1016/j.rser.2008.08.015*

146. Sharma, V.K., Colangelo, A., and Spagna, G., (1992): Investigation of an indirect type multi-shelf solar fruit and vegetable dryer. Renewable Energy, 2(6), pp. 577–586. *https://doi.org/10.1016/0960-1481(92)90021-T*

147. Shi, L., Zhang, G., Cheng, X., Guo, Y., Wang, J., and Chew, M.Y.L., (2016): Developing an empirical model for roof solar chimney based on experimental data from various test rigs. Building and Environment, 110, pp. 115–128. *https://doi.org/10.1016/j.buildenv.2016.10.002*

148. Shringi, V., Kothari, S., and Panwar, N.L., (2014): Experimental investigation of drying of garlic clove in solar dryer using phase change material as energy storage. Journal of Thermal Analysis and Calorimetry, 118(1), 533–539. *https://doi.org/10.1007/s10973-014-3991-0*

149. Simate, I.N., (2003): Optimization of mixed-mode and indirect-mode natural convection solar dryers. Renewable Energy, 28(3), pp. 435–453. *https://doi.org/10.1016/S0960-1481(02)00041-1*

150. Singh, S., (2017): Performance evaluation of a novel solar air heater with arched absorber plate. Renewable Energy, 114, pp. 879–886. *https://doi.org/10.1016/j.renene.2017.07.109*

151. Singh, S., and Kumar, S., (2012): Testing method for thermal performance-based rating of various solar dryer designs. Solar Energy, 86(1), 87–98. *https://doi.org/10.1016/j.solener.2011.09.009*

152. Soeder, D.J., (2021): Fossil Fuels and Climate Change. In Fracking and the Environment. Springer International Publishing, pp. 155-185. *https://doi.org/10.1007/978-3-030-59121-2_9*

153. Solargis. (2020): No title retrieved May 12,2020, from. https://solargis.com/maps-and-gis-data/download/hungary

154. Standard, A.S.H.R.A.E., 1977. Methods of testing to determine the thermal performance of solar collectors. ANSI/ASHRAE, pp. 93–1986.

155. Sreekumar, A., Manikantan, P.E., and Vijayakumar, K.P., (2008: Performance of indirect solar cabinet dryer. Energy Conversion and Management, 49(6), pp.1388–1395. *https://doi.org/10.1016/j.enconman.2008.01.005*

156. Stiling, J., Li, S., Stroeve, P., Thompson, J., Mjawa, B., Kornbluth, K., and Barrett, D. M., (2012): Performance evaluation of an enhanced fruit solar dryer using concentrating panels. Energy for Sustainable Development, 16(2), pp. 224–230. *https://doi.org/10.1016/j.esd.2012.01.002*

157. Sudprasert, S., Chinsorranant, C., and Rattanadecho, P., (2016): Numerical study of vertical solar chimneys with moist air in a hot and humid climate. International Journal of Heat and Mass Transfer, 102, pp. 645–656. *https://doi.org/10.1016/j.ijheatmasstransfer.2016.06.054*

158. Sunil, Varun, and Sharma, N., (2014): Experimental investigation of the performance of an indirect-mode natural convection solar dryer for drying fenugreek leaves. Journal of Thermal Analysis and Calorimetry, 118(1), 523–531. *https://doi.org/10.1007/s10973-014-3949-2*

159. Tan, A.Y.K., and Wong, N.H., (2013): Parameterization studies of solar chimneys in the tropics. Energies, 6(1), pp. 145–163. *https://doi.org/10.3390/en6010145*

160. Tashtosh, G.M., Jaradat, M., Zuraiakt, S., and Aljarah, M., (2014): A mathematical model of indirect solar drying of dairy products (*Jameed*). Energy and Environmental Engineering, 2(1), pp. 1–13. *https://doi.org/10.13189/eee.2014.020101*

161. Tedesco, F.C., Buhler, A., and Wortmann, S., (2019): Design, construction, and analysis of passive indirect solar dryer with chimney. Journal of Solar Energy Engineering, 141(3), pp. 1–9. *https://doi.org/10.1115/1.4041931*

162. Tomar, V., Tiwari, G.N., and Norton, B., (2017). Solar dryers for tropical food preservation: Thermophysics of crops, systems and components. Solar Energy, 154, pp. 2–13. https://doi.org/10.1016/J.SOLENER.2017.05.066

163. Udomkun, P., Romuli, S., Schock, S., Mahayothee, B., Sartas, M., Wossen, T., Njukwe, E., Vanlauwe, B., and Müller, J. (2020). Review of solar dryers for agricultural products in Asia and Africa: An innovation landscape approach. Journal of Environmental Management, 268, 110730. https://doi.org/10.1016/J.JENVMAN.2020.110730

164. Vengsungnle, P., Jongpluempiti, J., Srichat, A., Wiriyasart, S., and Naphon, P. (2020). Thermal performance of the photovoltaic-ventilated mixed mode greenhouse solar dryer with automatic closed loop control for Ganoderma drying. Case Studies in Thermal Engineering, 21(April), 100659. https://doi.org/10.1016/j.csite.2020.100659

165. Vijayan, S., Arjunan, T.V., and Kumar, A. (2016). Mathematical modeling and performance analysis of thin layer drying of bitter gourd in sensible storage based indirect solar dryer. Innovative Food Science and Emerging Technologies, 36, 59–67. https://doi.org/10.1016/j.ifset.2016.05.014

166. Vijayan, S., Arjunan, T.V., and Kumar, A. (2020). Exergo-environmental analysis of an indirect forces convection solar dryer for drying bitter gourd slices. Renewable Energy, 146, pp. 2210–2223. *https://doi.org/10.1016/j.renene.2019.08.066*

167. Vijayavenkataraman, S., Iniyan, S., and Goic, R. (2012). A review of solar drying technologies. In Renewable and Sustainable Energy Reviews (Vol. 16, Issue 5, pp. 2652–2670). https://doi.org/10.1016/j.rser.2012.01.007

168. Wang, C.Y., and Singh, R.P. (1978). A single layer drying equation for rough rice (Patent No. 78–3001). In American Society of Agricultural Engineers (No. 78–3001).

169. Yaciuk, G.I.D.R.C., (1982): Food drying: Proceedings of a workshop held at Edmonton Alberta, 6-9 July 1981. In International Development Research Centre Monographs IDRC-195e 104pp. The Centre.

170. Yaldýz, O., and Ertekýn, C., (2001): Thin layer solar drying of some vegetables. Drying Technology, 19(3–4), pp. 583–597. *https://doi.org/10.1081/DRT-100103936*

171. Zambrano, W., and Alvarado, S., (1984): Design, construction and testing of a chimney that reduces dangerous temperatures in a radiative convective solar dryer. Solar Energy, 32(5), pp. 581–584: *https://doi.org/ 10.1016/0038-092X(84)90132-4*

172. Zang, H., Guo, M., Wei, Z, and Sun, G., (2016): Determination of the optimal tilt angle of solar collectors for different climates of China. Sustainability, 8(7), pp. 654: *https://doi.org/10.3390/su8070654*

173. Zarezade, M., and Mostafaeipour, A., (2016): Identifying the effective factors on implementing the solar dryers for Yazd province, Iran. Renewable and Sustainable Energy Reviews, Vol. 57, pp. 765–775. *https://doi.org/10.1016/j.rser.2015.12.060*

174. Zhang, J., Gupta, A., and Baker, J., (2007): Effect of relative humidity on the prediction of natural convection heat transfer coefficients. Heat Transfer Engineering, 28(4), pp. 335–342. *https://doi.org/10.1080/01457630601122823*

175. Zhang, Q.A., Song, Y., Wang, X., Zhao, W.Q., and Fan, X.H., (2016): Mathematical modeling of debittered apricot (*Prunus armeniaca L.*) kernels during thin-layer drying. CyTA–Journal of Food, 14(4), pp. 509–517. *https://doi.org/10.1080/19476337.2015.1136843*

A2: Publications related to the dissertation

Refereed papers in foreign languages:

1. **Habtay, G.,** Buzas, J., Farkas, I. (2019): Mathematical modelling of cylindrical chimney effect in solar dyer, Hungarian Agricultural Engineering, No. 36/2019, pp. 69-74. *https://doi.org/10.17676/HAE.2019.36.69*
2. **Habtay, G.,** Buzas, J., Farkas, I. (2020): Heat transfer analysis in the chimney of indirect solar dryer under natural convection mode, FME Transactions, 48(3), pp. 701-706. *https://doi.org/10.5937/fme2003701H* (Scopus: Q2)
3. **Habtay, G**., Al-Neama, M. A., Buzas, J., and Farkas, I. (2021): Experimental performance of solar air collectors for drying applications. European Journal of Energy Research, 1(5), pp. 4-10. *https://doi.org/10.24018/ejenergy.2021.1.5.29*
4. **Habtay, G.**, Buzas, J., Farkas, I. (2021): Performance evaluation of solar air collector by chimney effect for drying applications. Acta Technologica Agriculturae, 24(4), pp.159-165. *https://doi.org/10.2478/ata-2021-0027*
5. Dhaundiyal, A., **Habtay, G**. (2022): The effect of psychrometry on the performance of a solar collector. Environmental Science and Pollution Research, 29(9), pp. 13445–13458. *https://doi.org/10.1007/s11356-021-16353-5* (Scopus: Q2, IF = 4.223).
6. **Habtay, G.**, Buzas, J., Farkas, I. (2022): Comparative study on the performance of solar dryer with finned plate solar chimney. Jurnal Tekno Insentif, 16(1), pp. 1–15. *https://doi.org/10.36787/jti.v16i1.453*

Refereed papers in Hungarian language:

7. Buzás, J., **Habtay, G.,** Farkas, I. (2021): Napenergiás kéményes szárító hőtechnikai vizsgálata, Energiagazdálkodás, 62. évf., 2-3. sz., 2021, 18-22. o. ISSN 0021-0757

International conference proceedings

8. **Habtay G.**, Farkas I. (2019): Heat transfer calculation of chimney applied for indirect solar dryer, Proceedings, 7th European Drying Conference, Politecnico di Torino, Italy, July 10-12, 2019, pp. 128-132.
9. **Habtay G.**, Buzas J., Farkas I. (2020): Performance enhancement of a chimney operated passive solar dryer, Proceedings of EuroSun 2020 Conference: 13th International Conference on Solar Energy for Buildings and Industry (ISES), Athens, Greece, September 1-4, 2020, pp. 278-285. ISBN 978-3-9820408-2-0.

International conference abstracts

10. **Habtay, G.**, Farkas, I. (2018): Effect of types of chimneys in an indirect passive solar dryer, Book of Abstracts, 24th Workshop on Energy and Environment, Gödöllő, Hungary, December 6-7, 2018, p. 24, ISBN 978-963-269-787-1.
11. **Habtay G.**, Farkas, I (2019): Free convection heat transfer in solar chimney for solar dryer, Book of abstracts, BioPhys Spring 2019: 18th International Workshop for Young Scientists, Gödöllő, Hungary, May 22-24, 2019, p. 17, ISBN 978-963-269-823-6.
12. **Habtay G.**, Buzas J., Farkas I. (2019): Analysis of the airflow in chimney based indirect solar dryer, Book of abstracts, 25th Workshop on Energy and Environment, Gödöllő, Hungary, November 28-29, 2019, p. 20, ISBN 978-963-9483-95-8.

13. **Habtay G.**, Buzas J., Farkas, I. (2020): Experimental study of chimney used in solar drying applications, Book of abstracts, BioPhys Spring 2020: 19th International Workshop for Young Scientists, Prague, Czech Republic, May 19-21, 2020, p. 36. ISBN: 978-83-89969-64-4.

14. **Habtay G.**, Buzas J., Farkas I. (2020): Solar energy potentials in Eritrea cities, Book of Abstracts, 26th Workshop on Energy and Environment, Gödöllő, Hungary, December 10-11, 2020, p. 10. ISBN 978-963-269-928-8.

15. **Habtay G.**, Buzas J., Farkas, I. (2021): Performance evaluation of chimney dependent solar dryer for apple drying, Book of abstracts, BioPhys Spring 2021, Lublin, Poland, May 18, 2021, p. 70. ISBN 978-83-89969-68-2.

16. **Habtay G.**, Buzas J., Farkas I. (2021): Comparative study on the performance of solar dryer with finned chimney, Book of Abstracts, 13th International Conference on Agrophysics: Agriculture in changing climate (ICA 2021), Lublin, Poland, November 15-16, 2021, p. 49., ISBN 978-83-89969-72-9.

17. **Habtay G.**, Buzas J., Farkas I. (2021): Performance of an indirect natural type of solar dryer, Book of Abstracts, 27th Workshop on Energy and Environment, Gödöllő, Hungary, December 9-10, 2021, p. 20. ISBN 978-963-269-972-1.

A3: Commonly used terms in psychrometry and psychrometry chart

Term	Definition
Capillary flow	The flow of liquid through the interstices and over the surface of a solid is caused by liquid-solid attraction.
Moisture content (*MC*)	A solid is usually expressed as moisture quantity per unit weight of the dry or wet solid.
Constant-rate period	The drying period during which the rate of water removal per unit of drying surface is constant.
Critical moisture content	The average moisture content when the constant-rate period ends.
Equilibrium Moisture content	The limiting moisture to which a given material can be dried under specific conditions of air temperature and humidity.
Falling-rate period	A drying period during which the instantaneous drying rate continually decreases.
Free-moisture content	The liquid which is removable at a given temperature and humidity may include bound/unbounded moisture.
Humidity ratio	The weight of water vapor is associated with the unit weight of dry air.
Relative humidity	The ratio of water vapor pressure in the air to the water vapor pressure of the saturated air.
Enthalpy	The specific heat of air with water vapor content.
Dry bulb temperature	The temperature of moist air is indicated by an ordinary thermometer.
Wet-bulb temperature	The temperature of moist air is indicated by a thermometer, the bulb of which is covered with a wet wick.
Dew point temperature	The temperature at which the condensation of water vapor begins if a mixture of air and water is cooled.

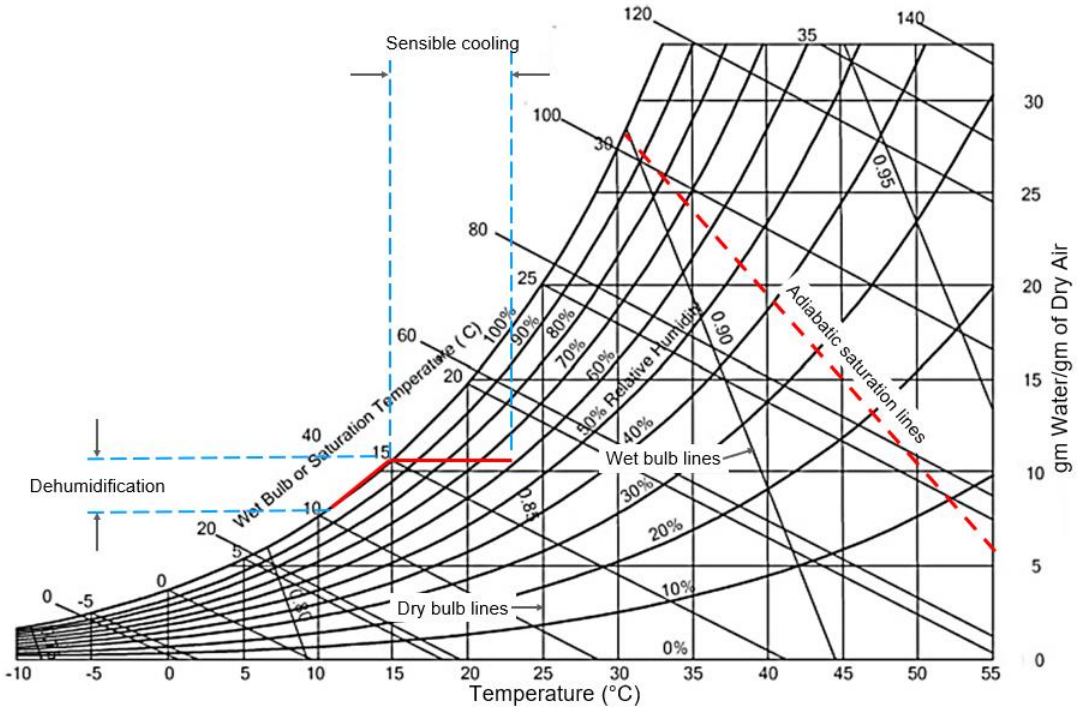

A4: Measuring devices used for the thermal analysis

Pyranometer

Solarimeter

Digital balance

T-type thermocouple

ADAM datalogger

Thermo-hygrometer outdoor

Testo anemometer

Thermo-hygrometer

Moisture analyzer

A5: Temperature profile for each setup without load

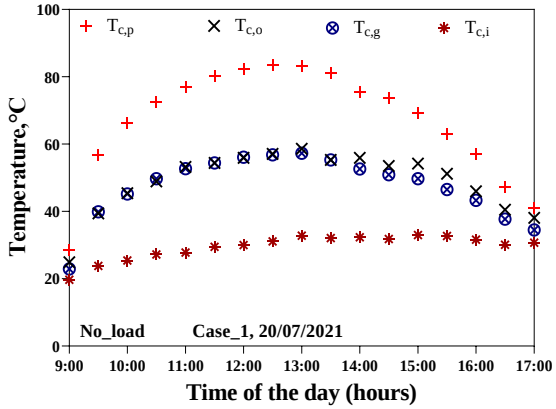

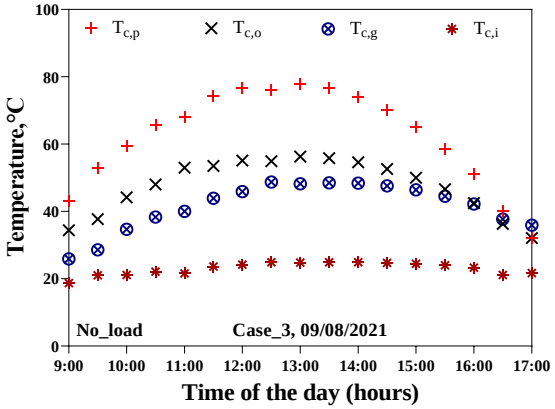

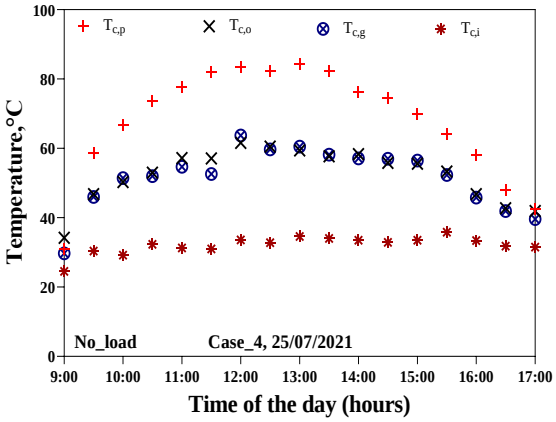

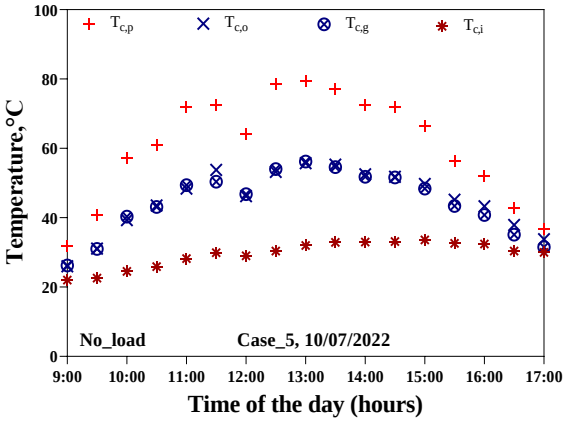

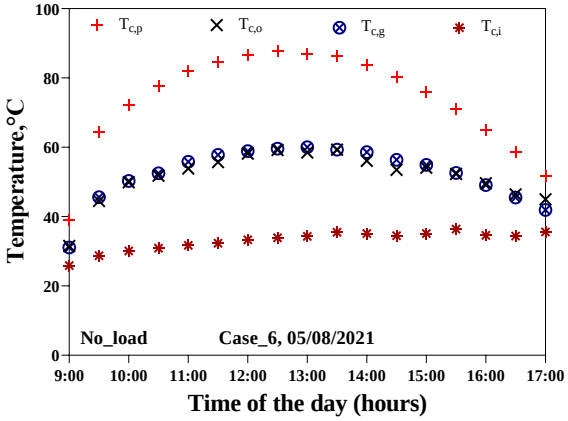

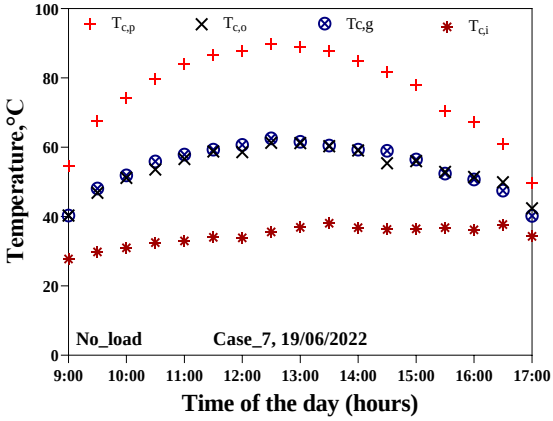

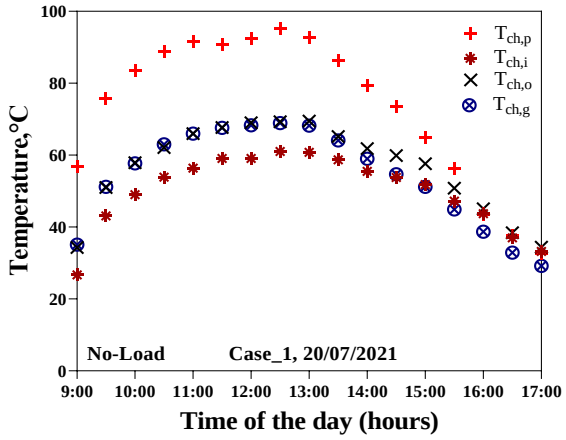
Temperature,°C
Time of the day (hours)
No-Load
Case_1, 20/07/2021
$T_{ch,p}$
$T_{ch,i}$
$T_{ch,o}$
$T_{ch,g}$

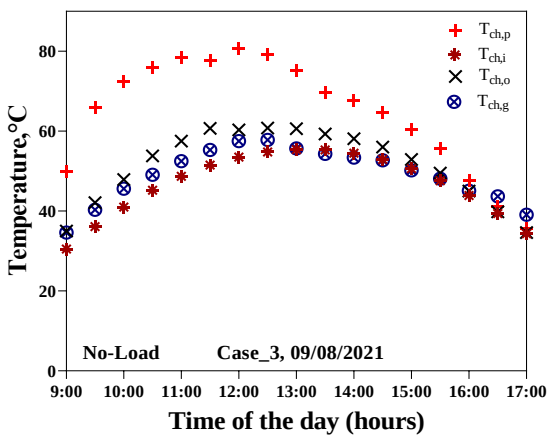
Temperature,°C
Time of the day (hours)
No-Load
Case_3, 09/08/2021
$T_{ch,p}$
$T_{ch,i}$
$T_{ch,o}$
$T_{ch,g}$

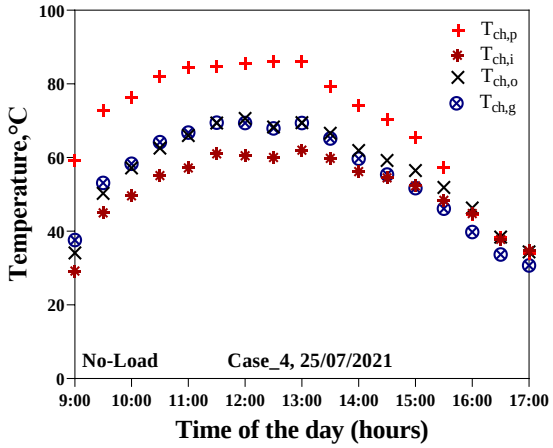
Temperature,°C
Time of the day (hours)
No-Load
Case_4, 25/07/2021
$T_{ch,p}$
$T_{ch,i}$
$T_{ch,o}$
$T_{ch,g}$

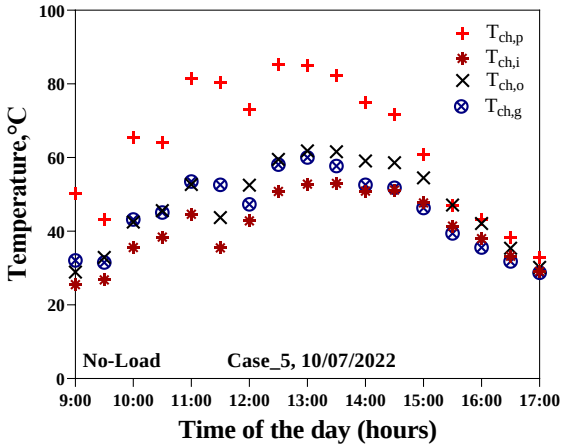
Temperature,°C
Time of the day (hours)
No-Load
Case_5, 10/07/2022
$T_{ch,p}$
$T_{ch,i}$
$T_{ch,o}$
$T_{ch,g}$

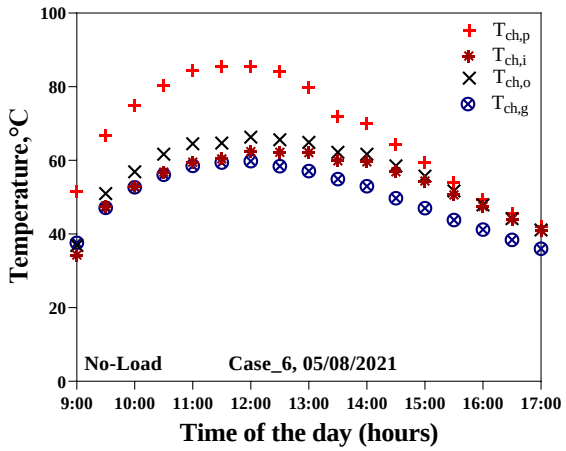
Temperature,°C
Time of the day (hours)
No-Load
Case_6, 05/08/2021
$T_{ch,p}$
$T_{ch,i}$
$T_{ch,o}$
$T_{ch,g}$

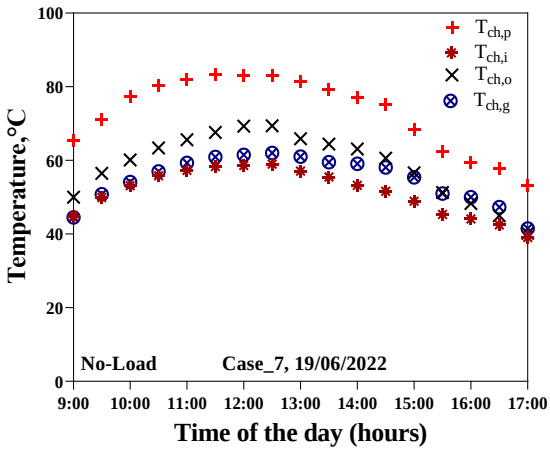
Temperature,°C
Time of the day (hours)
No-Load
Case_7, 19/06/2022
$T_{ch,p}$
$T_{ch,i}$
$T_{ch,o}$
$T_{ch,g}$

A6: Temperature profile for each setup under load conditions

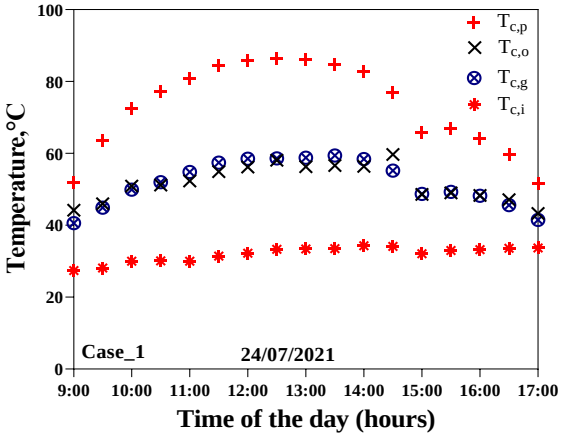

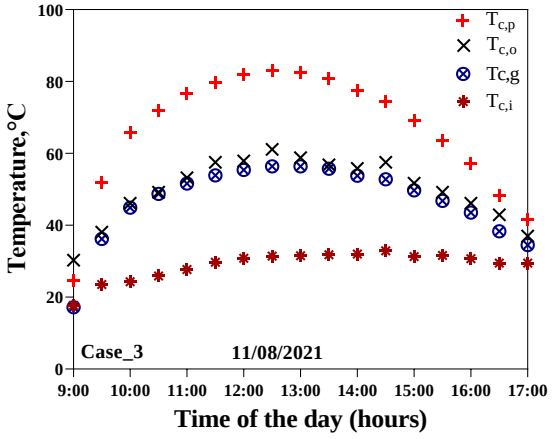

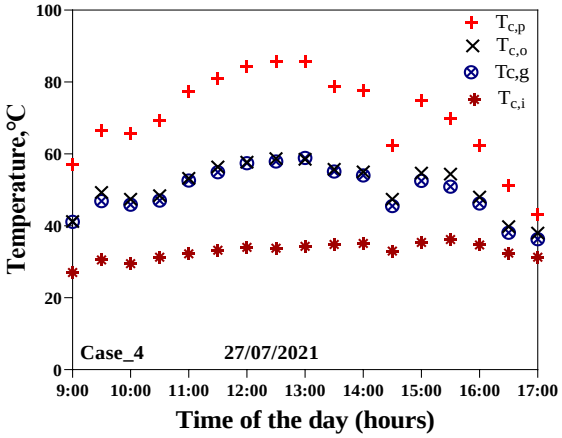

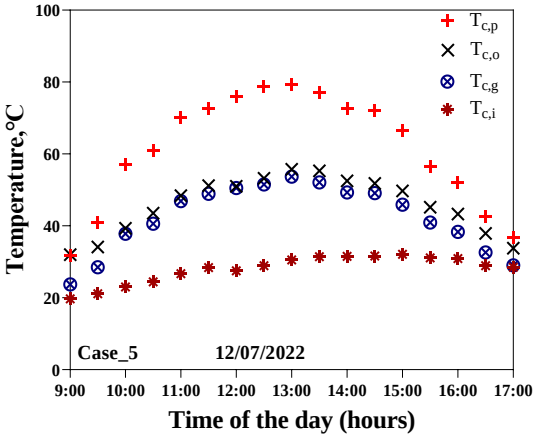

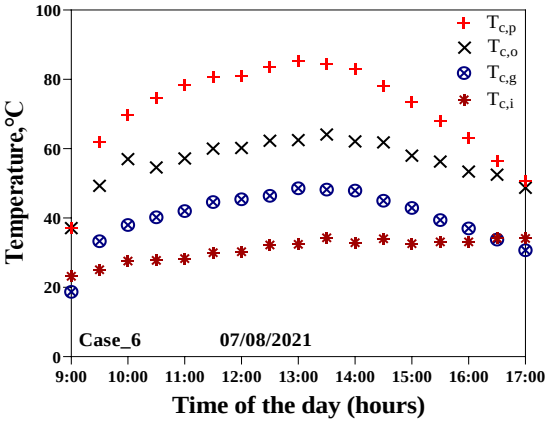

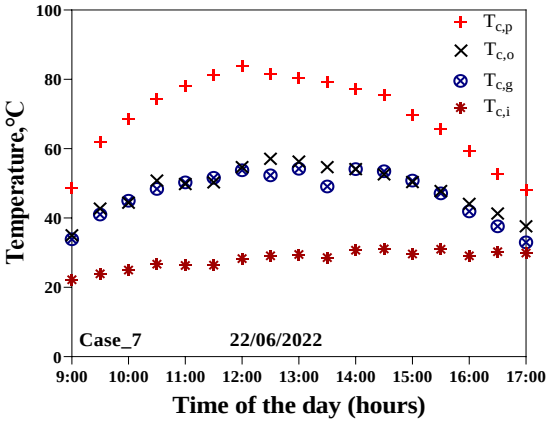

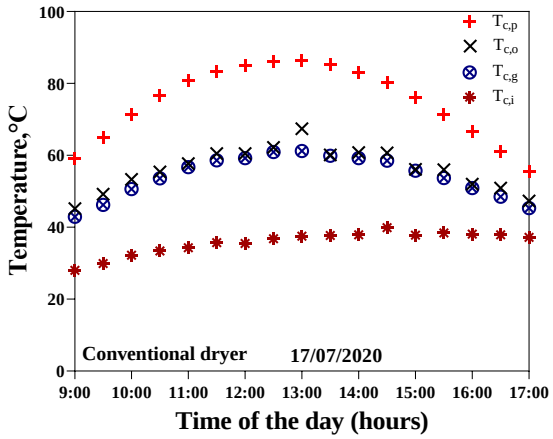
Temperature,°C
Time of the day (hours)
Conventional dryer
17/07/2020
$T_{c,p}$
$T_{c,o}$
$T_{c,g}$
$T_{c,i}$

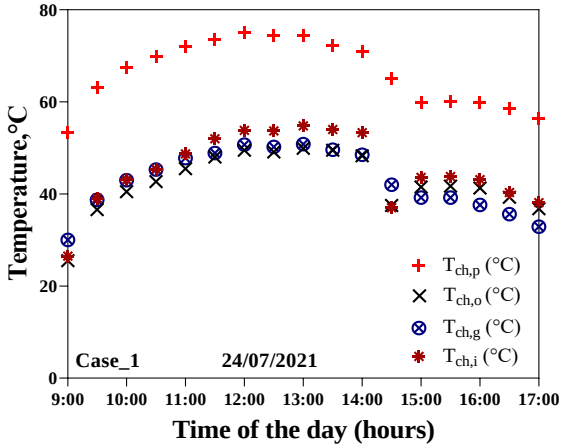
Temperature,°C
Time of the day (hours)
Case_1
24/07/2021
$T_{ch,p}$ (°C)
$T_{ch,o}$ (°C)
$T_{ch,g}$ (°C)
$T_{ch,i}$ (°C)

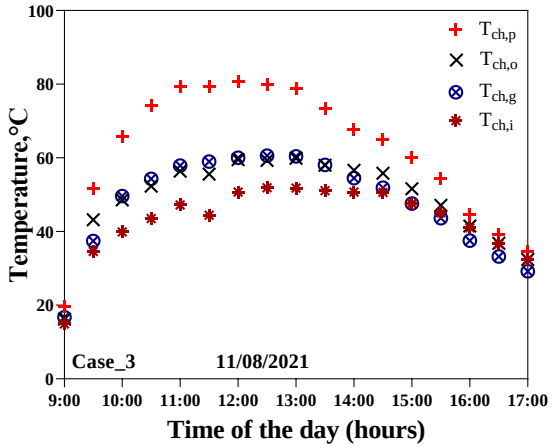
Temperature,°C
Time of the day (hours)
Case_3
11/08/2021
$T_{ch,p}$
$T_{ch,o}$
$T_{ch,g}$
$T_{ch,i}$

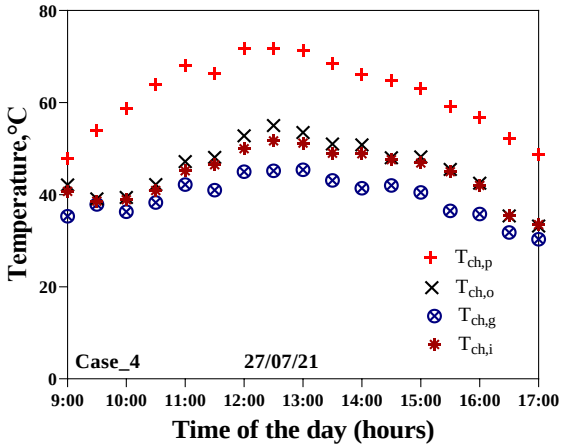
Temperature,°C
Time of the day (hours)
Case_4
27/07/21
$T_{ch,p}$
$T_{ch,o}$
$T_{ch,g}$
$T_{ch,i}$

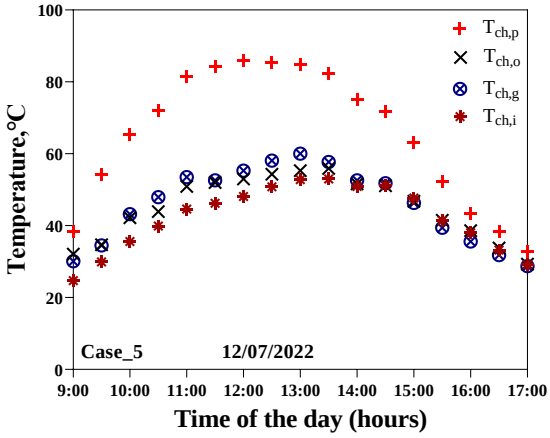
Temperature,°C
Time of the day (hours)
Case_5
12/07/2022
$T_{ch,p}$
$T_{ch,o}$
$T_{ch,g}$
$T_{ch,i}$

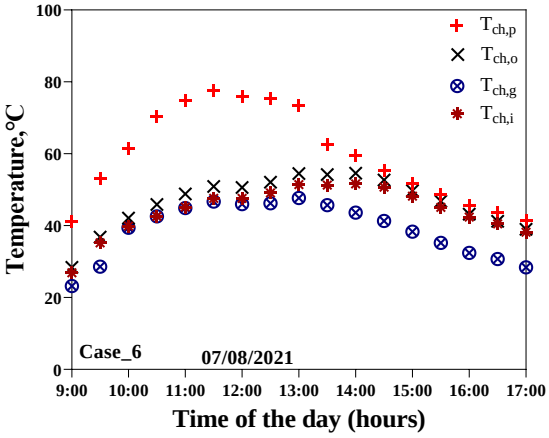
Temperature,°C
Time of the day (hours)
Case_6
07/08/2021
$T_{ch,p}$
$T_{ch,o}$
$T_{ch,g}$
$T_{ch,i}$

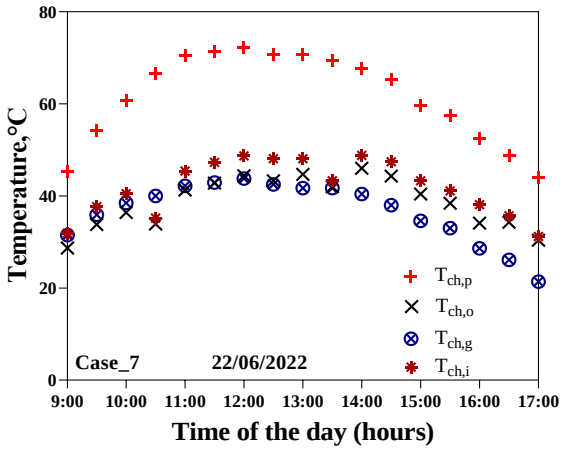

A7: Plot of energy efficiency against solar radiation for each configuration

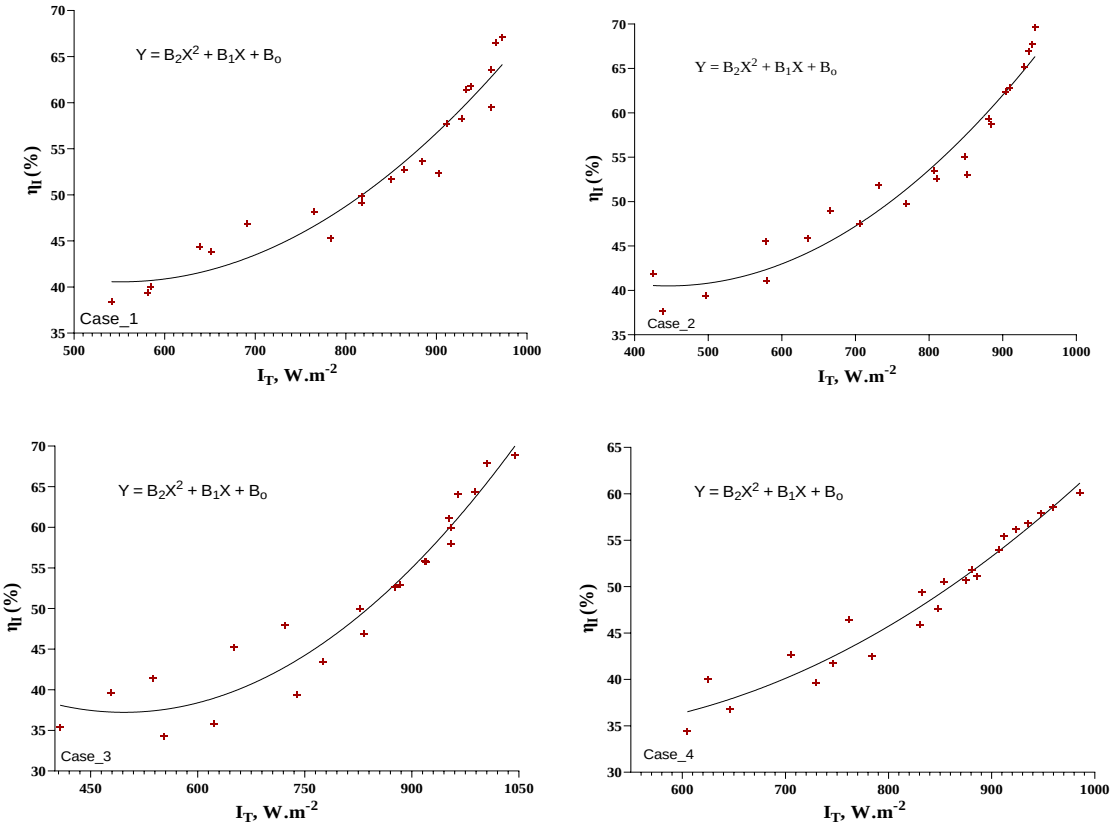

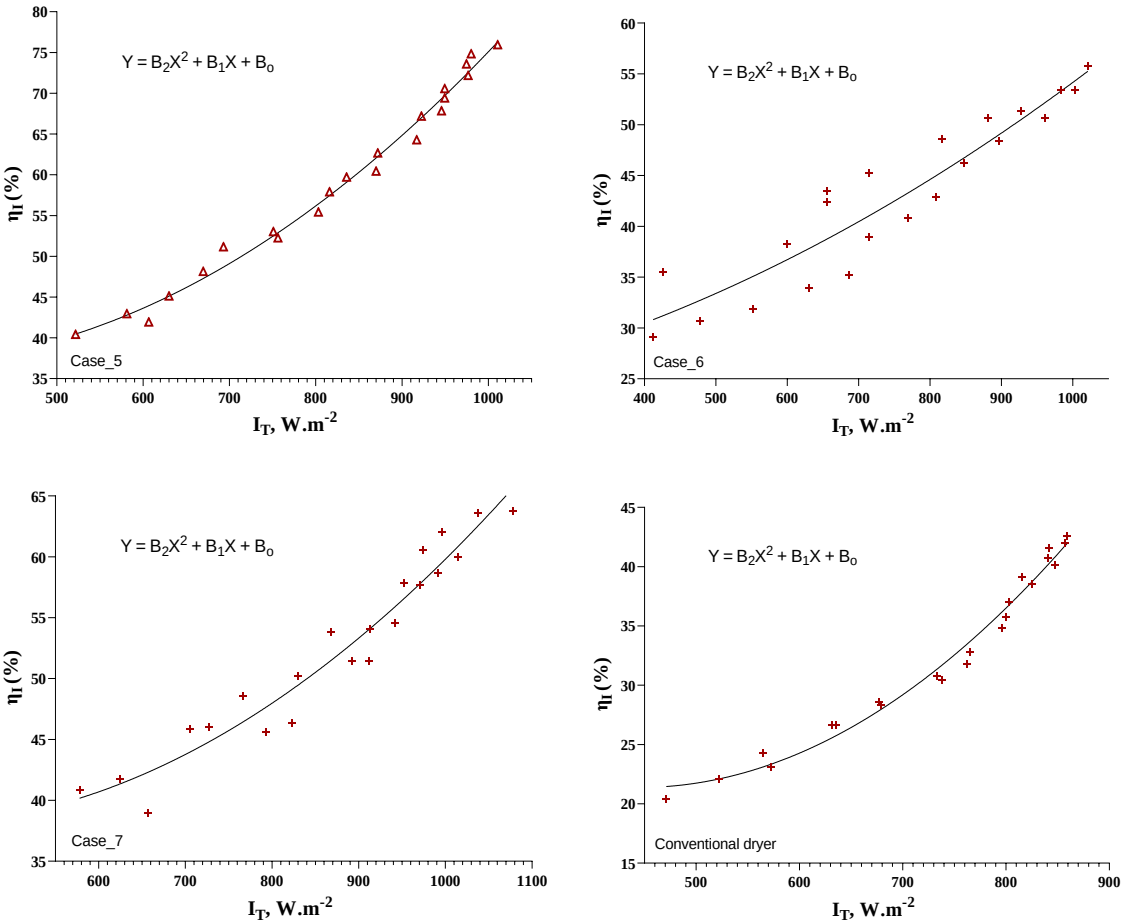

Table A7: Summary a second order polynomial constants

	B_2	B_1	B_o	R^2
Case_1	0.000133	-0.1467	81.04	0.9366
Case_2	0.0001041	-0.09275	61.17	0.9486
Case_3	0.0001093	-0.1086	64.19	0.9346
Case_4	9.428e-005	-0.08523	53.58	0.9558
Case_5	7.963e-005	-0.04878	44.24	0.9892
Case_6	2.071e-005	0.1044	23	0.8779
Case_7	5.686e-005	-0.04321	46.15	0.9418
Case_8	0.0001196	-0.1063	44.99	0.9825

A8: Plot of relative humidity against drying temperature for a solar chimney height of large, medium, small, non-uniform and for conventional dryer

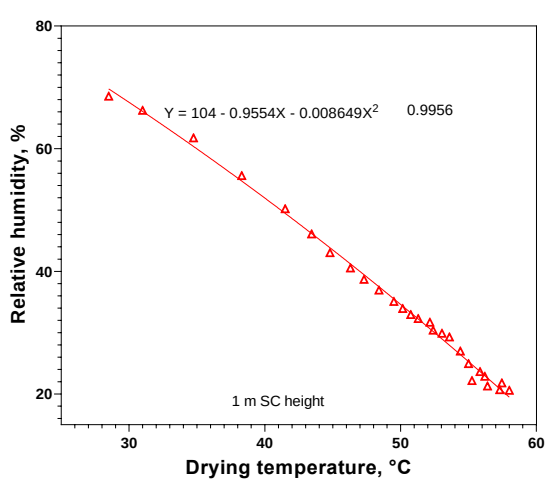

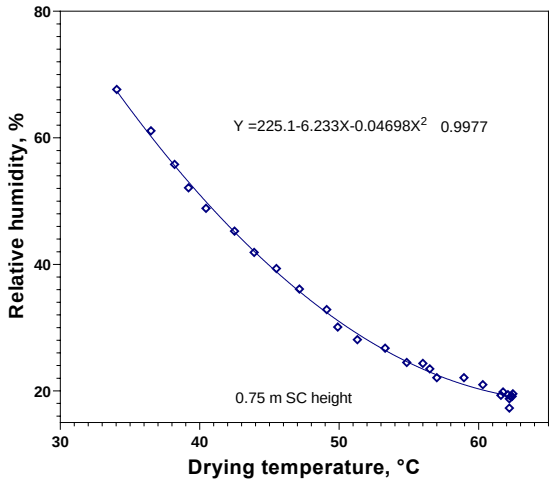

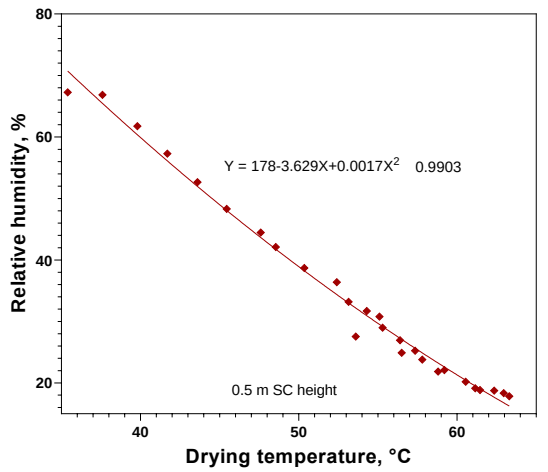

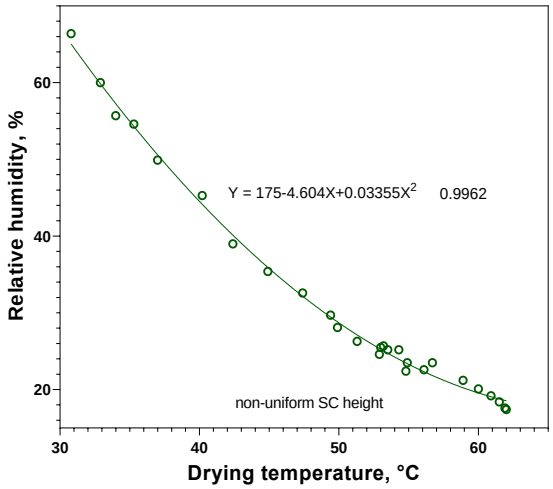

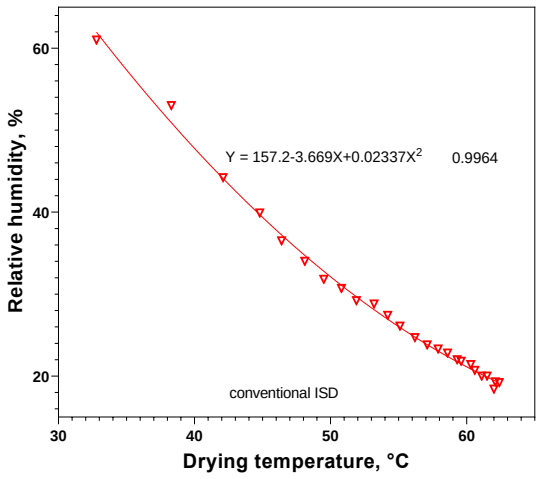

9. ACKNOWLEDGEMENT

This thesis work was supported financially by the Stipendium Hungaricum Scholarship Program and the Mechanical Engineering Doctoral School at Hungarian University of Agriculture and Life Sciences (MATE), Gödöllő, Hungary.

First of all, I would like to praise the Almighty God who has granted countless blessing and guidance during my studies.

I would like to express my deepest gratitude to my supervisors, Prof. Istvan Farkas and Dr Janos Buzas for their inestimable guidance, consistent encouragement and support. Their thoughtful suggestions, ideas were vital for the framework and outcome of this research. It has been a rewarding experience for me in working with them all these years and without them this thesis would not have materialized. I was indeed privileged to have been your supervisee.

I am very grateful to my beloved wife Mrs. Eden Kiflezgh, my mother Ghidey Berhe and all other family members for their immeasurable love and sacrifices which has made this feat possible. My most profound gratitude also goes to Tesfay Haile (Eritrean Honorary Consultante in Hungary), Prof. Tewolde Melles, Eng. Teferi Tsegaye.

Finally, I would like to give a special thank to the staff of the Doctoral School of Mechanical Engineering and the University administration staff for their kindness and cooperation with me during stay at the University.

Thank you for supporting and guiding me to where I am now. May the Almighty God continue to bless each and everyone of you!

Gödöllő, November 2022

Gebremicheal Gedion Habtay